

The SUMER Spectral Atlas of Solar-Disk Features

W. Curdt,¹ P. Brekke,^{2,3} U. Feldman,⁴ K. Wilhelm,¹ B. N. Dwivedi,^{1,5} U. Schühle,¹ and P. Lemaire⁶

¹ Max-Planck-Institut für Aeronomie, 37191 Katlenburg-Lindau, Germany

² Institute of Theoretical Astrophysics, University of Oslo, Blindern, N-0315 Oslo 3, Norway

³ ESA Space Science Department / NASA Goddard Space Flight Center, Greenbelt, Md. 20771, USA

⁴ E. O. Hulbert Center for Space Research, Naval Research Laboratory, Washington D.C., 20375, USA

⁵ Department of Applied Physics, Banaras Hindu University, Varanasi 221005, India

⁶ Institut d'Astrophysique Spatiale, Unité Mixte CNRS - Université de Paris XI, F-91405 Orsay, France

published as A&A 375, 591 (2001); updated: December 15, 2003

Abstract. A far-ultraviolet and extreme-ultraviolet (FUV, EUV) spectral atlas of the Sun between 670 Å and 1609 Å in first order of diffraction has been derived from observations obtained with the SUMER (Solar Ultraviolet Measurements of Emitted Radiation) spectrograph on the spacecraft SOHO (Solar and Heliospheric Observatory). The atlas contains spectra of the average quiet Sun, a coronal hole and a sunspot on disk. Different physical parameters prevalent in the bright network (BN) and in the cell interior (CI) – contributing in a distinct manner to the average quiet-Sun emission – have their imprint on the BN/CI ratio, which is also shown for almost the entire spectral range. With a few exceptions, all major lines are given with their identifications and wavelengths. Lines that appear in second order are superimposed on the first order spectra. These lines are clearly marked in the atlas. The spectra include emissions from atoms and ions in the temperature range $6 \cdot 10^3$ K to $2 \cdot 10^6$ K, i.e., continua and emission lines emitted from the lower chromosphere to the corona. This spectral atlas, with its broad wavelength coverage, provides a rich source of new diagnostic tools for studying the physical parameters in the chromosphere, the transition region and the corona. In particular, the wavelength range below 1100 Å as observed by SUMER represents a significant improvement over the spectra produced in the past. In view of the manifold appearance and temporal variation of the solar atmosphere it is obvious that our atlas can only be a – hopefully typical – snapshot. Brief descriptions of the data reduction and calibration procedures are given. The spectral radiances are determined with a relative uncertainty of 0.15 to 0.30 (1σ) and the wavelength scale is accurate to typically 10 mÅ. The atlas is also available in a machine readable form.

Key words. Sun: UV radiation, Sun: chromosphere, Sun: transition region, Sun: corona, line: identification, atlases

1. Introduction

The EUV portion of the electromagnetic spectrum extends from 100 Å to 1000 Å, whereas the wavelength range from 1000 Å to 2000 Å is commonly referred to as FUV portion in the literature. The solar spectrum in these ranges contains not only a large number of bright emission lines, mainly from the chromospheric and lower transition region plasmas, i.e., formed at electron temperatures $T_e \leq 2.5 \cdot 10^5$ K, but also many coronal lines formed at temperatures of one million kelvin and above. However, above 1216 Å no allowed lines from the upper transition region have previously been observed. Only a few forbidden lines that originate at coronal temperatures in plages had been reported in limb spectra (e.g., Brueckner 1981). In comparison, the solar spectrum in the range from 660 Å to 1200 Å includes a large number of lines from the upper transition region and corona, in addition to lines from the chromosphere and lower transition region (Curdt et al. 1997).

In this paper we present a spectral atlas representative of various solar features observed with SUMER on SOHO. SUMER is a high-resolution telescope and spectrograph designed to obtain stigmatic slit images with spatial and spectral resolution elements of $\approx 1''$ and ≈ 40 mÅ (in first order) as well as high temporal resolution over the wavelength range from 465 Å to 1610 Å. The accessible range depends on which of the detectors is used. While detector 'A' can in principle record spectra from 780 Å to 1610 Å in first order of diffraction, the range of detector 'B' reaches from 660 Å to 1500 Å. The gradual lower wavelength limit (for lines observed in second order) results from the steep fall-off of the reflectivity of the silicon carbide optics below 500 Å. The Ne VII line at 465 Å represents the shortest wavelength identified so far with this instrument. The range from 660 Å to 805 Å can be

covered in both orders. More than 1100 emission lines are available in the SUMER spectral range. These include resonance lines as well as previously unobserved faint inter-system lines, which can be detected by SUMER because of its more efficient low-noise detectors compared to previous instruments, as discussed by Feldman et al. (1997) and Curdt et al. (1997). Thus, the SUMER spectral atlas provides a rich source of new diagnostic tools for probing essential physical properties of the emitting plasma and studying electron densities, electron temperatures and elemental abundances throughout the solar atmosphere.

Earlier EUV/FUV high-resolution instruments made use of UV-sensitive photographic plates (or film) as detectors. Because of the fairly low efficiency of the photographic plates used, few (if any) spectra were obtained from regions that extended more than $20''$ above the limb. In comparison, SUMER has recorded line intensities extending out to $600''$ (Feldman et al. 1999). Off-limb features are, however, excluded here and will be covered by a separate communication.

Given the radiometric calibration of SUMER before and during the mission (Hollandt et al. 1996; Wilhelm et al. 1997a; Schühle et al. 1998, 2000), we are able to present the absolute spectral radiances of different solar features in the wavelength range from 660 \AA to 1485 \AA in first order of diffraction using the detector 'B'. For the sake of completeness, we have added the spectral range from 1485 \AA to 1609 \AA taken from a 'A'-detector spectrum of the quiet Sun. The calibrated radiance spectra have been compared to well-calibrated full disk irradiance measurements and reasonable agreement is found. (Damasch et al. 1999a). The absolute value of the radiation in the EUV/FUV region is important for studying not only the solar transition region and corona, but also the atmosphere of the Earth. This radiation is an important source of energy in the upper atmosphere of the Earth and changes the temperature, chemistry and dynamics in these layers.

In Sect. 1, a brief summary is given of the most important EUV/FUV instruments and previously published solar spectral catalogues and line lists. In Sect. 2 we describe the instrument and the observation, while Sect. 3 deals with data reduction and calibration. The actual atlas is presented in Sect. 4. A list of all observed lines is added as annex to this atlas.

2. Earlier Spectral Atlases

Space astronomy started in 1946 in the United States when W. von Braun's A4 rocket engines (during war named V-2 missile) became available to scientists for launching free-flying, high-altitude observatories. It was not surprising, under these circumstances, that a group from the US Naval Research Laboratory (NRL) became the first to observe the ultraviolet radiation of the Sun with a spectrograph mounted on the tail

fin of a A4 rocket. Since then much progress has been made in solar high-resolution spectroscopy from space (see Feldman et al. 1988). A large number of experiments have been launched to observe the EUV and FUV portions of the solar spectrum. High spectral and spatial resolutions were achieved by several instruments at wavelengths above 1150 \AA . At shorter wavelengths, however, the spectral and spatial resolution were moderate and only strong lines could be observed and/or identified. Spectral catalogues and line lists covering the FUV and EUV portions of the spectrum have previously been published by Burton et al. (1967)¹, Burton & Ridgeley (1970)¹, Dupree & Reeves (1971), Gabriel et al. (1971)¹, Huber et al. (1973)¹, Malinovsky & Heroux (1973), Kjeldseth-Moe et al. (1976), Doschek et al. (1976)¹, Feldman et al. (1976a, 1976b)¹, Vernazza & Reeves (1978), Dere (1978)¹, Feldman & Doschek (1978), Cohen et al. (1978)¹, Cohen (1981), Sandlin et al. (1986)¹, Brekke et al. (1991), Feldman & Doschek (1991)¹, Brekke (1993), Thomas & Neupert (1994), Brooks et al. (1999).

In particular, two instruments made a significant impact on solar spectroscopy: The NRL/S082B EUV spectrograph on the Skylab ATM (Apollo Telescope Mount) and the NRL/High Resolution Telescope and Spectrograph (HRTS). The S082B instrument operated in the 970 \AA to 3940 \AA range, but due to the coating ($\text{Al} + \text{MgF}_2$) of the optical surfaces, the instrument was very inefficient below 1100 \AA (Bartoe et al. 1977). A spectral atlas covering the 1175 \AA to 1950 \AA wavelength range based on the S082B spectrometer was published by Cohen (1981). The $2'' \times 60''$ slit defined the spatial resolution element. Line lists based on the S082B data include those of Doschek et al. (1976), Feldman et al. (1976a, 1976b), Feldman & Doschek (1978), and Cohen et al. (1978), the latter being the most comprehensive. A few very long exposures of bright solar features resulted in useful spectra at wavelengths as short as 970 \AA . A line list compiled from these observations was published by Feldman & Doschek (1991).

During the Skylab mission, several calibration rocket (CALROC) flights were carried out as part of a programme for calibration of the S082B spectrograph. A FUV spectral atlas in the wavelength range from 1170 \AA to 2100 \AA was prepared by Kjeldseth-Moe et al. (1976). The CALROC atlas contains the absolute intensity of an averaged quiet region located $300''$ inside the solar limb. During the observations the slit was rastered across its linear extension, thus averaging over an area of about $60'' \times 60''$ on the solar disk. In addition the atlas contains a quiet region $50''$ inside the solar limb while an active region is presented for wavelengths above 1680 \AA . During these observations the full spatial resolution of the instrument was used. The spectral resolution of the data is $\approx 70\text{ m\AA}$

¹ References contain line lists with line identification, line strengths, etc., but no detailed spectral scans.

and the radiance measurements have estimated relative uncertainties of $\pm 25\%$ (1σ) (Kjeldseth-Moe et al. 1976). This atlas was used as a reference calibration source for other FUV spectra for many years.

HRTS, which operated at wavelengths longer than 1150 Å, was the first spectrometer to combine both high spectral resolution (50 mÅ) and good angular resolution ($1''$) with extensive wavelength and spatial coverage (Bartoe & Brueckner 1975). It was launched several times on sounding rockets and was part of the 5 day Spacelab 2 mission. Spectral catalogues based on the HRTS material covering the wavelength range from 1190 Å to 1710 Å have been published by Brekke et al. (1991) and Brekke (1993). These atlases represented different solar features that intercepted the $950''$ long slit extending from disk centre to the limb. The features included quiet Sun, plages, a sunspot (including a lightbridge), and an explosive event. A very comprehensive line list based on the HRTS material (and to some extent on the Skylab data) was published by Sandlin et al. (1986). The HRTS instrument has provided very important information on the properties of the solar chromosphere and transition region. Excellent reviews of some of the HRTS results can be found in the book "The Solar Transition Region" (Mariska 1992), and in Cook & Brueckner (1979).

The LASP (Laboratory of Atmospheric and Space Physics) EUV spectrometer has been flown on sounding rockets (Hassler et al. 1991). This instrument has been the only solar instrument with an onboard wavelength calibration lamp to provide an absolute wavelength reference with high spectral resolution. During the first flight the wavelength range was 1520 Å to 1600 Å (760 Å to 800 Å in second order). During a later rocket flight on March 12, 1998 the spectrometer was tuned to cover the spectral ranges from 1200 Å to 1280 Å in the first order and 600 Å to 640 Å in the second order.

Before the SOHO mission, the wavelength region between 660 Å and 1175 Å remained poorly observed. Spectra covering the 300 Å to 2950 Å wavelength range with a spectral resolution of about 0.4 Å were obtained during a series of rocket flights in the late 1960s and early 1970s by Burton et al. (1967), Burton & Ridgeley (1970), and Gabriel et al. (1971). Due to low spectral resolution, line shapes could not be obtained. However, many intense solar lines were identified. Improved observations of the EUV solar spectrum in the range from 280 Å to 1340 Å were obtained with the Harvard College Observatory (HCO) spectroheliometer S055 on Skylab (Reeves et al. 1977) and smaller instruments flown earlier on Orbiting Solar Observatories OSO-4 and OSO-6 (cf., Huber et al. 1973).

The S082A on Skylab was a slitless objective-type grating spectrograph covering the wavelength range from 170 Å to 630 Å (Tousey et al. 1977). Each exposure included numerous images of the entire solar disk with a spatial resolution of $2'' \times 2''$. An atlas of EUV spectrohe-

liograms from 170 Å to 625 Å has been made available by Feldman et al. (1987).

Spectral catalogues at shorter wavelengths are those of Vernazza & Reeves (1978) and Malinovsky & Heroux (1973). Based on observations with the S055 spectrometer on Skylab, Vernazza & Reeves (1978) presented a spectral atlas of different solar features in the wavelength range from 280 Å to 1350 Å with a spectral resolution of 1.6 Å. Until now this atlas represented the most complete set of quiet-Sun spectra in this wavelength range. But due to poor spectral resolution of this spectrometer, many lines reported in this atlas are incorrectly identified. More recently an active region EUV atlas in the range from 230 Å to 450 Å was obtained with the SERTS (Solar EUV Rocket Telescope and Spectrometer) rocket experiment (Thomas & Neupert 1994). Emission lines of molecular hydrogen, which are present in sunspot spectra, have been measured and/or predicted by Bartoe et al. (1979). Brooks et al. (1999) have presented a spectral line list in the ranges 308 Å to 381 Å and 513 Å to 633 Å based on measurements of the normal incidence channel (NIS) of the SOHO/CDS instrument (Coronal Diagnostic Spectrometer, Harrison et al. 1995). A calibrated solar EUV spectrum in the same wavelength range has also been presented by Brekke et al. (2000).

3. Instrumentation and Observations

SUMER is part of the SOHO mission of ESA and NASA. SOHO was launched on December 2, 1995 by an Atlas II-AS Centaur into a transfer trajectory to the first Lagrangian point, L1. It was injected into a halo orbit around L1 on February 14, 1996 where, in continuous view of the Sun, it accompanies the Earth at a sunward distance of $1.5 \cdot 10^6$ km. SOHO lost its attitude control on June 25, 1998, but was subsequently recovered later in 1998.

This section describes details of the instrument and the data acquisition which are relevant for the interpretation of the data. A comprehensive description of the instrument is given by Wilhelm et al. (1995), and first results and inflight performance characteristics are given by Wilhelm et al. (1997b) and Lemaire et al. (1997).

3.1. Instrument

SUMER is a stigmatic normal-incidence spectrograph operating in the range from 465 Å to 1610 Å with optical elements made of silicon carbide (SiC) and three normal-incidence reflections. Only few lines below 500 Å have so far been observed with SUMER. The off-axis parabola telescope mirror has a plate scale in the slit plane of $6.3 \mu\text{m}/\text{arcsec}$. It can be moved to obtain disk and off-limb spectra in the lower corona. Four slits with angular dimensions of $4'' \times 300'', 1'' \times 300'', 1'' \times 120'',$ and $0.3'' \times 120''$ are available, the two short slits can be placed at

three different spatial positions with respect to the detector. We have used the $1'' \times 300''$ slit (slit #2) during the coronal-hole and quiet-Sun observations given in this atlas. The sunspot was observed using the narrow $0.3'' \times 120''$ slit (slit #7).

Two diffraction orders can be observed by SUMER; first order lines and second order lines appear superimposed in the spectrum. A few lines could also be observed in third order (Feldman et al. 1997). The dispersion of the instrument is slightly wavelength dependent. For detector 'B', it varies from $44.7 \text{ m}\text{\AA}/\text{pixel}$ (first order) and $22.3 \text{ m}\text{\AA}/\text{pixel}$ (second order) at 660 \AA to $41.2 \text{ m}\text{\AA}/\text{pixel}$ and $20.6 \text{ m}\text{\AA}/\text{pixel}$ at 1500 \AA .

The instrument is equipped with two photon-counting detectors ('A' and 'B') with image encoding in cross-delay-line technique (XDL), for details see Siegmund et al. (1994). Only one detector can be operated at a time. Each detector has 1024 spectral and 360 spatial pixels. The pixel size of approximately $26.5 \mu\text{m} \times 26.5 \mu\text{m}$ is defined by the analogue electronics. The plate scale in the focal plane of the spectrometer is $\approx 1 \text{ pixel/arcsec}$ resulting in an effective focal length of the instrument of 5.5 m. By centroiding, wavelength measurements can be performed with a precision of $5 \text{ m}\text{\AA}$ and better if sufficient lines are available for this purpose (cf., Dammasch et al. 1999b). The central area of the detector is coated with KBr (potassium bromide). This coating increases the detection quantum efficiency (DQE) mainly in the range from 900 \AA to 1500 \AA . Fig. 1 shows a detector readout as raw data in the spectral range from 746 \AA to 791 \AA in the bottom panel. Observations of lines on both sections of the photocathode can be used to discriminate second order lines from first order lines, since the photocathode responsivity changes differently for lines in different orders. Approximately 50 spectral pixels at the extreme ends of the detectors are covered by a mesh providing a 1:10 attenuation for H I Ly α observations.

During the radiometric laboratory calibration (Hollandt et al. 1996), the responsivity of SUMER was determined for both detectors with a transfer standard light source. In-flight calibration refinements indicate that this calibration has been valid and stable until the SOHO accident in June 1998. The dark signal of the detectors is extremely low, and for disk observation, scattered light can be neglected.

Both detectors show non-uniformity effects typical for micro-channel-plate (MCP) intensifiers. These effects stem from the MCP structure, the inhomogeneity of the electric field, electronic non-linearities, and individual pixel deficiencies. These effects, which are very worrisome for the purpose of imaging, can be compensated to some extent by flat-field and geometric corrections. SUMER regularly generates a flat-field matrix, which can be applied either on board or on the ground.

3.2. Data Acquisition

The standard observing sequence for the "reference spectrum" consists of a series of full detector readouts at different wavelengths. To cover the wavelength range of detector 'B' from 670 \AA to 1500 \AA , a set of 61 spectral sections, each offset by $\approx 12.8 \text{ \AA}$ (in first order), were obtained sequentially. This offset was used to record the entire spectral range on both the bare and the KBr-coated part of the MCP, which allows us to discriminate second order lines from first order lines. For this exercise, it was extremely helpful that the range from 670 \AA to 750 \AA was recorded in both orders on this detector. The spectral catalogues, presented here, have been extracted from the KBr-coated portion of the detector, except for the wavelength region around a telemetry gap (see below) and around H I Ly α where only the bare part is available. Note that we have to place this strong line on the attenuator section located at the extreme pixel positions of the detector. Also, the extreme sections of our spectral range can only be recorded on the bare part of the detector. The sunspot spectrum was obtained using a modified observing sequence for faster data acquisition, which was composed of 37 spectral windows, displaced by larger increments of $\approx 20.8 \text{ \AA}$ each.

Whenever possible, the reference spectrum was preceded by a raster sequence where the spectrometer slit moves perpendicular to the slit direction to map an area of $120''$ width. This raster contains 157 slit positions with a step size of $0.75''$. With an exposure time of 10 s at each spatial position the complete raster scan takes 26 min. Three spectral windows centred on selected emission lines were extracted from the detector at each slit position. Monochromatic images at different wavelengths can be constructed from the raster sequence by summing up the counts in the line profiles at each spatial location. Images of the Extreme-Ultraviolet Imaging Telescope (EIT) onboard SOHO (Delaboudinière et al. 1995) were also taken as context images and used to find the exact slit position during the observation as well as to co-align the SUMER observations with those obtained with other instruments. After the raster sequence, the pointing returns to the target position at the centre of the raster image where the reference spectrum is to be acquired. This solar position is maintained if the solar-rotation tracker is activated.

About 300 SUMER reference spectra have been recorded from different locations of the Sun so far. We have selected the reference spectrum obtained on April 20, 1997 as a good choice for the quiet Sun, because neither eruptive phenomena are found in this data set nor telemetry gaps deteriorate the data quality. From 1485 \AA onwards, we have added quiet-Sun 'A'-detector spectra taken on August 12, 1996 in order to present the entire SUMER spectrum of the quiet Sun up to 1609 \AA .

The criteria for typical coronal-hole spectra provide ground for debate. There seems to be a gradual scale of the strengths of coronal holes. While our spectrum, recorded near disk centre on October 12, 1996, is characterized

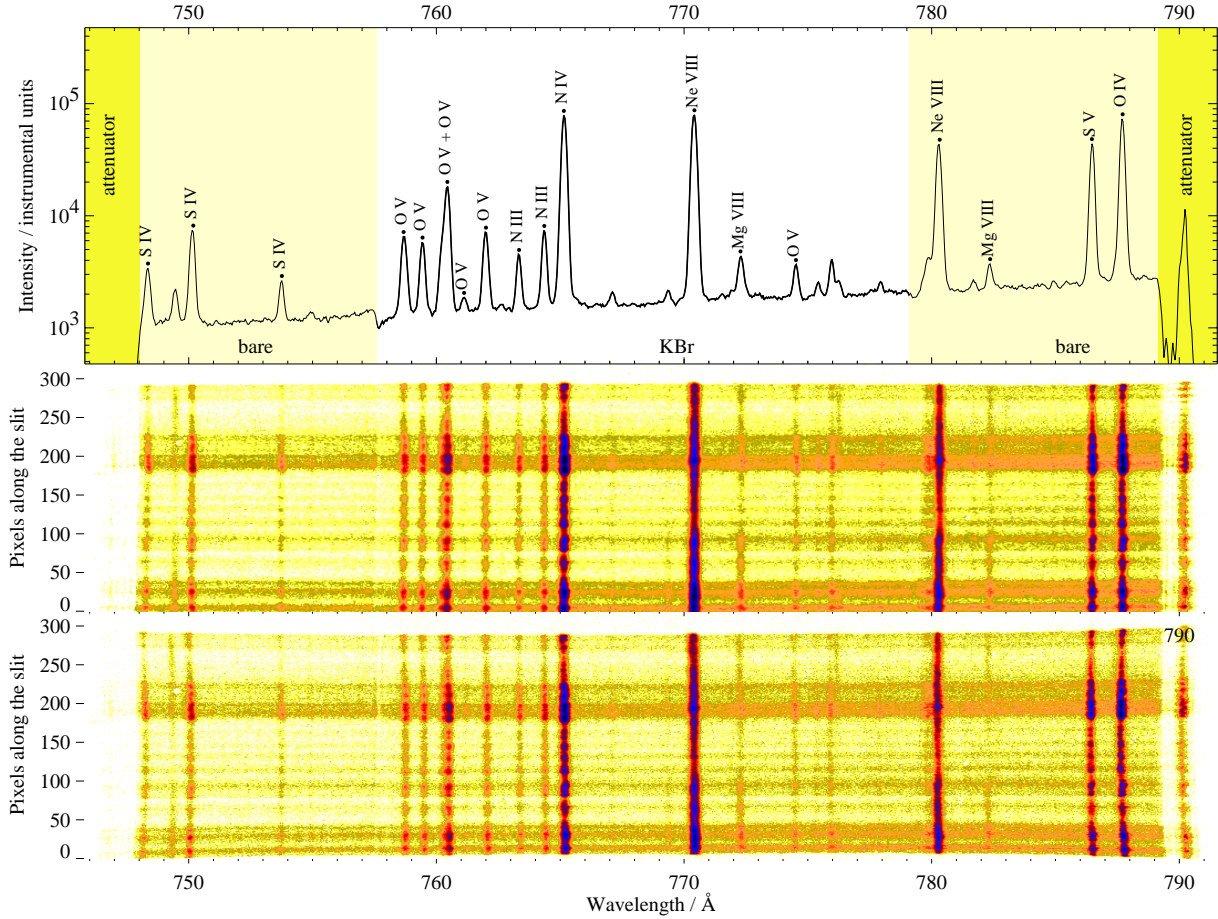


Fig. 1. The SUMER spectral window centred around the Ne VIII 770 Å line, with an exposure time of 300 s, obtained near disk centre of the quiet Sun. The entire detector readout is shown in the lower panel as raw data and after flat-field correction and geometrical distortion correction in the central panel. The spectral profile in the upper panel, integrated from spatial pixels 35 to 174, provides some line identifications. The changes in the continuum counts at 758 Å and 780 Å, which are caused by the different responsivity of the KBr photocathode compared to the bare MCP, are much more prominent at longer wavelengths.

by a depression of approximately a factor of two through the entire wavelength range, this difference is only found at wavelengths below 1000 Å in a polar coronal-hole spectrum (cf., Schühle et al. 1999). This aspect is not yet understood and needs further investigation.

We have selected the sunspot spectrum obtained on March 18, 1999 for our atlas, because this spot was one of the largest observed by SUMER so far and also because the slit seems to have been placed right through the central umbral part. However, we lost a small portion of this spectrum (2 Å) during a telemetry gap. A spectroscopic analysis of this spectrum has been published in more detail by Curdt et al. (2000a). Context images showing the position of the slit during data acquisition are presented in Fig. 2. All observational parameters are summarized in Table 1.

4. Data Reduction

The spectra presented here have been recorded with detector 'B' and compressed during downlink. After decompression, the data set has been flat-field corrected and the geometric distortion of the detector has been removed. Finally, spectral pixels have been converted to wavelengths and the intensity has been given in physical units. Standard procedures have been applied for the basic data processing.

4.1. Correction for Flat-Field and Geometric Distortions

As mentioned in Sect. 3.1, the responsivity of the detector is nonuniform on scales of about 20 pixels or less. Several flat-field matrices have been acquired by long exposures of three hours in the H I Lyman continuum at 880 Å while the spectrometer was defocussed. This provides a deep, al-

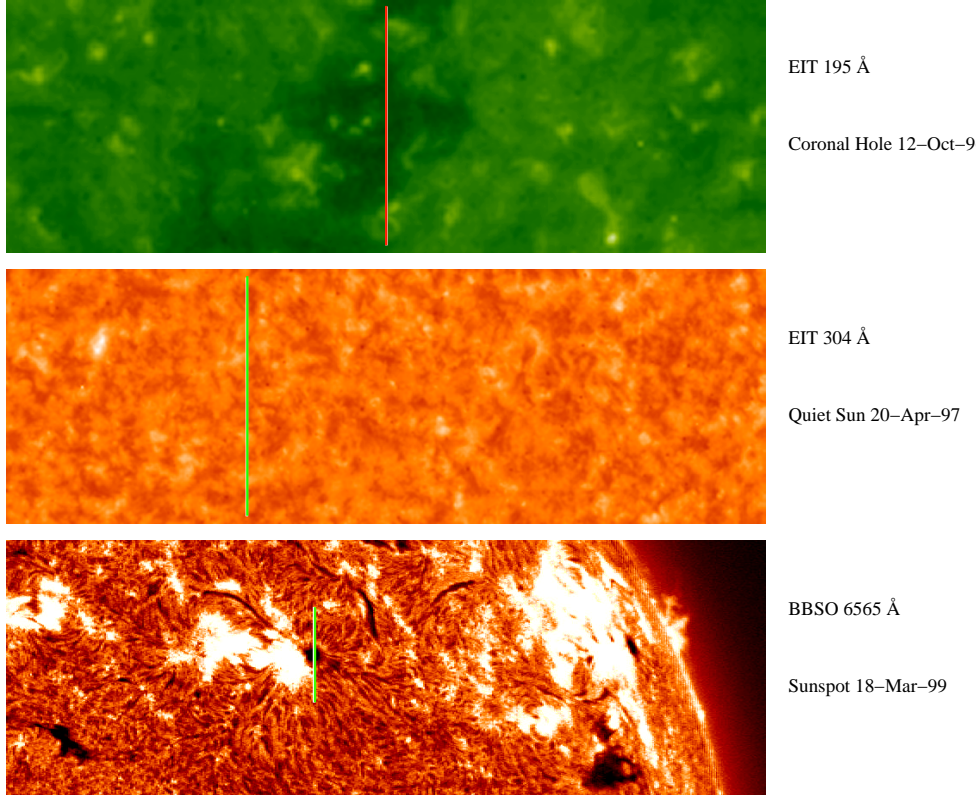


Fig. 2. Context images showing the position of the SUMER slit during data acquisition. The field of view is $937'' \times 320''$ in all three cases. Top: The equatorial coronal hole seen as a dark structure in the Fe XII/195 Å channel (also seen in other EIT channels, courtesy: EIT consortium). Centre: A quiet-Sun area near disk centre in the He II/304 Å channel (courtesy EIT consortium). Bottom: The leading sunspot of active region NOAA 8487 as seen on a H I H α filtergram (courtesy: Big Bear Solar Observatory).

Table 1. Observational parameters of the data sets presented in this atlas. The pointing in x and y is given in seconds of arc (SOHO co-ordinates) and refers to slit centre at the start of the observation, t_0 . T is the exposure time in seconds and d is the total duration of the spectral scan in hours. n_{px} gives the number of pixels which have been used for averaging along the slit. The solar rotation tracking was active in all cases.

target	detector	date	t_0	d	x	y	T	n_{px}	slit	rotcomp
			UT	h	''	''	s	pixel	#	
coronal hole	B	October 12, 1996	20:45	5:15	-66	-26	300	171	2	on
quiet Sun	B	April 20, 1997	00:03	5:09	0	0	300	300	2	on
sunspot	B	March 18, 1999	17:36	2:51	468	360	90	17	7	on
quiet Sun	A	August 12, 1996	01:13	2:07	0	0	113	115	4	on

though not entirely uniform exposure which the SUMER processor compares against a median-20 filtered array in order to extract all non-uniformities smaller than 20 pixels. The small-scale variation amounts to as much as 50%. This includes a pixel-to-pixel variation of approximately 20% in the spatial dimension caused by an analogue-to-digital converter differential non-linearity.

The properties of the detector vary as a function of the extracted charge as the detector is being 'scrubbed' by the accumulated counts. Thus, the flat-field data need to be updated quite frequently. In all cases, we selected the latest flat-field image obtained before the considered observation for this process.

The fringe fields in the detector MCP-anode gap lead to a geometric distortion which makes the image of the slit shorter at the centre of the detector compared to areas closer to the edges. As a result, the spectral lines are curved (cf., Fig. 1). An artificial 'rectangular grid' has been produced using averaged stable solar spectral lines and continuum data, from which the distortion has been parametrized. This correction is then applied to the data in order to overcome this shortcoming. The SUMER standard "destretching procedure" (Moran 1996), also contains a compensation for the small inclination of the slit image relative to the detector pixel direction, which is caused by a residual alignment error between detector anode and spectrometer grating.

Fig. 1 shows a full-detector image centred at $\approx 769 \text{ \AA}$ before and after the corrections for flat-field and geometric distortions are made. As seen in the central panel, the continuum features appear to be horizontal in the dispersion direction and the emission lines are straight to within one spectral pixel after this correction.

4.2. Wavelength Calibration

Since there is no absolute wavelength reference available in the spectrometer, a wavelength scale can only be derived using solar chromospheric lines. The dispersion changes as a function of wavelength, and so each exposure needs an individual calibration. The wavelength calibration is based on identifying the position of chromospheric lines on the detector and the assumption of negligible net Doppler flows for these lines. In quiet regions atomic lines and lines from singly ionized species are formed over a limited range in temperature and other physical conditions, and are known to show relatively small average absolute shifts (e.g., Samaain 1991). Also, the observed small velocity variations along the slit in these lines indicate that these lines are very useful for establishing an absolute wavelength scale.

The pixel-to-wavelength relation is achieved by a correlation of the line centroids in the entire 43 \AA window with all known reference wavelengths in this window, preferably emission lines from neutrals and singly ionized species, which are fairly strong and unblended in the solar spectrum and for which the absolute wavelengths are known with high accuracy. Since the non-linear dispersion is known very accurately from the optical design, this correlation leads to a constant offset for each exposure. In an iterative process, we inspected the preliminary wavelength calibration of each individual exposure for inconsistencies and deviations. This exercise has been very useful in eliminating misidentifications or finding problems with literature values for some of the reference lines.

The identification of reference lines is sometimes difficult due to the presence of many overlapping lines and also due to the presence of prominent lines both in first and second order in the SUMER spectrum. Except for a

few close blends, the line centroids could be determined by multi-Gauss fits with estimated uncertainties of the order of 0.1 pixel ($\approx 5 \text{ m\AA}$ in first order). The accuracy of the laboratory wavelengths of atomic lines is generally better than 2 m\AA . Most of the laboratory wavelengths used for the wavelength calibration were taken from Kelly (1987).

After the spectra have been calibrated, the wavelengths should be accurate to typically 10 m\AA or 2 to 5 km/s on a velocity scale which is relative to quiet-Sun chromospheric layers. We do not claim this accuracy for the sunspot spectra, where this value can easily reach 40 m\AA in cases where either the measured line or the reference lines or both are shifted by net Doppler flows. It is also evident that the sunspot spectrum is more noisy, due to an accumulative effect of the narrow slit, the shorter exposure time, and the reduced number of averaged pixels, which amounts to a factor of ≈ 100 less counts.

In several cases our measured wavelength values, which are reported in the annexed line list, suggest that the literature values have to be revised, in particular, this is the case for wavelengths of forbidden transitions in highly-ionized species, which are difficult to measure in the laboratory. Examples of more accurate measurements, which are beyond the scope of this atlas, are reported by Dammasch et al. (1999b) and Peter & Judge (1999).

4.3. Radiometric Calibration

The calibration of the spectral response of the SUMER instrument is based on a comparison with a radiometric transfer standard source, which had been calibrated against the Berlin Electron-Storage ring for SYnchrotron radiation (BESSY I) as primary radiometric standard (Hollandt et al. 1996). The transfer source provided 16 emission lines with known photon fluxes of rare gases in the SUMER wavelength range. These have been used as the basis for establishing the spectral responsitivity curves of the instrument in first and second order for both detectors.

Based on the experience with previous solar UV missions the stability of the calibration was a major concern. The combined effects of molecular organic contamination and solar irradiation was known to cause degradation of the optical performance in space. Therefore, a comprehensive cleanliness control programme was made part of the SUMER project, which successfully avoided this type of contamination. This could be verified by monitoring the sensitivity during the mission (Schühle et al. 1998). The responsivity of the instrument has been monitored from the moment when first light was received on the telescope. The count rates for well known solar lines at quiet solar conditions were measured and found to be the same as predicted by the calibration made on the ground. During the entire mission, calibration measurements have been carried out at regular time intervals to track the responsivity of the instrument. The radiance at selected wave-

lengths of a quiet-Sun area was monitored to detect possible changes in the response. Despite the high variability of the Sun as a source, these measurements confirmed the stability of the calibration within uncertainty limits of $\pm 15\%$ (1σ) for detector 'A' (Wilhelm et al. 1997a) and $\pm 20\%$ for detector 'B', in the range from 537 Å to 1250 Å (Schühle et al. 2000). In addition, the spectral calibration curves could be refined during flight by measuring solar line ratios and by observation of standard UV stars (Wilhelm et al. 1997a).

Thus we believe that in the wavelength range from 537 Å to 1250 Å the radiometric calibration has been valid until June 1998, the time when the loss of the SOHO attitude control occurred. Our spectrum of the sunspot was taken after recovery of the spacecraft when a change of sensitivity of the SUMER instrument was discovered. Data after the recovery are treated with a correction factor of 43 % to account for the average loss of sensitivity attributable to the loss of SOHO. The uncertainty in the determination of this change affects also the overall uncertainty of the radiometric calibration after recovery which we estimate to 30 %. At wavelengths longer than 1250 Å the uncertainties are 30 % before and 40 % after the SOHO recovery.

However, some corrections are necessary for bright lines. The count-rate capabilities of the detectors are slightly exceeded if bright lines are placed onto the KBr part of the photocathode, leading to a local-gain depression of the detector channel plates and dead-time effects of the electronics (Wilhelm et al. 2000). As a result the intensities of the lines affected (C III 977 Å, H I Ly β 1026 Å, O VI 1032 Å, O VI 1037 Å, H I Ly α 1216 Å, O I 1302–1306 Å, C II 1335/1336 Å) are underestimated in the raw data. The corrections, which amount to as much as 30% for the C III line and about 17% for the O VI, H I, O I, and C II lines have been applied in our atlas. The given intensity of the H I Ly α 1216 Å line is only an approximation, since this bright line could only be observed with the attenuator. Since the brightness of structures observed on the Sun may have changed while the spectral range was covered, the intensities of lines may become less comparable with increasing difference in wavelength.

In the sunspot spectrum, the photon rate of some emission lines heavily exceeded the detector capabilities. Then, in addition to dead-time losses, some pulses are registered at a displaced position and appear in both dimensions as ghosts in an image. These electronic ghosts have been eliminated and appear as gaps in our spectrum. This correction was needed for H I Ly γ 973 Å, C III 977 Å, O VI 1032 Å, O VI 1037 Å, H I Ly α 1216 Å, O V 1218 Å & Mg X 1219 Å/2, N V 1238 Å, and N V 1242 Å.

To confirm the consistency of the radiometric results further, we compared our calibration and checked it with other solar spectral instruments which measure the irradiance from the full solar disk. In using the spectral radiance of this atlas for a comparison with irradiance data

from the full Sun, one has to take into account contributions from different features on the disk, such as active regions and coronal holes, and center-to-limb variation (limb brightening), which are not resolved in full-disk measurements. Full-disk irradiances have been reported for a number of selected emission lines for which full-Sun raster scans have been made with the SUMER instrument (Wilhelm et al. 1998). From these measurements the effects of active regions, coronal hole deficiencies, and detailed center-to-limb radiance variations have been determined. Most lines of the solar transition region are from optically thin plasmas and show substantial limb brightening, which leads to an average radiance of the solar disk of approximately twice the radiance at disk centre. Therefore, the irradiance from the full Sun will be higher than from the disk centre for most of the lines in this spectral range. Work has been done to compare the irradiances of the quiet Sun measured with SUMER with previous results in the literature, and whenever a comparison could be made we found agreement within the uncertainty margins (Damasch et al. 1999a). A comparison of the SUMER radiance spectrum has also been made with the irradiance spectrum of the Solar-Stellar Irradiance Comparison Experiment (SOLSTICE) on the Upper Atmospheric Research Satellite (above 1150 Å) and the EUV Grating Spectrograph (EGS) (below 1190 Å), which was flown on sounding rockets (Woods et al. 1998a). The latter two instruments have been calibrated against the Synchrotron Ultraviolet Radiation Facility (SURF) of the US National Institute of Standards and Technology (NIST) as primary radiometric standard. The comparison between the SOLSTICE/EGS irradiance spectrum and the SUMER quiet-Sun radiance spectrum was made between 800 Å and 1600 Å at a spectral resolution of 3 Å (Schühle et al. 1998). For most parts of the spectrum the agreement was found to be very good, except where we have dominating second-order lines in the SUMER spectrum and a spectral region around 950 Å, which could be attributed to an instrumental effect (Woods 1998b). A detailed comparison between SOLSTICE and SUMER in the range from 1200 Å to 1560 Å was given by Wilhelm et al. (1999). The comparison of stellar FUV spectra with the spatially resolved spectra of the Sun is also of great interest. Fig. 3 compares the average quiet-Sun radiance spectrum in the range from 1287 Å to 1307 Å to the irradiance spectrum of the solar twin G2 V star α Cen A (for details, cf., Ayres 2000) as measured by the Hubble Space Telescope Imaging Spectrograph (HST-STIS). Both spectra are very similar, except for second order lines, which are not present in STIS spectra. Faint lines can be easier seen in the SUMER spectrum, which has a better photon statistic. The STIS spectrum with its better spectral resolution is very useful for studying line blends and line reversals due to optical thickness effects. A more detailed analysis and a radiometric comparison are beyond the scope of this atlas.

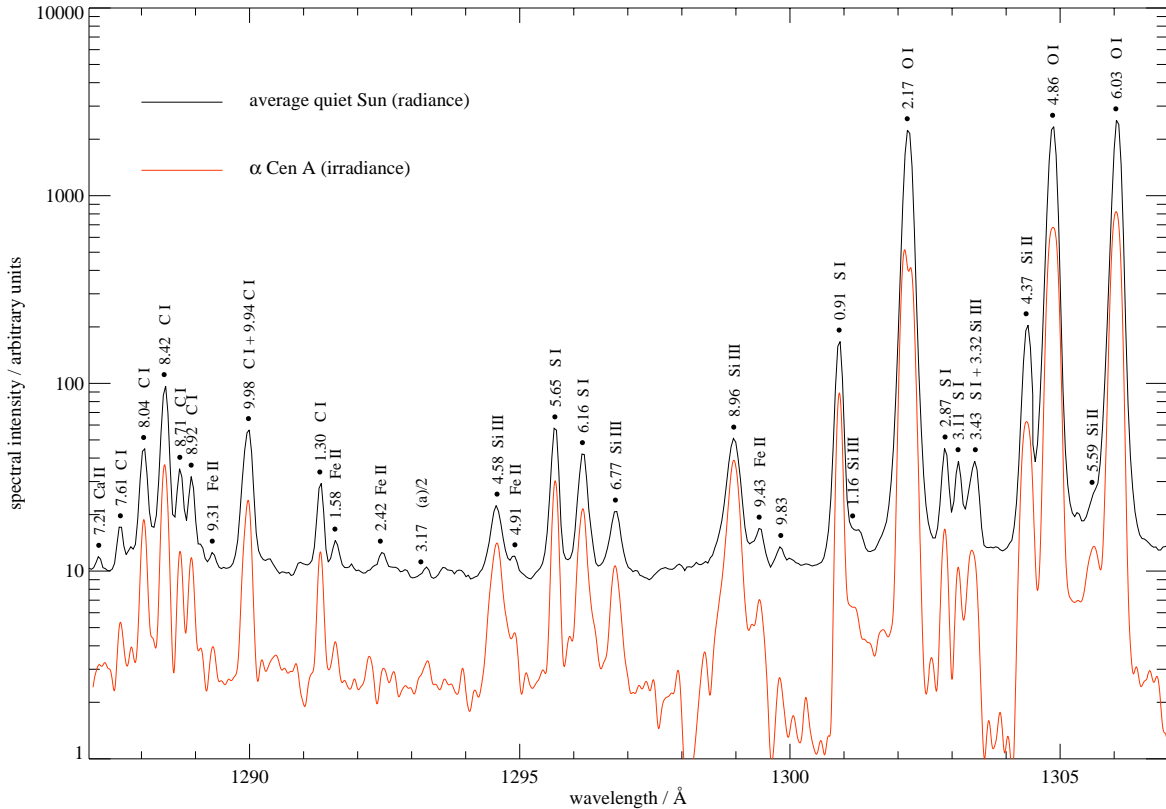


Fig. 3. Comparison of the FUV irradiance spectrum of α -Cen A and of the quiet Sun radiance spectrum at disk centre in the range from 1270 \AA to 1310 \AA . The stellar spectrum (courtesy: HST-STIS consortium) has been degraded to the SUMER resolution by a convolution with a Gaussian of standard deviation $\sigma=60$ m \AA .

5. Description of the Atlas

The spectra presented in this atlas are composites of individual exposures, most of them on the KBr photocathode. The separation wavelengths are indicated by broken vertical lines at the bottom. Although we have used the onboard solar rotation tracker for all spectra presented here, there are clear indications of evolution in the network structures observed. This has to be taken into account, if radiances of lines from different exposures are compared. The variability of the solar atmosphere on all temporal and spatial scales is amazing. These include periodic phenomena (cf., e.g., Curdt & Heinzel 1998 and references therein) and explosive phenomena (cf., e.g., Innes et al. 1997 and references therein). To give an example, the emission measure of some lines increased by a factor of ≈ 5 during the sunspot observation as derived from a comparison of lines recorded in both orders of diffraction (i.e., at the beginning of the sequence and at the end of the sequence).

The spectra are displayed as profiles in different colours, the quiet-Sun spectrum as black line, the coronal-hole spectrum as blue line, and the sunspot spectrum as red line. In the sunspot profile the continuum background has been moderately noise-filtered. The BN/CI ratio of the

quiet-Sun spectrum is overlayed as green, solid line using a separate axis scale. In Fig. 4 the spectrum is presented in portions of 42 \AA per page with 2 \AA of overlap. The atlas is also available in machine readable form via ftp or the internet². This atlas represents our most up-to-date knowledge of the solar-disk spectrum in the given spectral range. Coronal and flare spectra have also been analyzed (Curdt et al. 2000b; Feldman et al. 2000), but are not the subject of this communication.

5.1. Line Identification

Each resolved emission line is indicated by a mark, the measured wavelength in angstrom (\AA), and the identification, if available. For the sake of a concise presentation, the wavelength values are restricted to three digits, one digit before and two rounded digits after the decimal point (e.g., the Ne VIII line observed at 770.423 \AA reads 0.42 in first order and 0.85 in second order). The mark can be used as a cross-reference to line lists available in the literature, where additional spectroscopic information is found.

² Profiles and line list available via <http://cdsweb.u-strasbg.fr/Simbad.html> or <http://www.linmpi.mpg.de/~curdt>

observations, circles to Curdt et al. (1997) and squares to Feldman et al. (1997), respectively. Diamonds point to the older lists of Kelly (1987), Cohen et al. (1978), Sandlin et al. (1986), and Bartoe et al. (1979). We have checked the line lists in this order and emphasize that marks are not meant in a sense of 'first identification by', but, on the contrary, in general are pointing to the most recent list. Triangles denote lines observed for the first time or new identifications, these are mainly found in the sunspot spectrum. Open marks represent lines which are observed in second order of diffraction. Questionable identifications are marked by a question mark (?). Only 4% of the lines in the quiet-Sun spectrum remain unidentified at this stage, most of them being faint. This percentage increases to 12%, if we also consider the sunspot spectrum, which seems to be dominated by 3- to 6-fold ionized species and is more difficult to interpret. In these cases we have given the temperature classification of Feldman et al. (1997), if available (cf., Fig. 4). A list of all lines observed in the SUMER spectral range is given electronically in the Annex.

5.2. Bright Network/Cell Interior Ratio

In the quiet-Sun spectrum, the SUMER slit cuts five partly sub-structured supergranular cells. We have separated 21 pixels representative of bright network and 71 pixels of cell interior, respectively. The BN/CI ratio, thus derived from the same exposures, is ≥ 1 at all wavelengths. It shows an interesting variation, depending on the particular emission line under consideration. This feature is a direct consequence of the plasma temperature and density of the emitting source. For lines with high formation temperature, the BN/CI ratios are not far from 1, while they can reach values > 10 for transition region lines.

6. Summary

The spatially resolved solar EUV/FUV spectra studied in this atlas, cover a wide spectral range from 670 Å to 1609 Å and provide a wealth of information on solar plasma structures from the upper chromosphere through the transition region to the corona. This information has, therefore, a tremendous diagnostic value for the emitting source. Together with the high spatial resolution of the SUMER spectrograph, compared to other solar EUV spectrometers flown during the last decades, plasma parameters of small solar features can be investigated. The atlas also provides an excellent reference for astrophysical applications. The SUMER spectrograph combines better spectral and spatial resolutions as well as coverage than any previous observations in the same wavelength range, and permits the extensive use of spectroscopic techniques in determining temperatures, pressures, densities and velocities in the upper solar atmosphere. The atlas also presents a powerful tool for the planning of future observations, i.e., to determine adequate integration times, to identify possible blends, and to select proper data extraction windows in upcoming solar studies.

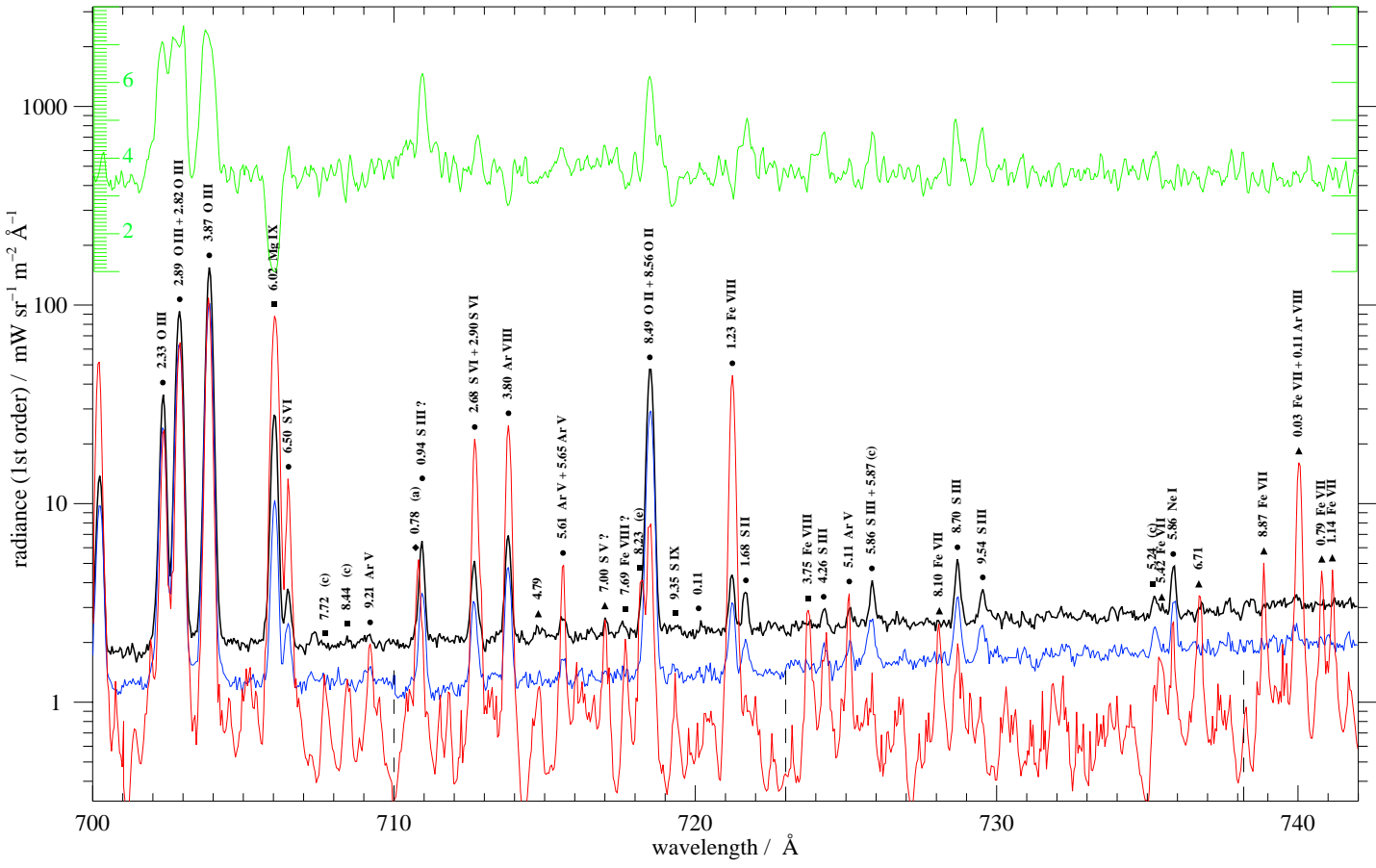
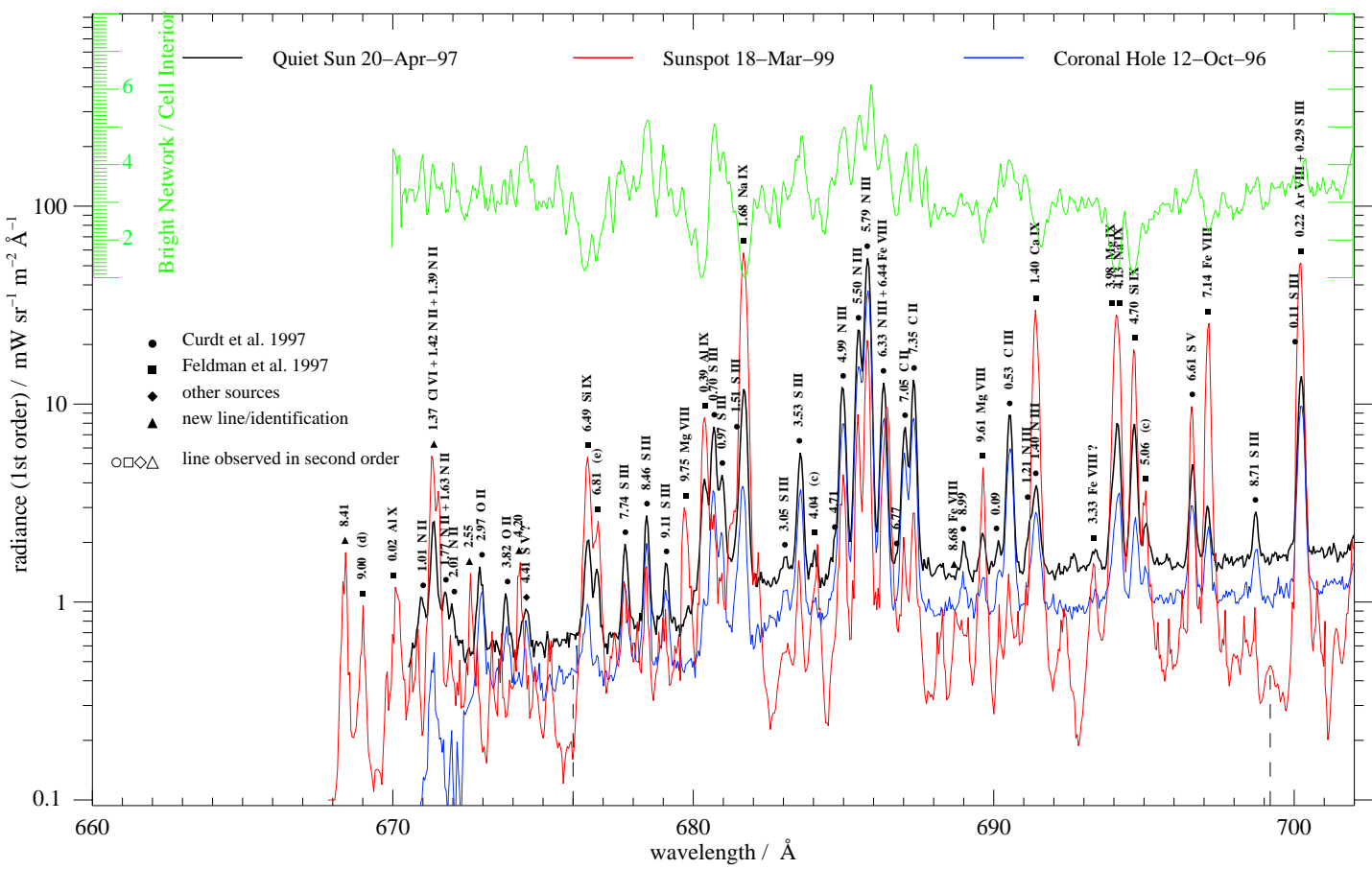
7. Acknowledgements

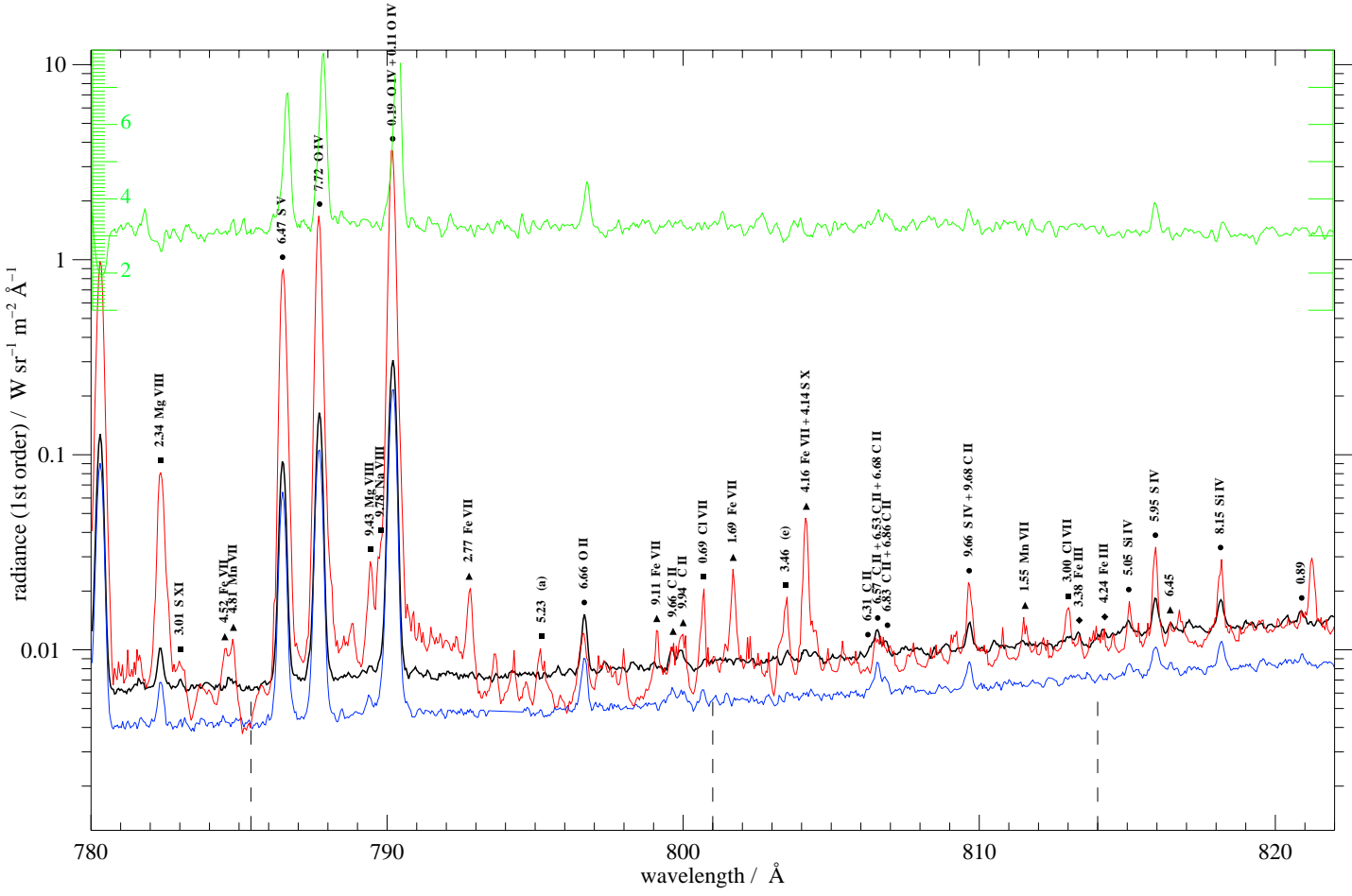
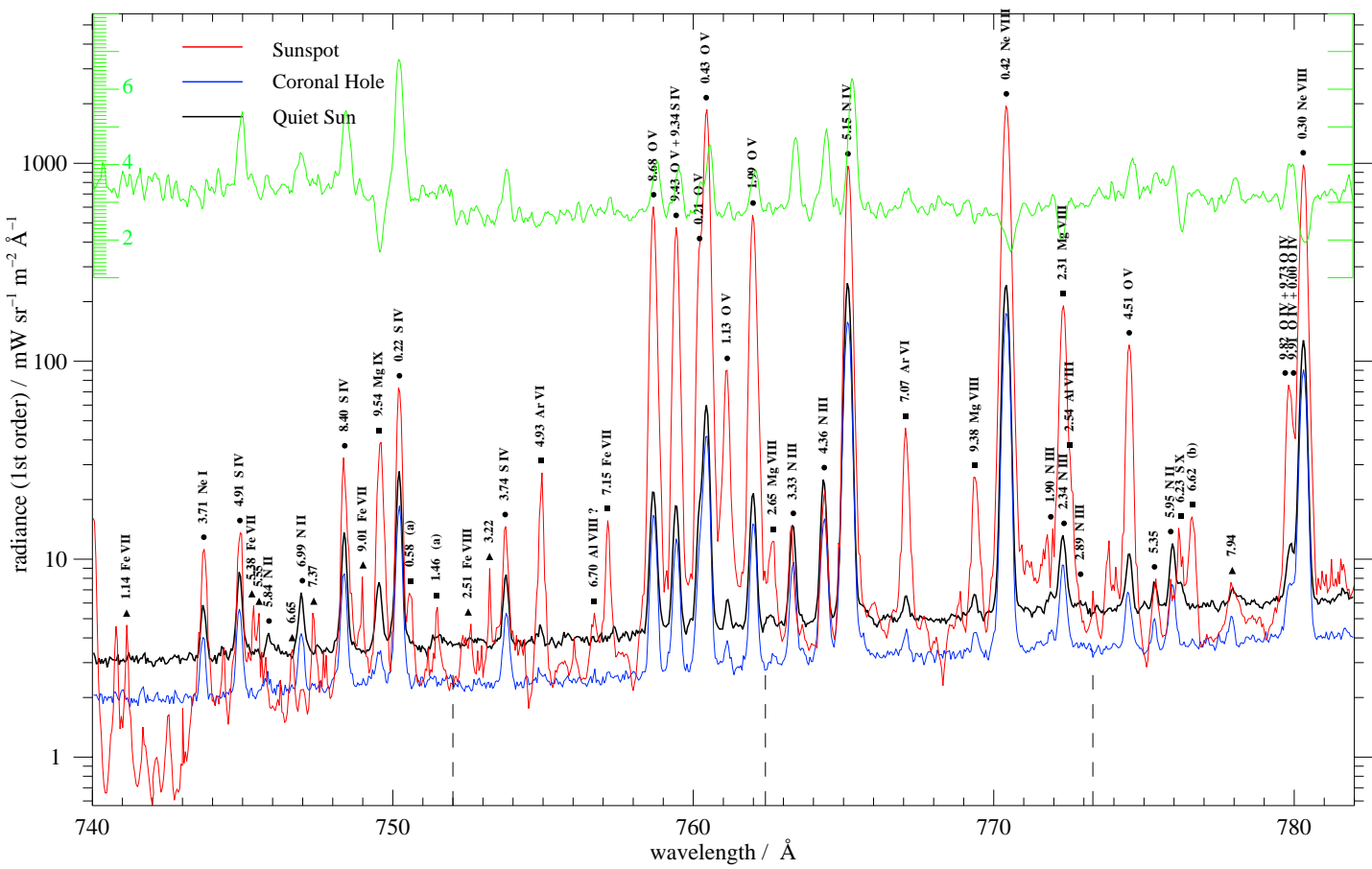
We thank Tom Ayres for his help in retrieving the stellar data from the HST-ST Science Institute archive. The SUMER project is financially supported by DLR, CNES, NASA and the ESA PRODEX Programme (Swiss contribution). SUMER is part of SOHO, the Solar and Heliospheric Observatory, of ESA and NASA. U. F. acknowledges financial support from NRL/ONR 6.1 basic research programs and NASA grants.

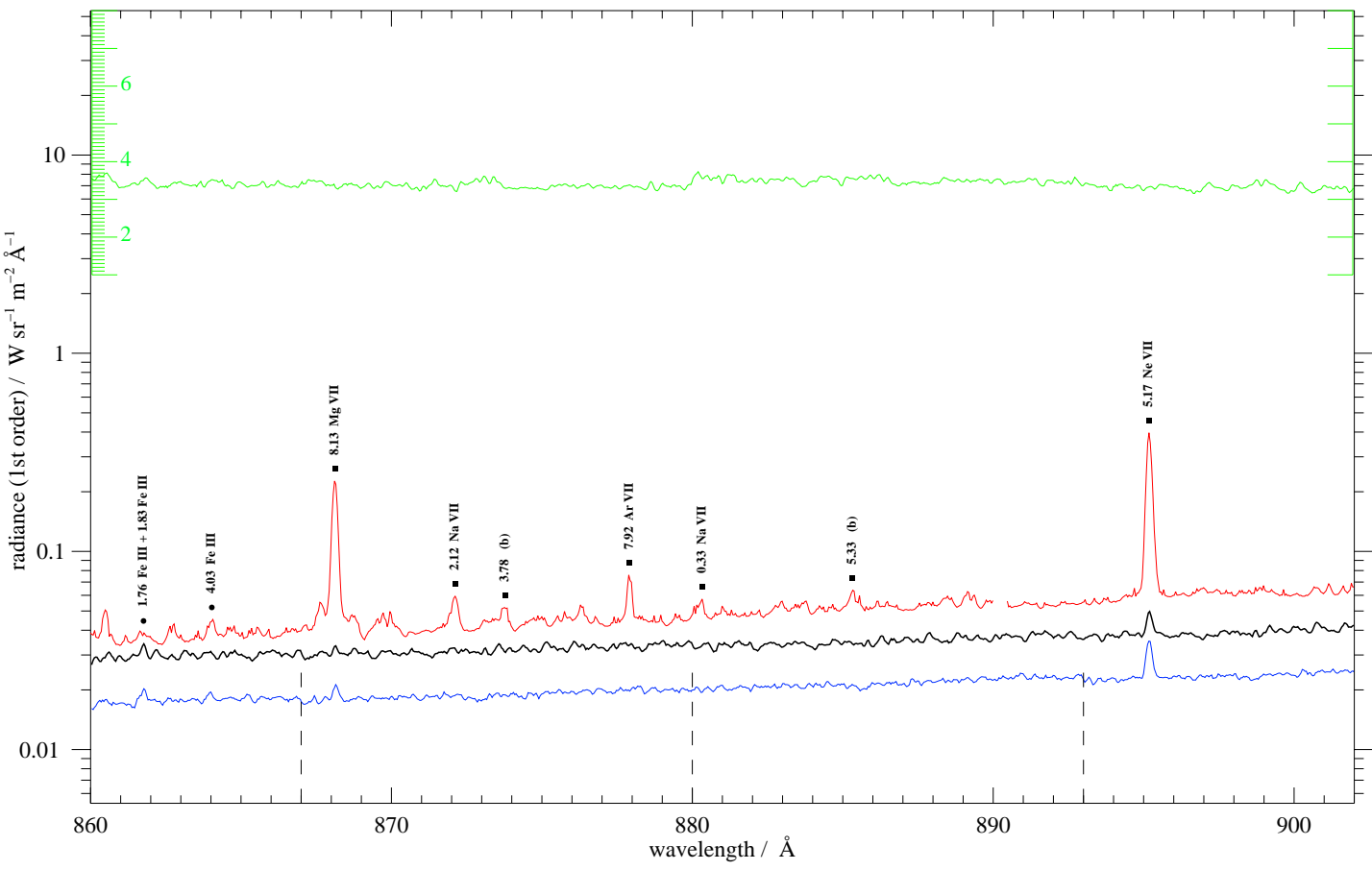
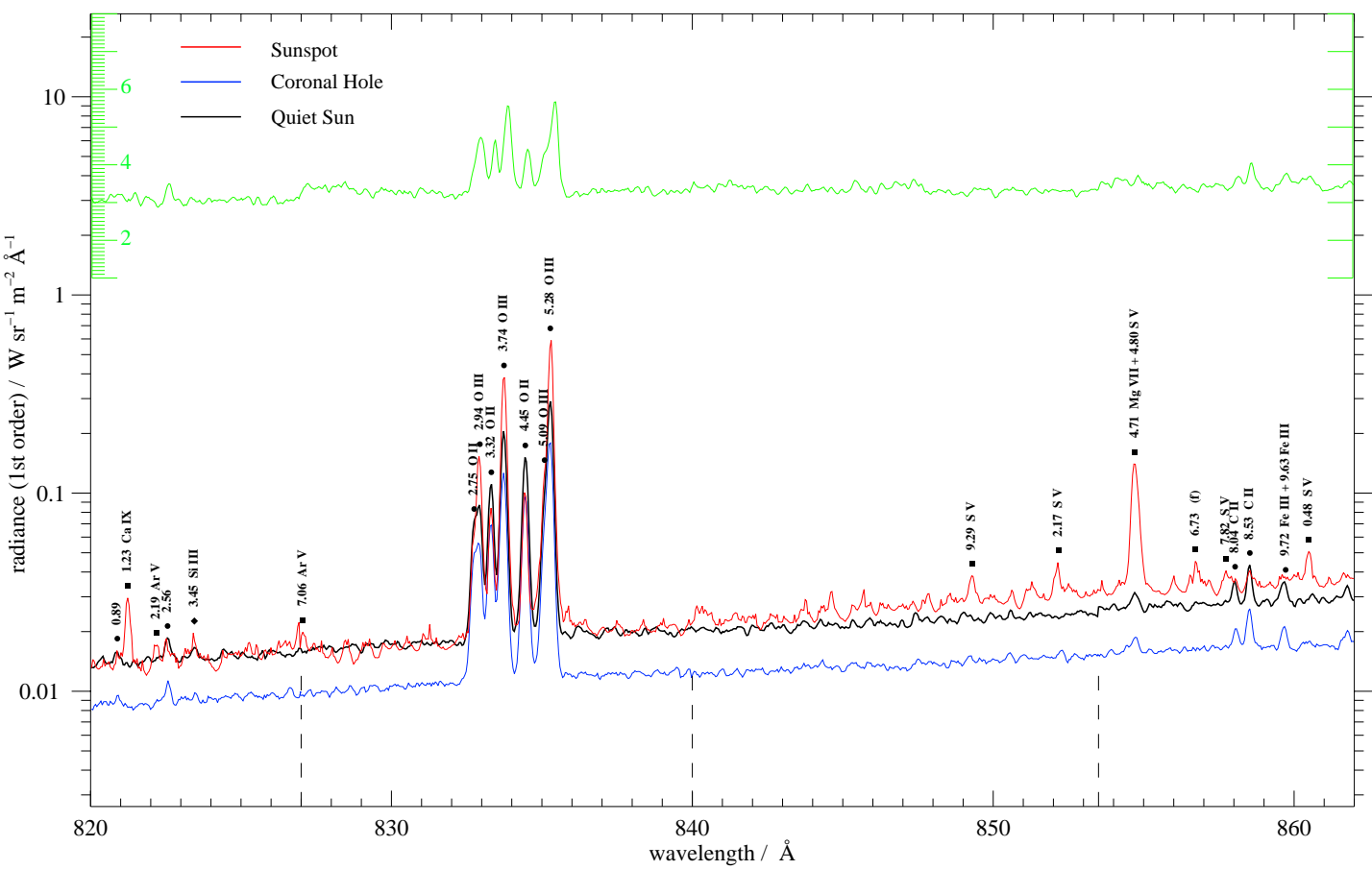
References

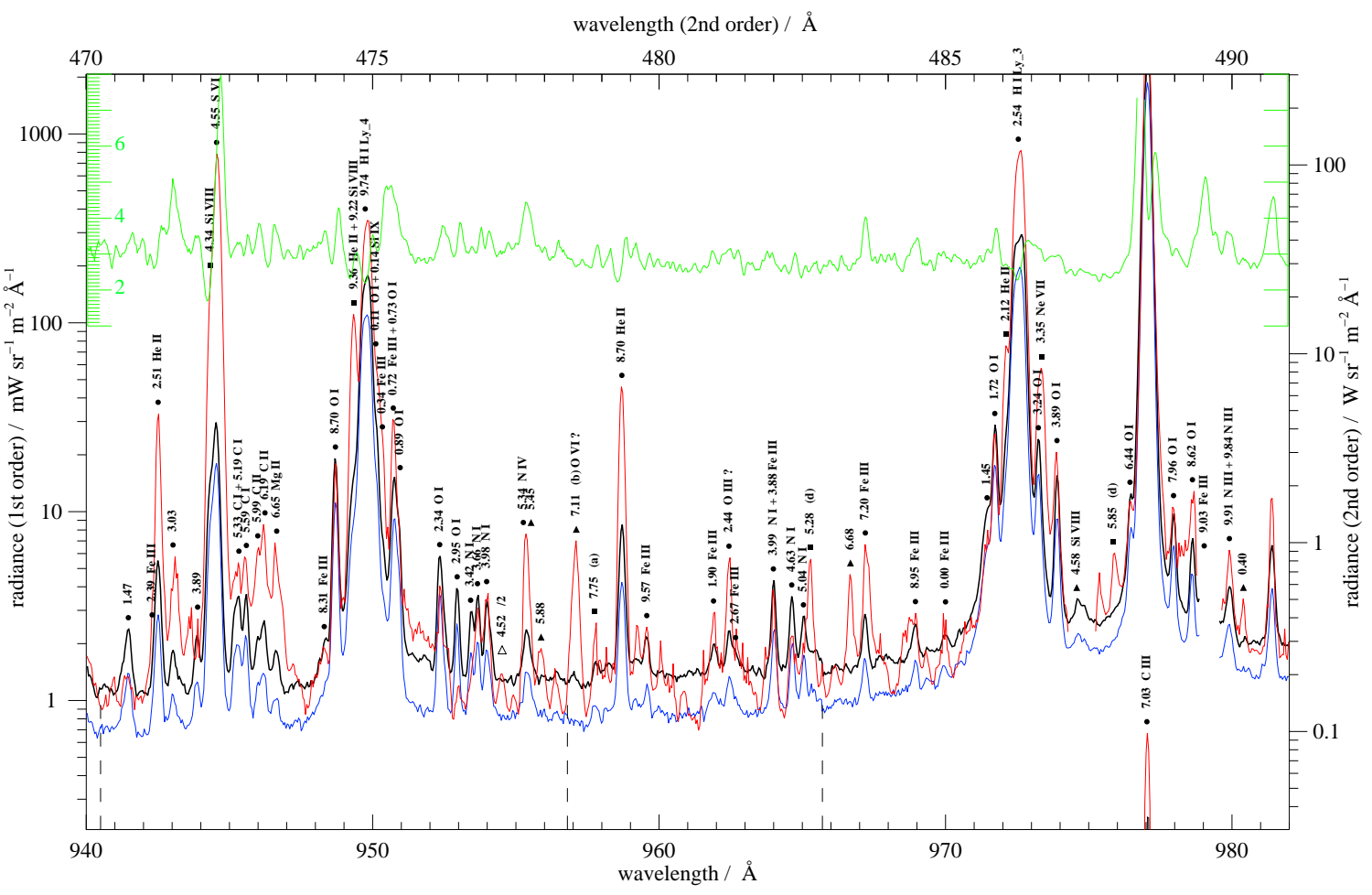
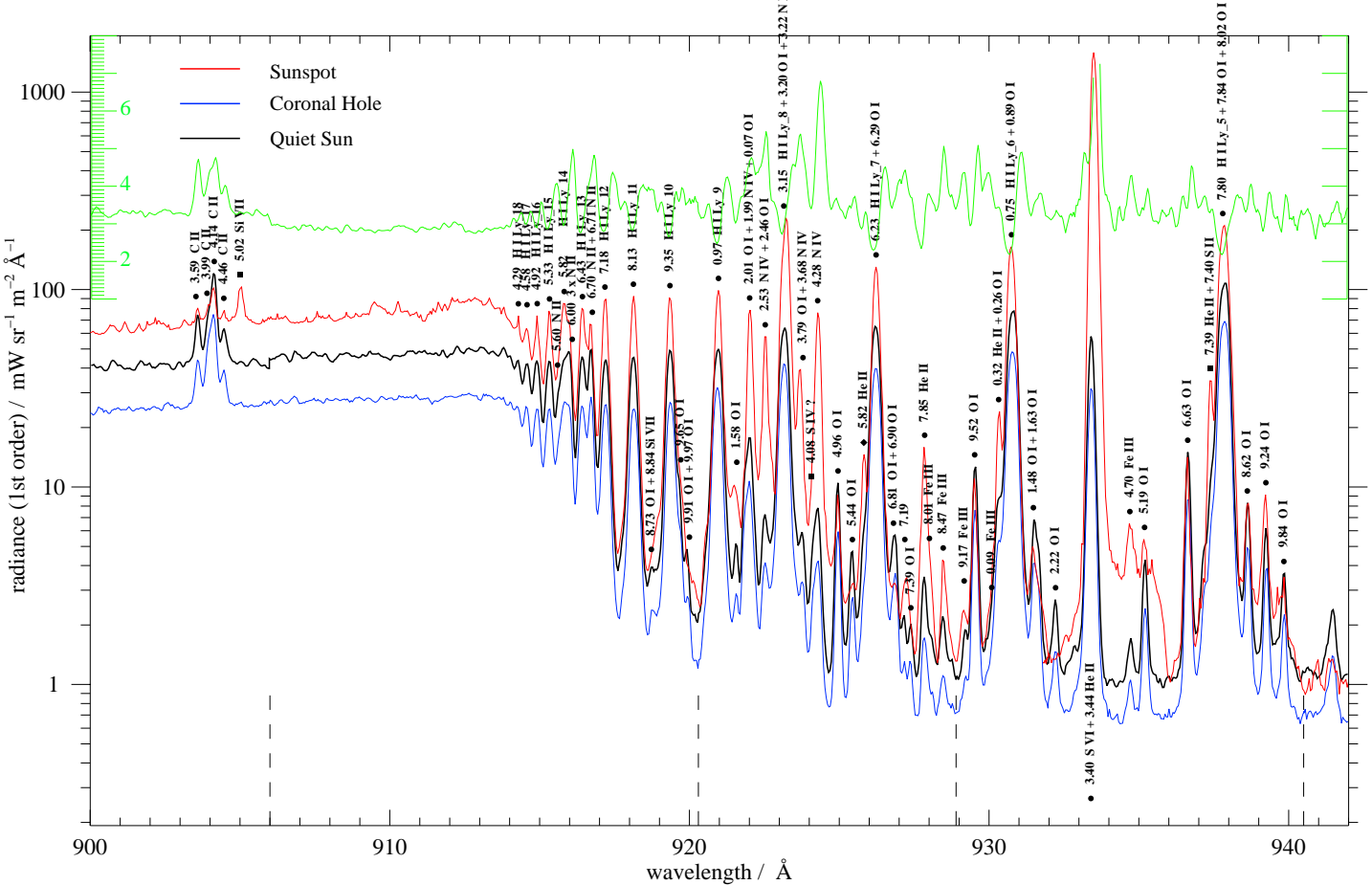
- Ayres, T.R. 2000, Sol. Phys. 193, 273
- Bartoe, J.-D.F., & Brueckner, G. E. 1975, J. Opt. Soc. Am. 65, 13.
- Bartoe, J.-D.F., Brueckner, G.E., Purcell, J.D., & Tousey, R. 1977, Appl. Opt. 16, 879
- Bartoe, J.-D.F., Brueckner, G.E., Nicolas, K.R. et al. 1979, MNRAS 187, 463
- Brekke, P., Kjeldseth-Moe, O., Bartoe, J.-D.F., & Brueckner, G.E. 1991, ApJS 75, 1337
- Brekke, P. 1993, ApJS 87, 443
- Brekke, P., Thompson, W.T., Woods, T.N., & Eparvier, F.G. 2000, ApJ 536, 959
- Brooks, D.H., Fischbacher, G.A., Fludra, A. et al. 1999, A&A 347, 277
- Brueckner, G.E. 1981, in F.Q. Orrall (ed.) *Solar Active Regions*, Colorado Associated University Press, Boulder, p. 113
- Burton, W.M., Ridgeley, A., & Wilson, R. 1967, MNRAS 135, 207
- Burton, W.M., & Ridgeley, A. 1970, Solar Phys. 14, 3
- Cohen, L., Feldman, U., & Doschek, G.A. 1978, ApJS 37, 393
- Cohen, L. 1981, *An Atlas of Solar Spectra between 1175 and 1950 Angstroms Recorded on Skylab with the NRL's Apollo Telescope Mount Experiment* NASA Ref. Pub. 1069
- Cook, J.W. & Brueckner, G.E. 1979, ApJ 227, 645
- Curdt, W., Feldman, U., Laming, J.M. et al. 1997, A&AS 126, 281
- Curdt, W. & Heinzel, P. 1998, ApJ 503, L95
- Curdt, W., Dwivedi, B.N., & Feldman, U. 2000a, J. Astrophys. Astr. 21 (3&4), 397
- Curdt, W., Landi, E., Wilhelm, K., & Feldman, U. 2000b, Phys. Rev. A 62, 022502
- Dammasch, I.E., Wilhelm, K., Curdt, W., & Schühle, U. 1999a, in A. Wilson (ed.) *Magnetic Fields and Solar Processes*, Proc. 9th EPS meeting, Florence, 1999, ESA-SP-448, 1165
- Dammasch, I.E., Wilhelm, K., Curdt, W., & Hassler, D.M. 1999b, A&A 346, 285
- Delaboudinière, J.-P., Artzner, G.E., Brunaud, J. et al. 1995, Sol. Phys. 162, 291
- Dere, K.P. 1978, ApJ 221, 1062
- Doschek, G.A., Feldman, U., VanHoosier, M.E., & Bartoe, J.-D.F. 1976, ApJS 31, 417
- Dupree, A.K., & Reeves, E.M. 1971, ApJ 165, 599
- Feldman, U., Doschek, G.A., VanHoosier, M.E., & Purcell, J.D. 1976a, ApJS 31, 445
- Feldman, U., Brown, C.M., Doschek, G.A. et al. 1976b, J. Opt. Soc. Am. 66, 853
- Feldman, U., Doschek, G.A. 1978, ApJS 37, 443
- Feldman, U., Purcell, J. D., & Dohne, B. 1987, *An Atlas of Extreme Ultraviolet Spectroheliograms from 170-625 Å*, NRL Report
- Feldman, U., Doschek, G.A., Seely, J.S. 1988, J. Opt. Soc. Am. 5, 2237
- Feldman, U. & Doschek, G.A. 1991, ApJS 75, 925
- Feldman, U., Behring, W.E., Curdt, W. et al. 1997, ApJS 113, 195
- Feldman, U., Doschek, G.A., Schühle, U., & Wilhelm, K. 1999, ApJ 518, 500
- Feldman, U., Curdt, W., Landi, E., & Wilhelm, K. 2000, ApJ 544, 508
- Gabriel, A.H., Garton, W.R.S., Goldberg, L. et al. 1971, ApJ 169, 595
- Harrison et al. 1995, Sol. Phys. 162, 233
- Hassler, D.M., Rottman, G.J., & Orrall, F.Q. 1991, ApJ 372, 710
- Hollandt, J., Schühle, U., Paustian, W. et al. 1996, Appl. Opt. 35, 5125
- Huber, M.C.E., Dupree, A.K., Goldberg, L. et al. 1973, ApJ 183, 291
- Innes, D.E., Inhester, B., Axford, W.I., & Wilhelm, K. 1997, Nature 386, 811
- Kelly, R.L. 1987, J. Phys. Chem. Ref. Data 16, 1
- Kjeldseth-Moe, O., VanHoosier, M.E., Bartoe, J.-D.F., & Brueckner, G.E. 1976, *A Spectral Atlas of the Sun between 1175-2100 Å*, NRL Report 8056
- Lemaire, P., Wilhelm, K., Curdt, W. et al. 1997, Sol. Phys. 170, 105
- Malinovsky, M. & Heroux, L. 1973, ApJ 181, 1009
- Mariska, J.T. 1992, *The Solar Transition Region*, Cambridge University Press, Cambridge
- Moran, T. 1996, private communication
- Peter, H. & Judge, P.G. 1999, ApJ 522, 1148
- Reeves, E.M., Huber, M.C.E. & Timothy, J.G. 1977, Appl. Opt. 16, 837
- Samain, D. 1991, A&A 244, 217
- Sandlin, G.D., Bartoe, J.-D.F., Brueckner, G.E. et al. 1986, ApJS 61, 801
- Schühle, U., Brekke, P., Curdt, W. et al. 1998, Appl. Opt. 37, 2646
- Schühle, U., Curdt, W., Wilhelm, K. et al. 1999, Space Sci. Rev. 87, 299
- Schühle, U., Curdt, W., Hollandt, J. et al. 2000, Appl. Opt. 39, 418
- Siegmund, O.H.W., Gummin, M.A., Stock, J.M. et al. 1994, Proc. SPIE 2280, 89
- Thomas, R.J. & Neupert, W. 1994, ApJS 91, 461
- Tousey, R., Bartoe, J.-D.F., Brueckner, G.E. & Purcell, J.D. 1977, Appl. Opt. 16, 870
- Vernazza, J.E. & Reeves, E.M. 1978, ApJS 37, 485
- Wilhelm, K., Curdt, W., Marsch, E. et al. 1995, Sol. Phys. 162, 189
- Wilhelm, K., Lemaire, P., Feldman, U. et al. 1997a, Appl. Opt. 36, 6416
- Wilhelm, K., Lemaire, P., Curdt, W. et al. 1997b, Sol. Phys. 170, 75
- Wilhelm, K., Lemaire, P., Dammasch, I.E. et al. 1998, A&A 334, 685
- Wilhelm, K., Woods, T.N., Schühle, U. et al. 1999, A&A 352, 321
- Wilhelm, K., Schühle, U., Curdt, W. et al. (2000), Metrologia 37(5), 393
- Woods, T.N., Rottman, G.J., Bailey, S.M. et al. 1998a, Sol. Phys. 177, 133
- Woods, T.N. 1998b, private communication

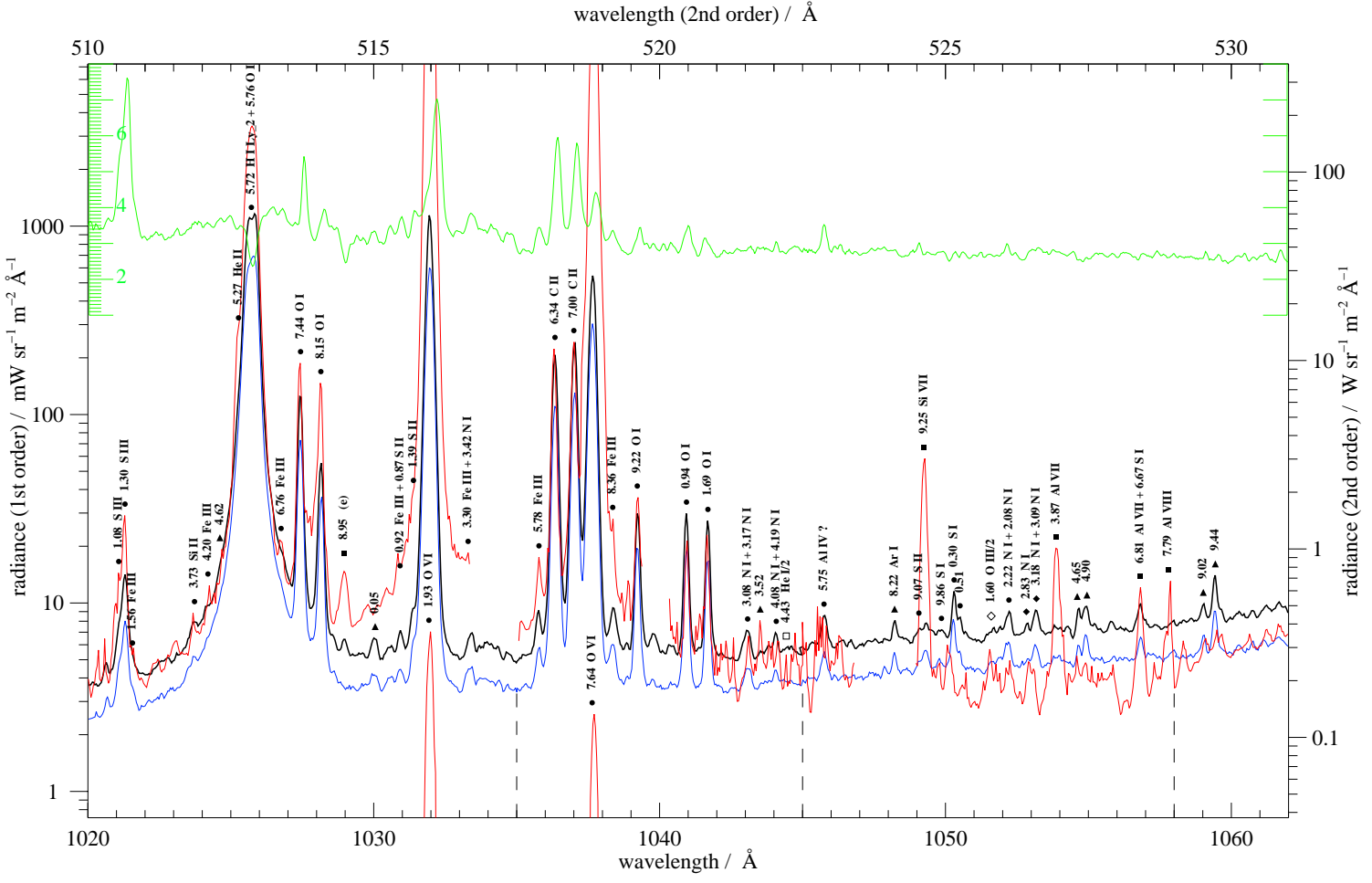
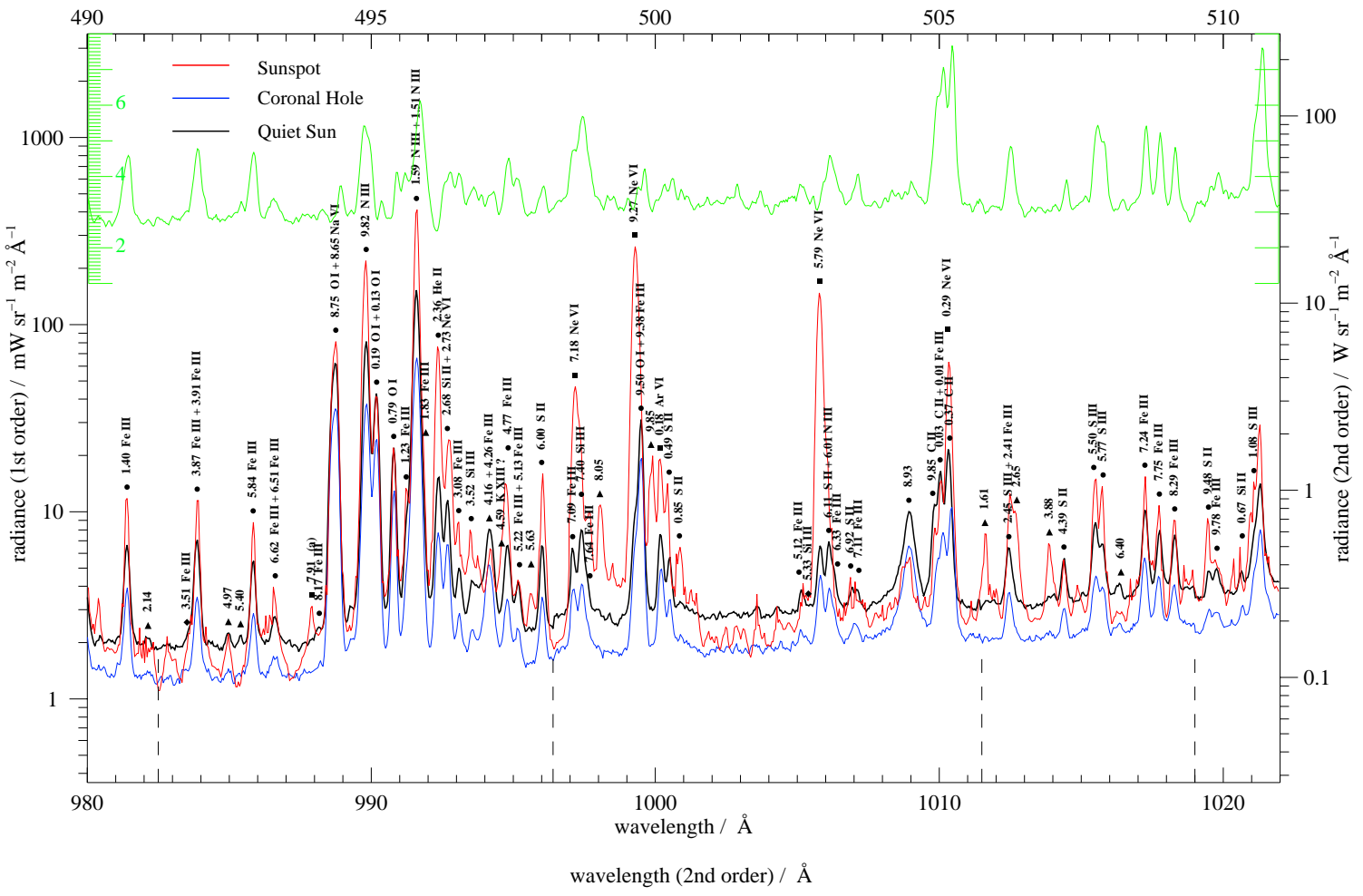
Fig. 4. The SUMER solar-disk spectral atlas includes profiles of the average quiet Sun (black), an equatorial coronal hole (blue), and a sunspot (red). Resolved emission lines are indicated by a mark, the measured wavelength in angstrom (\AA), and the identification, if available. The marks point to line lists available in the literature, where additional information about a specific line can be found. Squares (\square) point to Feldman et al. (1997), circles (\circ) to Curdt et al. (1997), diamonds (\diamond) to Kelly (1987), Cohen et al. (1978), or Sandlin et al. (1986). Triangles (\triangle) are new lines or identifications. Filled symbols denote lines observed in first order of diffraction, open symbols are second-order lines. Only the three least-significant digits of the wavelength values are given. If available, unidentified lines are characterized by the temperature classification of Feldman et al. (1997) (a: $T_e < 3 \cdot 10^5$; b: $T_e \approx 3 \cdot 10^5$; c: $T_e \approx 4 \cdot 10^5$; d: $6 \cdot 10^5 < T_e < 9 \cdot 10^5$; e: $T_e \approx 1.4 \cdot 10^6$; f: $T_e \approx 1.8 \cdot 10^6$). The profiles have been radiometrically calibrated assuming first order of diffraction and the radiance axis is scaled to $\text{mW sr}^{-1} \text{ m}^{-2} \text{ \AA}^{-1}$. We have taken care of the type of photocathode (bare or KBr) when applying the radiometric calibration to different sections of the spectrum. For lines observed in second order, the right vertical axis is applicable. Note, that the sensitivity ratio between both orders, which is wavelength dependent, has been chosen for (and is only correct for) the central wavelength. Also note, that second order lines are always superimposed on a first order background. We also display in green the BN/CI ratio, which is a useful parameter for electron temperature classification.

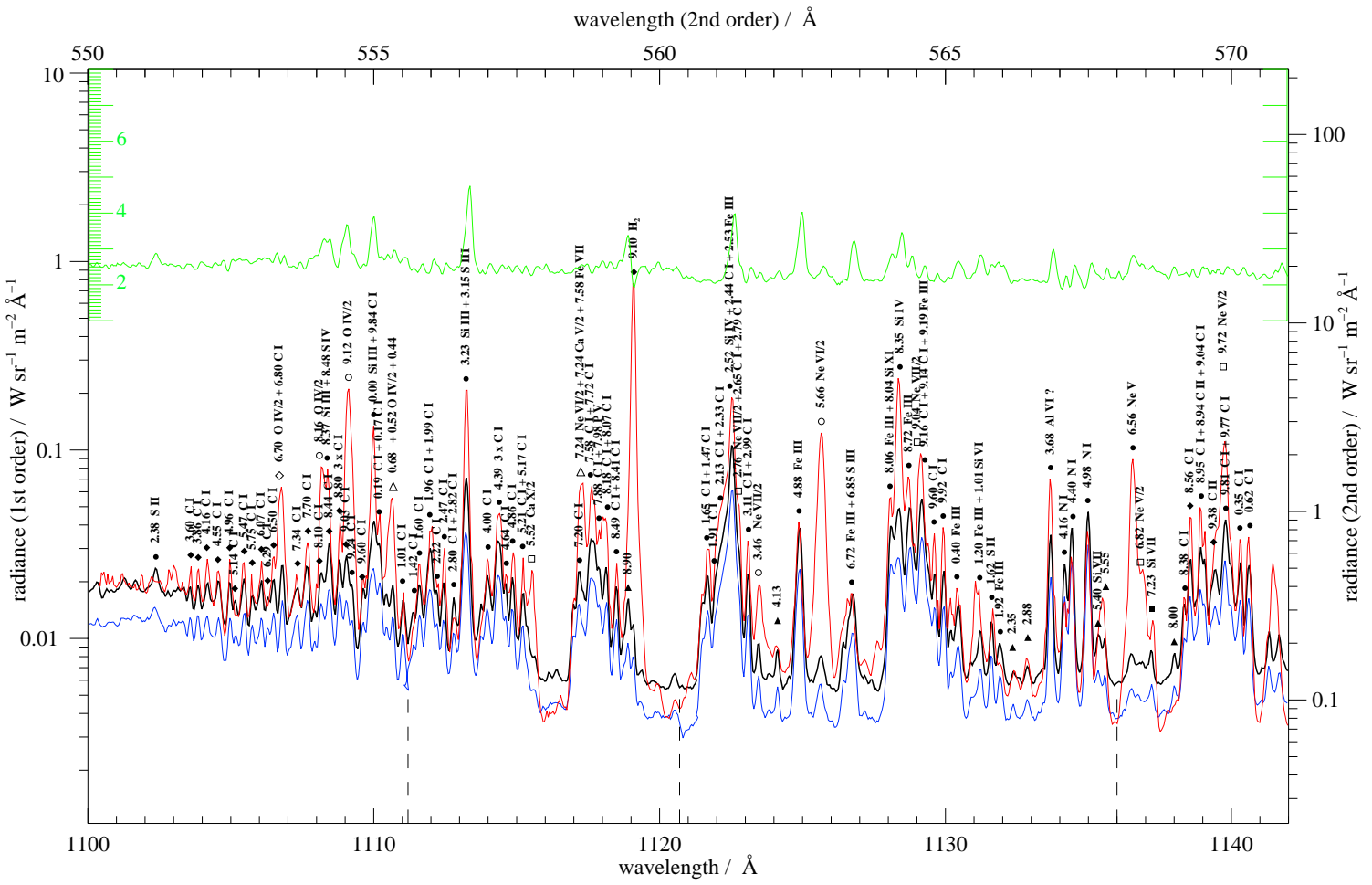
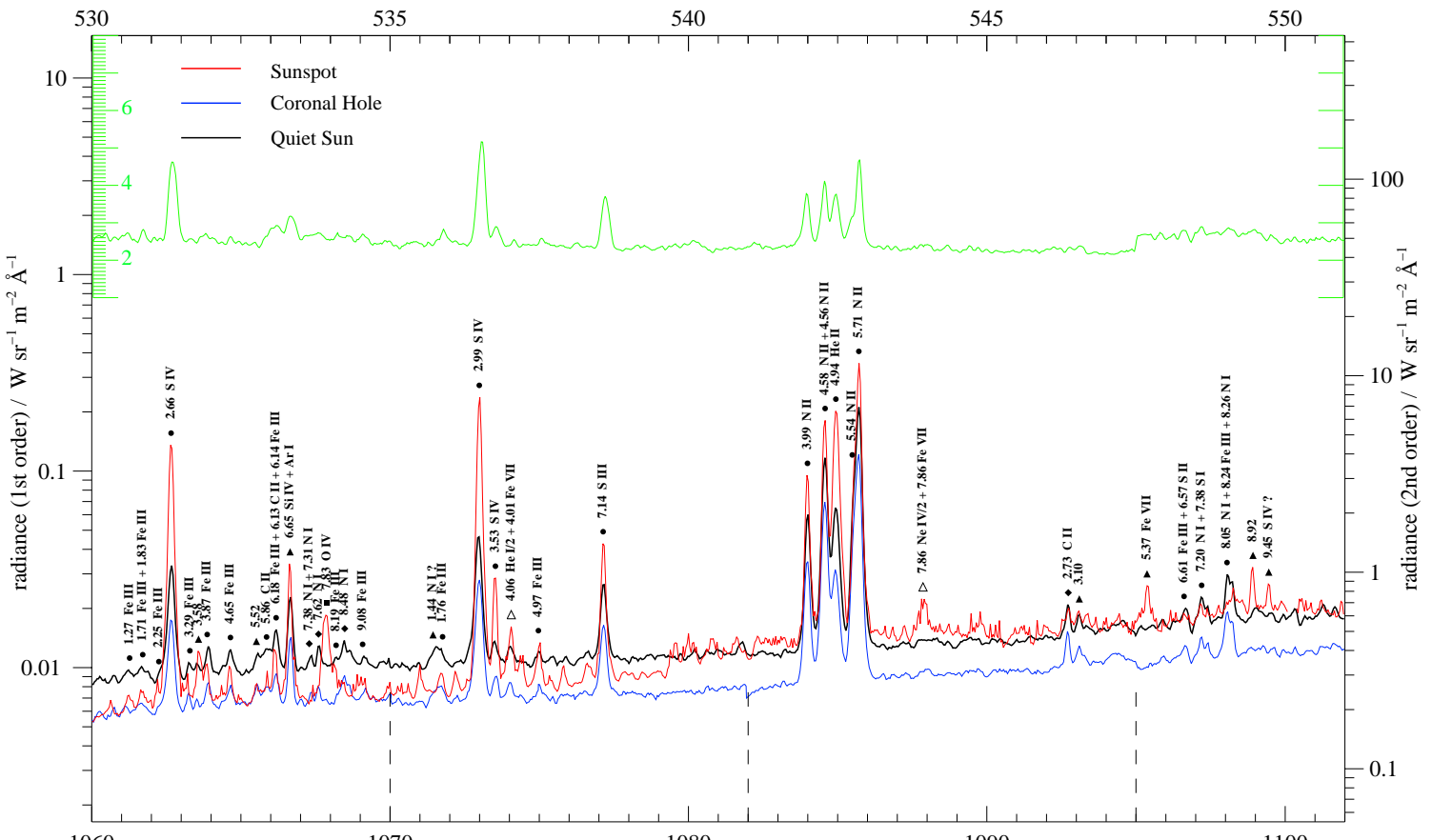


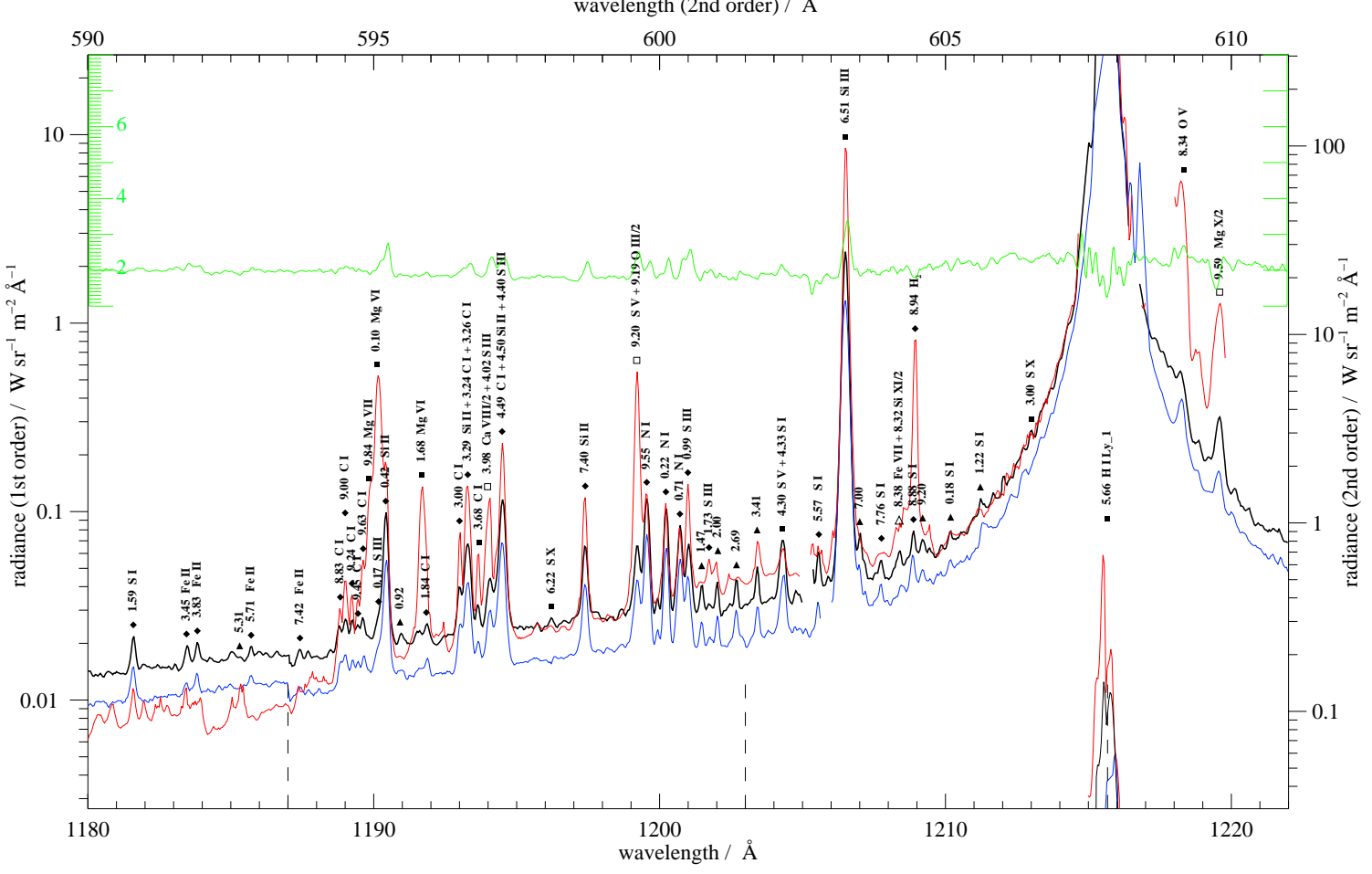
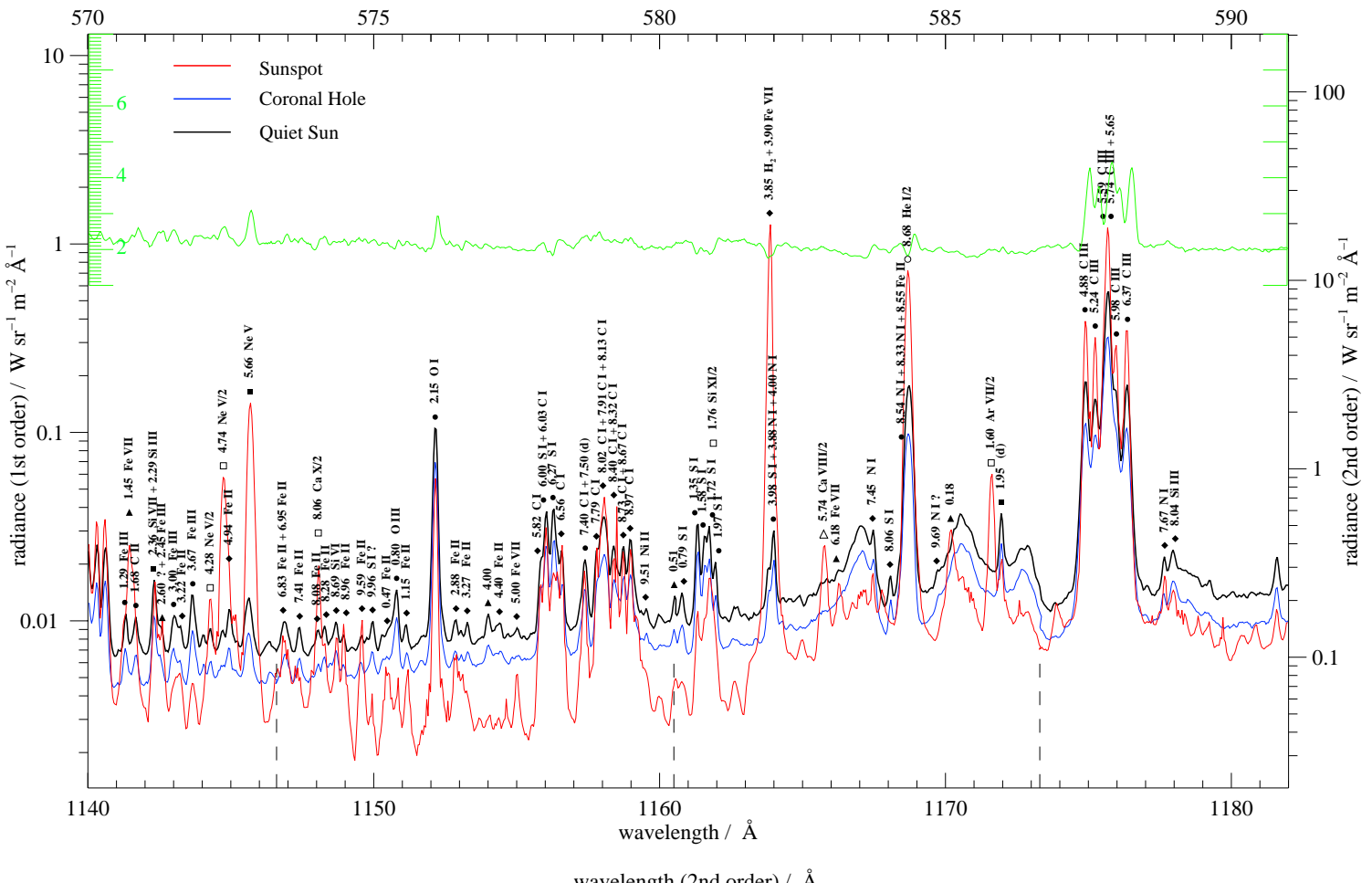


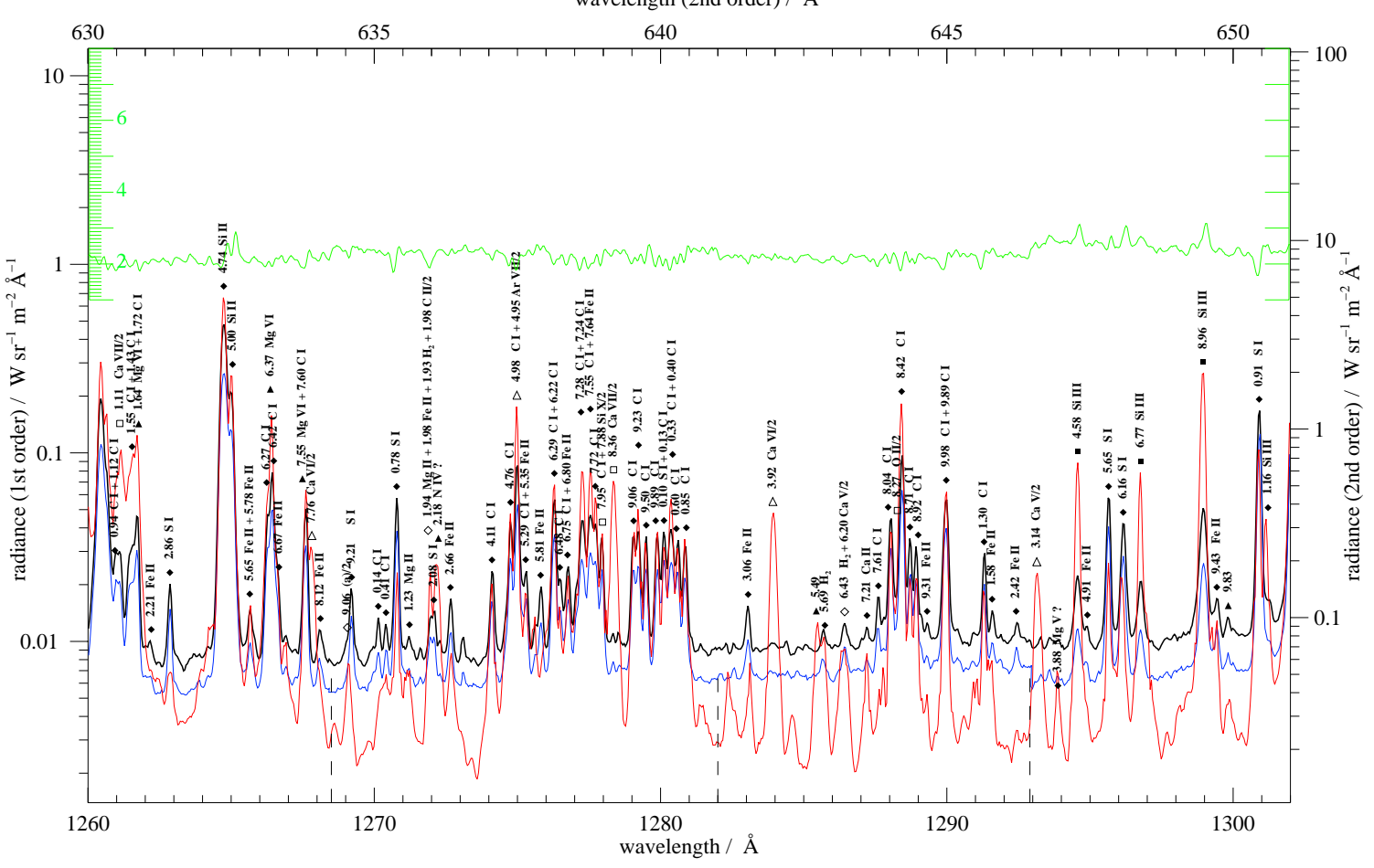
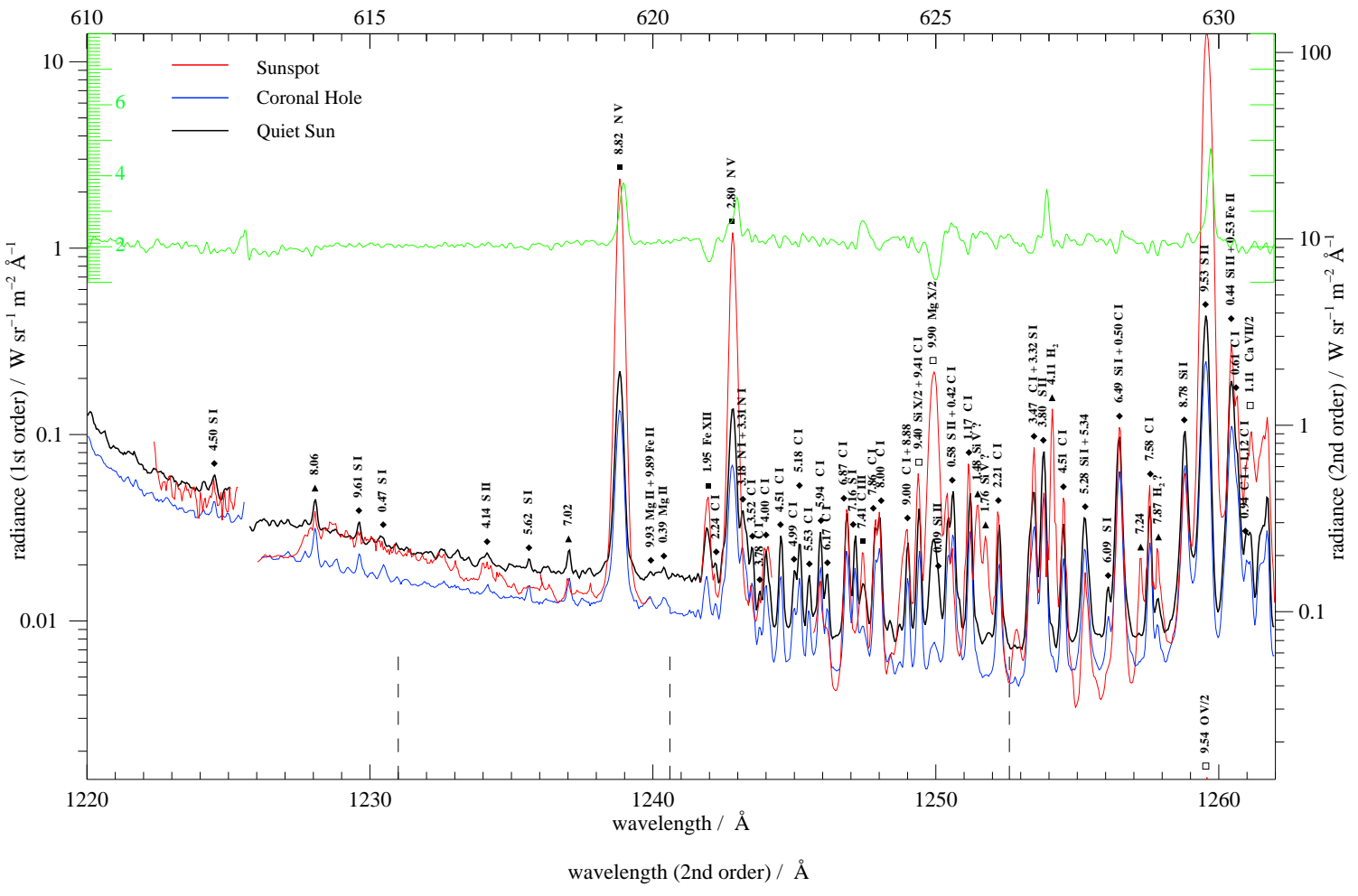


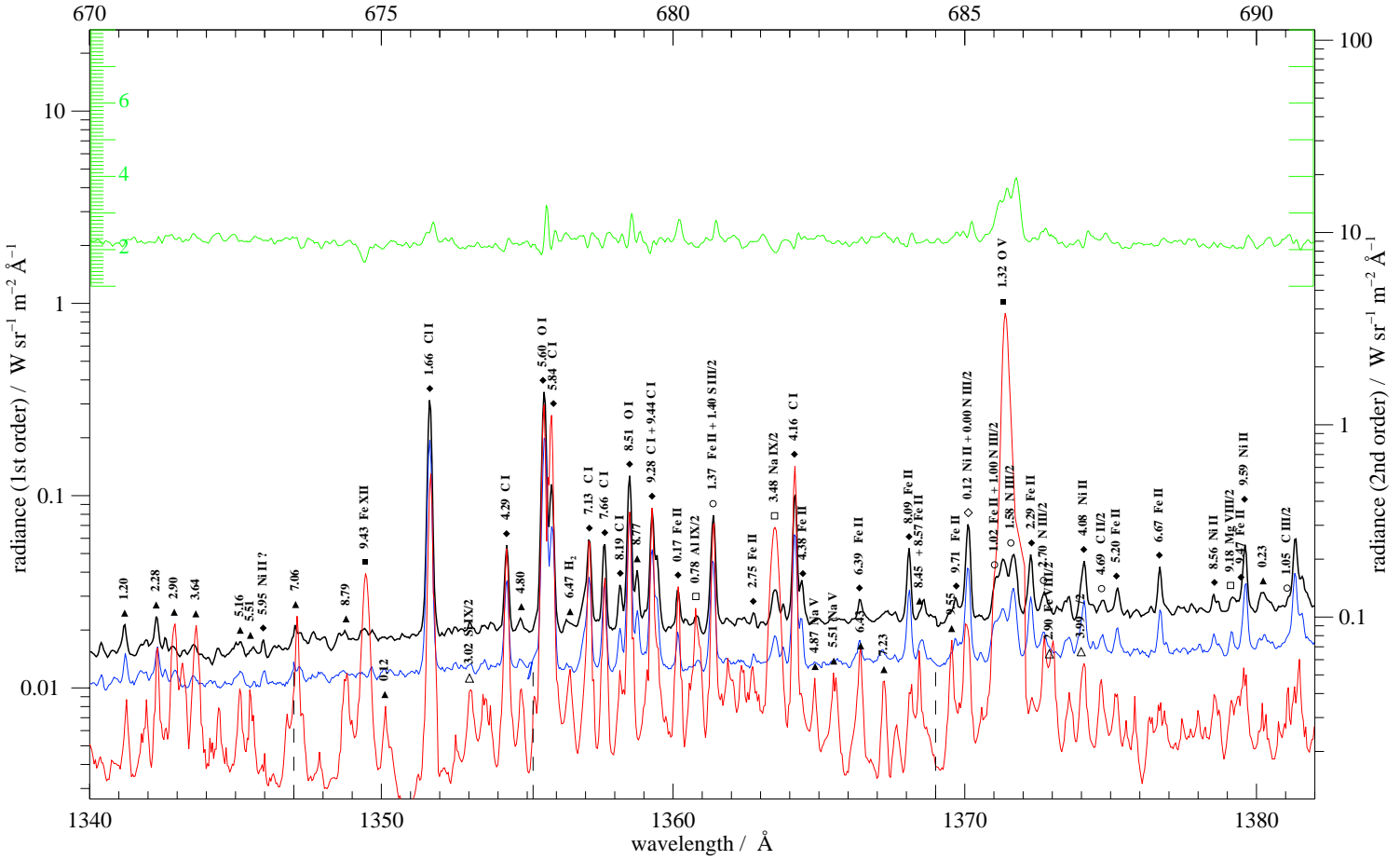
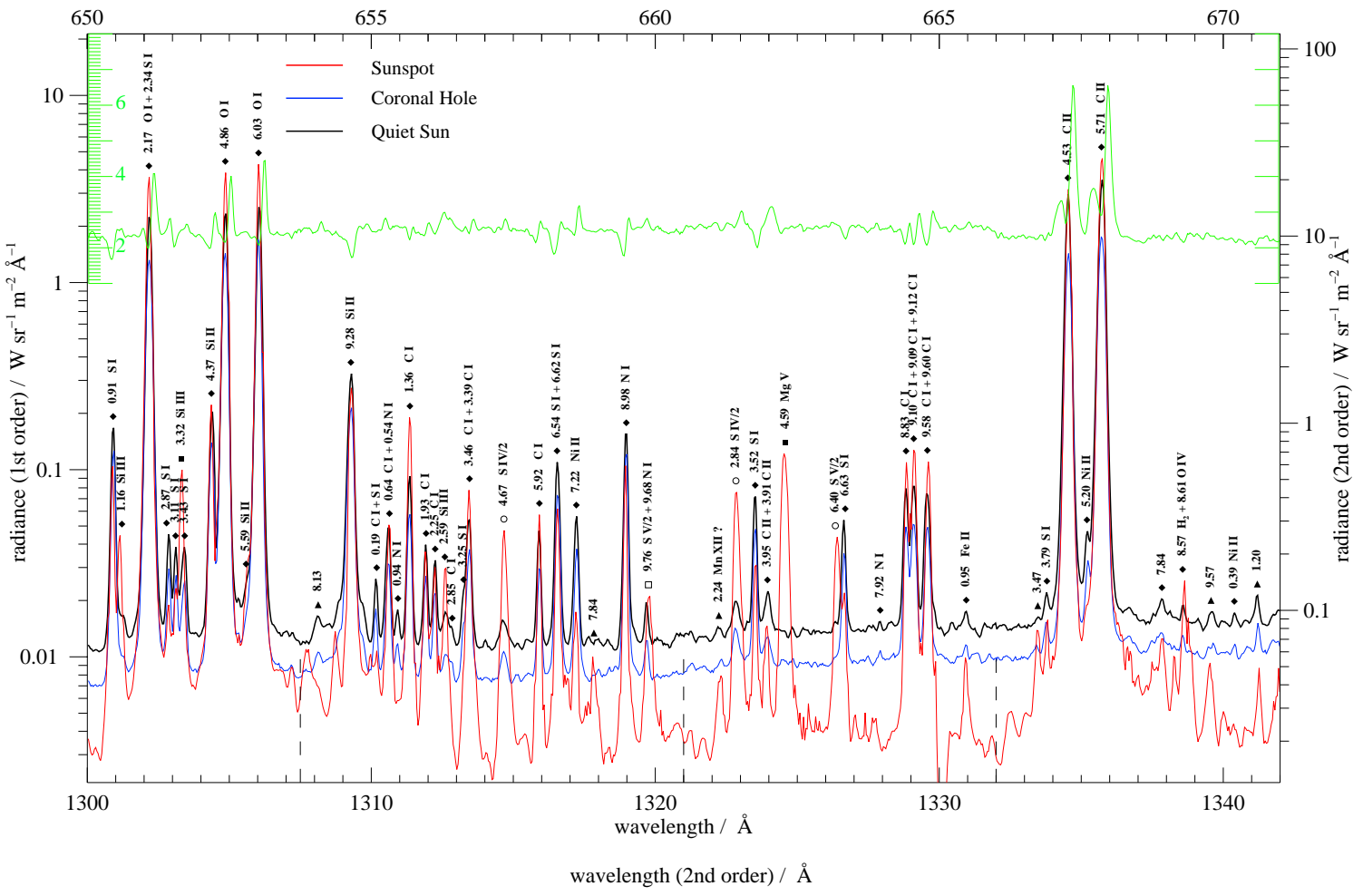


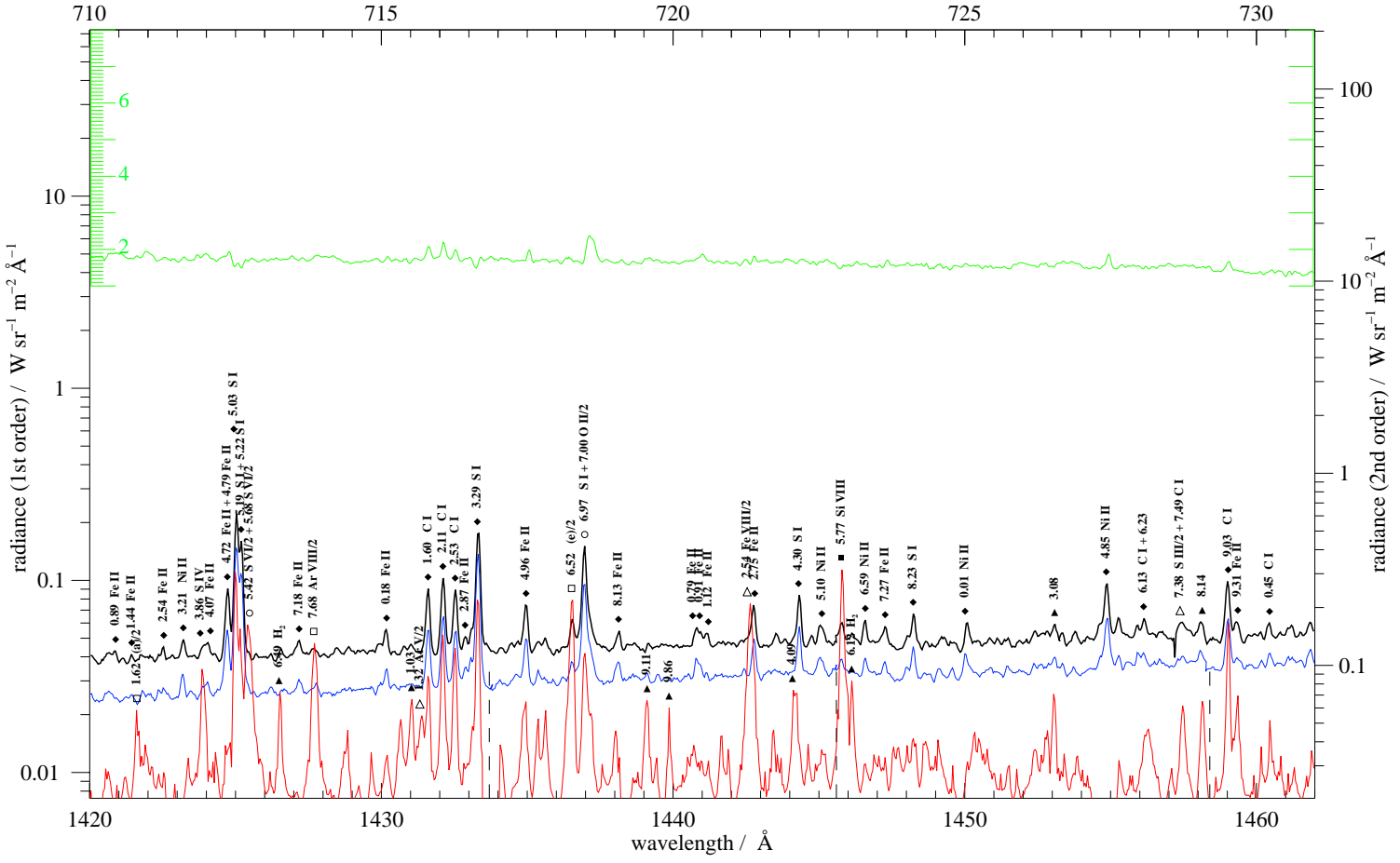
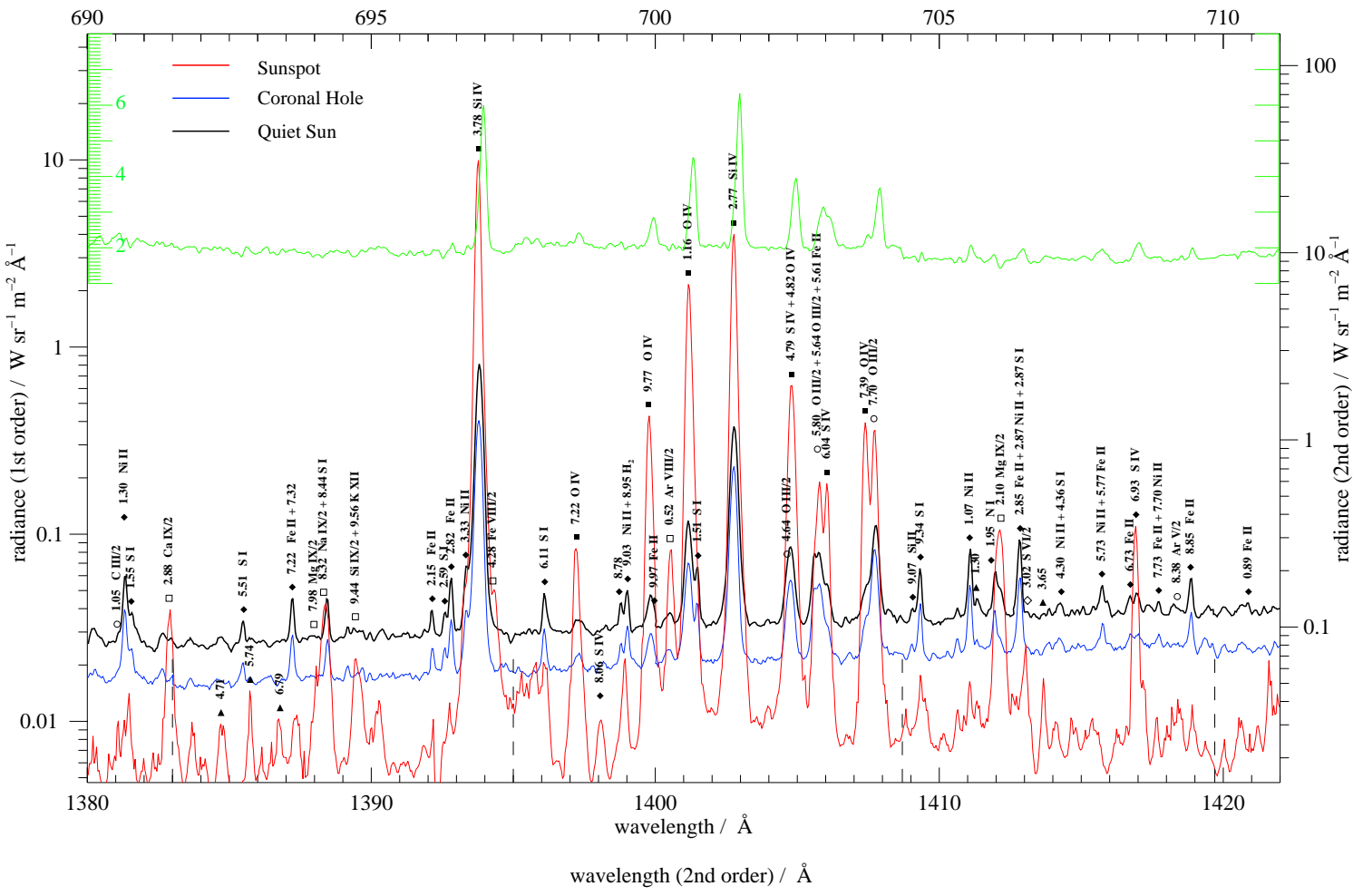


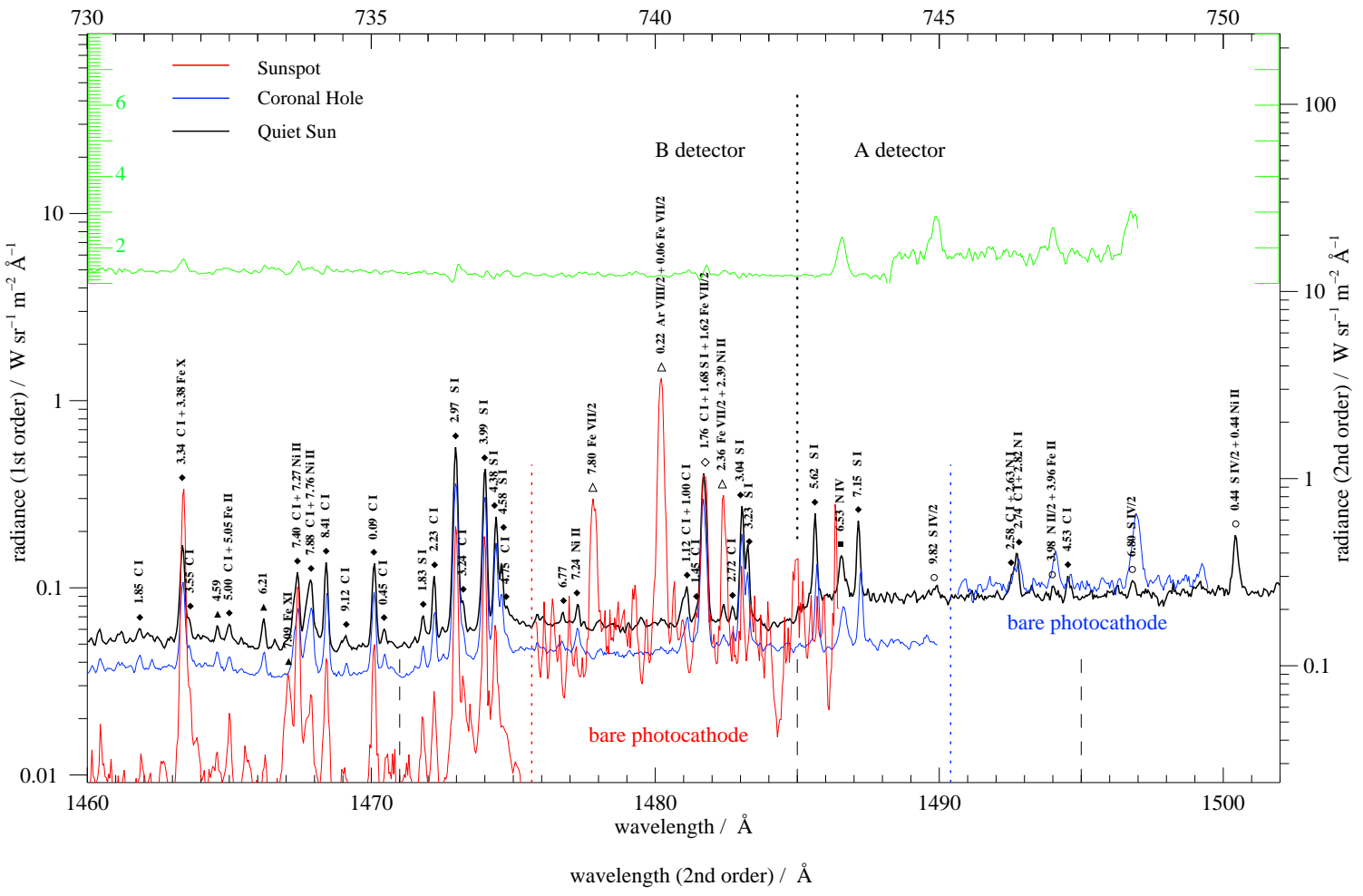












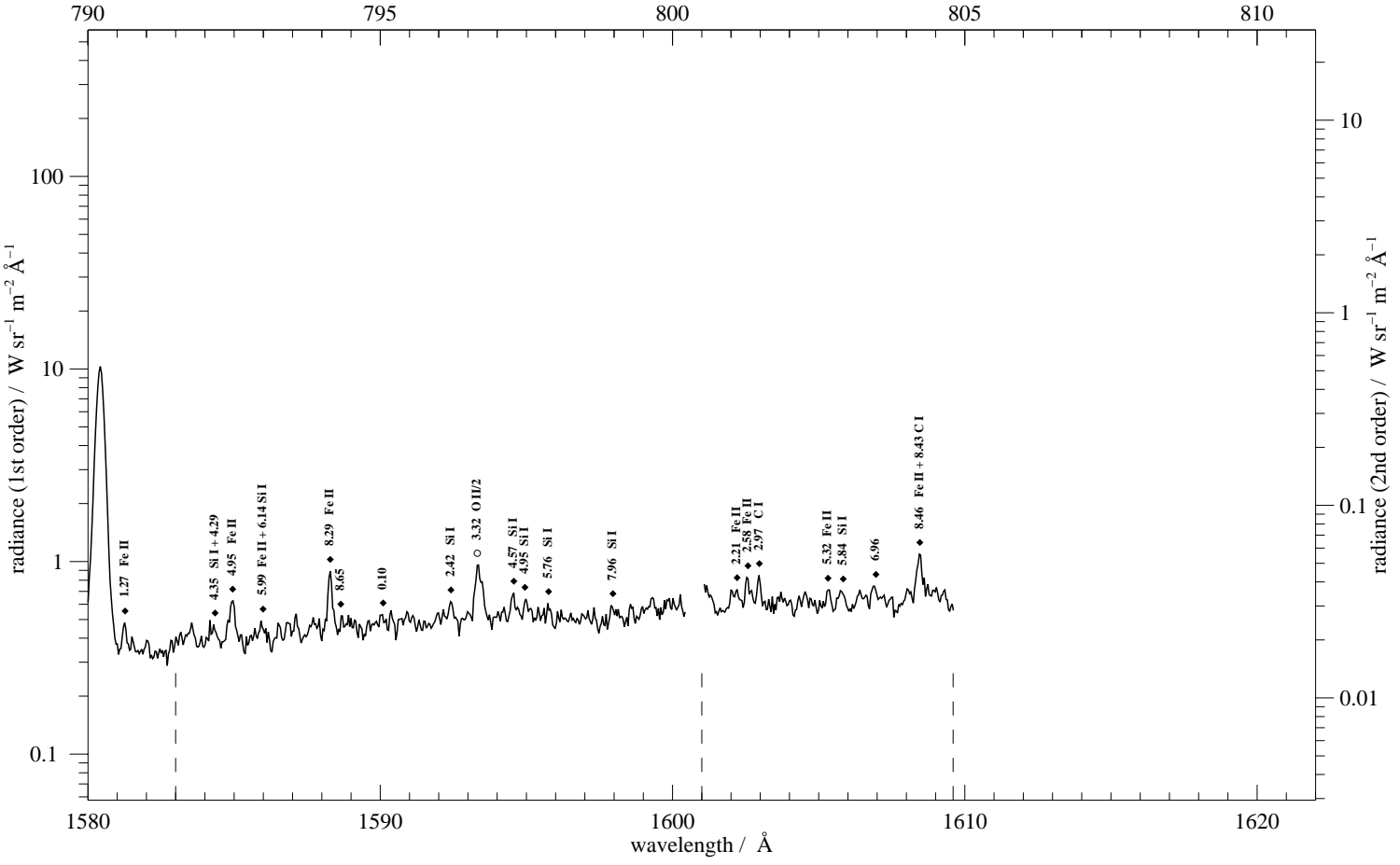
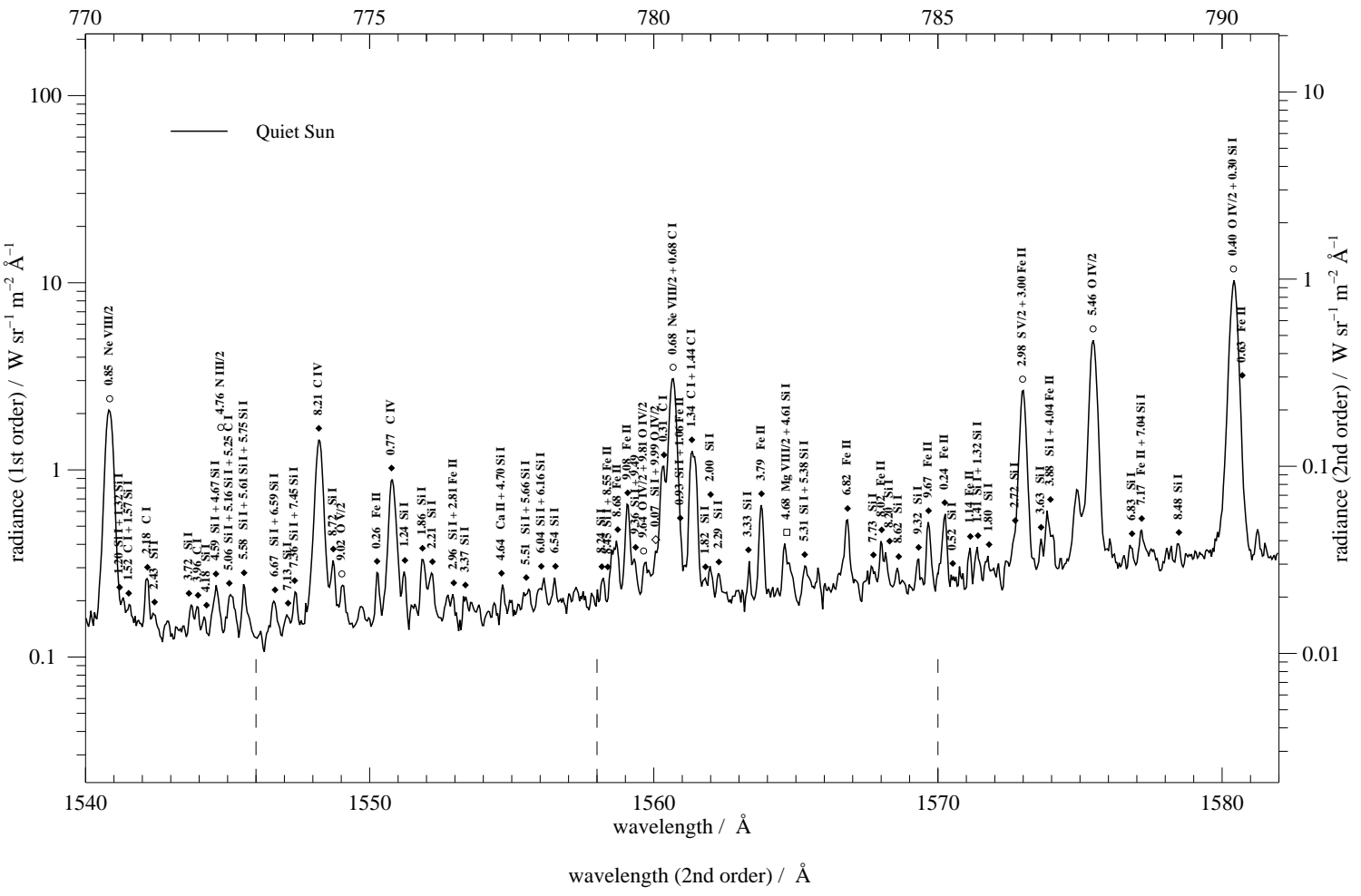


Table 1. Line List - List of spectral lines in the wavelength range from 668 Å to 1611 Å identified in SUMER spectra of the average quiet Sun (QS), a coronal hole (CH) and a sunspot on disk (SS). Spectral lines observed in second order of diffraction which are also given here, extend the lower wavelength limit to below 500 Å. For each entry we give the observed wavelengths in angström, the identification, the transition, the peak of spectral radiance, L^{peak} , in mW (sr m² Å)⁻¹ (incl. background), and a cross-reference to other line lists available in the literature (cf., Sect. 5.1). For second-order lines radiance entries are generally not provided, since the background separation in both orders of diffraction is a non-trivial task, which can not be automated. Only a few radiance values of strong second-order lines with negligible first-order contribution are given, which are marked by an asterisk (*). References in last column: (0) Curdt et al. (1997), (1) Feldman et al. (1997), (3) new line or new identification, (4) Kelly (1987) or Cohen (1978) or Sandlin (1986). This line list complements Fig.4 of the SUMER Spectral Atlas.

λ_{obs} Å	Line	Transition	L_{QS}^{peak} mW (sr m ² Å) ⁻¹	L_{CH}^{peak} mW (sr m ² Å) ⁻¹	L_{SS}^{peak} mW (sr m ² Å) ⁻¹	Ref.
668.41					1.8	3
669.00	(d)				1.0	0
670.02	Al X	$2s\ 2p\ ^1P_1 - 2p^2\ ^1D_2$			1.2	0
671.01	N II	$2s^2\ 2p^2\ ^3P_1 - 2s^2\ 2p\ 3s\ ^3P_2$	1.1		0.2	1
671.37	Cl VI	$3s^2\ ^1S_0 - 3s\ 3p\ ^1P_1$	2.5		5.5	3
671.39	N II	$2s^2\ 2p^2\ ^3P_2 - 2s^2\ 2p\ 3s\ ^3P_2$				1
671.42	N II	$2s^2\ 2p^2\ ^3P_0 - 2s^2\ 2p\ 3s\ ^3P_1$				1
671.63	N II	$2s^2\ 2p^2\ ^3P_1 - 2s^2\ 2p\ 3s\ ^3P_1$				1
671.77	N II	$2s^2\ 2p^2\ ^3P_1 - 2s^2\ 2p\ 3s\ ^3P_0$	1.1	0.2	0.3	1
672.01	N II	$2s^2\ 2p^2\ ^3P_2 - 2s^2\ 2p\ 3s\ ^3P_1$	1.0	0.2	0.7	1
672.55					1.4	3
672.97	O II	$2s^2\ 2p^3\ ^2P_{3/2} - 2s^2\ 2p^2\ 3s\ ^2P_{3/2}$	1.5	1.1	0.2	1
673.82	O II	$2s^2\ 2p^3\ ^2P_{1/2} - 2s^2\ 2p^2\ 3s\ ^2P_{1/2}$	1.1	0.8	0.4	1
674.20			0.7		1.6	3
674.41	S V ?		0.9	0.8	0.6	4
676.49	Si IX	$2s^2\ 2p^2\ ^3P_1 - 2s\ 2p^3\ ^5S_2$	2.0	1.0	5.4	0
676.81	(e)		1.5	0.5	2.6	0
677.74	S III	$3s^2\ 3p^2\ ^3P_0 - 3s^2\ 3p\ 3d\ ^3D_1$	2.0	1.3	1.2	1
678.46	S III	$3s^2\ 3p^2\ ^3P_1 - 3s^2\ 3p\ 3d\ ^3D_2$	2.7	2.0	1.5	1
679.11	S III	$3s^2\ 3p^2\ ^3P_1 - 3s^2\ 3p\ 3d\ ^3D_1$	1.6	1.1	0.9	1
679.75	Mg VIII	$2s\ 2p^2\ ^2P_{1/2} - 2p^3\ ^2D_{3/2}$	1.0	0.5	3.0	0
680.39	Al IX	$2s^2\ 2p\ ^2P_{1/2} - 2s\ 2p^2\ ^4P_{3/2}$	4.2	1.0	8.5	0
680.70	S III	$3s^2\ 3p^2\ ^3P_2 - 3s^2\ 3p\ 3d\ ^3D_3$	7.7	3.6	2.8	1
680.97	S III	$3s^2\ 3p^2\ ^3P_2 - 3s^2\ 3p\ 3d\ ^3D_2$	4.4	2.2	1.4	1
681.51	S III	$3s^2\ 3p^2\ ^3P_0 - 3s^2\ 3p\ 4s\ ^3P_1$	3.5	2.0	6.7	1
681.68	Na IX	$1s^2\ 2s\ ^2S_{1/2} - 1s^2\ 2p\ ^2P_{3/2}$	11	3.9	58	0

Table 1—Continued

λ_{obs}	Line	Transition	L_{QS}^{peak}	L_{CH}^{peak}	L_{SS}^{peak}	Ref.
Å			mW	(sr m ² Å) ⁻¹		
683.05	S III	$3s^2 3p^2 {}^3P_1 - 3s^2 3p {}^4s {}^3P_0$	1.7	1.1	0.6	1
683.53	S III	$3s^2 3p^2 {}^3P_2 - 3s^2 3p {}^4s {}^3P_2$	5.7	3.7	1.6	1
684.04	(c)		1.8	1.1	2.0	0
684.71			2.1	1.3	0.7	1
684.99	N III	$2s^2 2p {}^2P_{1/2} - 2s 2p^2 {}^2P_{3/2}$	12	7.9	4.4	1
685.50	N III	$2s^2 2p {}^2P_{1/2} - 2s 2p^2 {}^2P_{1/2}$	23	15	8.9	1
685.79	N III	$2s^2 2p {}^2P_{3/2} - 2s 2p^2 {}^2P_{3/2}$	54	37	20	1
[686.33	N III	$2s^2 2p {}^2P_{3/2} - 2s 2p^2 {}^2P_{1/2}$	12	8.4	9.7	1
686.43	Fe VIII	$3p^5 3d^2 {}^2P_{3/2} - 3p^6 4d {}^2D_{5/2}$			5	
686.77			1.7	1.0	1	
687.05	C II	$2s^2 2p {}^2P_{1/2} - 2s^2 3d {}^2D_{3/2}$	7.6	5.7	2.1	1
687.35	C II	$2s^2 2p {}^2P_{3/2} - 2s^2 3d {}^2D_{5/2}$	13	8.5	2.8	1
688.68	Fe VIII	$3p^5 3d^2 {}^2P_{3/2} - 3p^6 4d {}^2D_{3/2}$			5	
688.99			2.0	1.4	0.8	1
689.61	Mg VIII	$2s 2p^2 {}^2P_{3/2} - 2p^3 {}^2D_{5/2}$	2.2	1.3	4.8	0
690.09			2.0	1.4	1.0	1
690.53	C III	$2s 2p {}^1P_1 - 2s 3s {}^1S_0$	8.8	6.0	1.4	1
691.21	N III	$2s 2p^2 {}^2D_{5/2} - 2s^2 3p {}^2P_{3/2}$	2.5	1.6	2.9	1
691.40	N III	$2s 2p^2 {}^2D_{3/2} - 2s^2 3p {}^2P_{1/2}$	3.9	2.8	29	1
691.40	Ca IX	$3s^2 {}^1S_0 - 3s 3p {}^3P_1$	3.9	2.8	29	0
693.33	Fe VIII ?	$3p^6 4p {}^2P_{1/2} - 3p^6 4d {}^2D_{3/2}$	1.8	1.2	1.6	0
693.98	Mg IX	$2s^2 {}^1S_0 - 2s 2p {}^3P_2$	4.3	1.9	28	0
694.13	Na IX	$1s^2 2s {}^2S_{1/2} - 1s^2 2p {}^2P_{1/2}$	8.0	3.6	28	0
694.70	Si IX	$2s^2 2p^2 {}^3P_2 - 2s 2p^3 {}^5S_2$	7.9	2.7	18	0
695.06	(c)		2.5	1.5	3.7	0
696.61	S V	$3s 3p {}^1P_1 - 3s 3d {}^1D_2$	5.0	3.1	9.7	1
697.14	Fe VIII	$3p^6 4p {}^2P_{1/2} - 3p^6 4d {}^2D_{3/2}$	3.1	25	5	
698.71	S III	$3s^2 3p^2 {}^3P_0 - 3s^2 3p 3d {}^3P_1$	2.9	1.8	0.9	1
700.11	S III	$3s^2 3p^2 {}^3P_1 - 3s^2 3p 3d {}^3P_2$	6.0	9.7	17	1
[700.22	Ar VIII	$2p^6 3s {}^2S_{1/2} - 2p^6 3p {}^2P_{3/2}$	13	9.7	51	0
700.29	S III	$3s^2 3p^2 {}^3P_1 - 3s^2 3p 3d {}^3P_0$			1	
702.33	O III	$2s^2 2p^2 {}^3P_0 - 2s 2p^3 {}^3P_1$	35	24	23	1
[702.82	O III	$2s^2 2p^2 {}^3P_1 - 2s 2p^3 {}^3P_0$			1	
[702.89	O III	$2s^2 2p^2 {}^3P_1 - 2s 2p^3 {}^3P_2$	92	63	64	1
703.87	O III	$2s^2 2p^2 {}^3P_2 - 2s 2p^3 {}^3P_2$	154	101	108	1
706.02	Mg IX	$1s^2 2s^2 {}^1S_0 - 1s^2 2s 2p {}^3P_1$	27	10	87	0
706.50	S VI	$2p^6 3p {}^2P_{1/2} - 2p^6 3d {}^2D_{3/2}$	3.7	2.5	13	1

Table 1—Continued

λ_{obs} Å	Line	Transition	L_{QS}^{peak} mW	L_{CH}^{peak} (sr m ² Å) ⁻¹	L_{SS}^{peak} (sr m ² Å) ⁻¹	Ref.
707.72	(c)		1.9	1.4	1.4	0
708.44	(c)		2.2	1.3	1.3	0
709.21	Ar V	$3s^2 3p^2 {}^3P_1 - 3s 3p^3 {}^3P_2$	2.2	1.5	2.0	1
710.78	(a)		2.6	1.5	5.2	5
710.94	S III ?		6.5	3.5	2.3	1
712.68	S VI	$2p^6 3p {}^2P_{3/2} - 2p^6 3d {}^2D_{5/2,3/2}$	5.1	3.2	21	1
713.80	Ar VIII	$2p^6 3s {}^2S_{1/2} - 2p^6 3p {}^2P_{1/2}$	6.9	4.8	24	1
714.79			2.4	1.4	1.2	3
715.61	Ar V	$3s^2 3p^2 {}^3P_2 - 3s 3p^3 {}^3P_{1,2}$	2.7	1.7	4.9	1
717.00	S V ?		2.7	1.4	2.6	3
717.69	Fe VIII ?	$3p^6 4p {}^2P_{3/2} - 3p^6 4d {}^2D_{5/2}$	2.6	1.5	2.1	0
718.23	(e)		3.7	2.0	4.1	0
718.49	O II	$2s^2 2p^3 {}^2D_{5/2} - 2s 2p^4 {}^2D_{5/2}$	47	29	7.9	1
	O II	$2s^2 2p^3 {}^2D_{3/2} - 2s 2p^4 {}^2D_{5/2}$				1
719.35	S IX	$2s^2 2p^3 3p {}^3F_4 - 2s^2 2p^3 3d {}^3G_5$	2.4	1.4	1.4	0
720.11			2.6	1.5	0.8	1
721.23	Fe VIII	$3p^6 4p {}^2P_{1/2} - 3p^6 4d {}^2D_{3/2}$	3.2	44	5	
721.68	S II	$3s^2 3p^3 {}^2D_{5/2} - 3s^2 3p^2 4d {}^4F_{7/2}$	3.6	2.1	1.1	1
723.75	Fe VIII	$3p^6 4p {}^2P_{3/2} - 3p^6 4d {}^2D_{3/2}$			2.9	5
724.26	S III	$3s^2 3p^2 {}^3P_0 - 3s 3p^3 {}^3S_1$	3.0	2.0	2.2	1
725.11	Ar V	$3s^2 3p^2 {}^1D_2 - 3s 3p^3 {}^1D_2$	3.0	2.0	3.5	1
725.86	S III	$3s^2 3p^2 {}^3P_1 - 3s 3p^3 {}^3S_1$	4.1	2.6	1.4	1
	(c)					1
725.87	(c)					
728.10	Fe VII	$3d 4p {}^3D_2 - 3d 4d {}^3F_3$			2.5	5
728.70	S III	$3s^2 3p^2 {}^3P_2 - 3s 3p^3 {}^3S_1$	5.2	3.4	2.0	1
729.54	S III	$3s^2 3p^2 {}^1D_2 - 3s^2 3p 4s {}^1P_1$	3.7	2.4	1.1	1
735.24	(c)		3.4	2.4	1.2	0
735.42	Fe VII	$3d 4p {}^3P_1 - 3d 4d {}^3P_2$			1.7	5
735.86	Ne I	$2p^6 {}^1S_0 - 2p^5 3s {}^1P_1$	4.8	3.2	2.5	1
736.71					3.4	3
738.87	Fe VII	$3d 4p {}^3P_2 - 3d 4d {}^3P_2$			5.0	5
740.03	Fe VII	$3d 4p {}^1F_3 - 3d 4d {}^1G_4$				5
	Ar VIII	$2p^6 4d {}^2D_{5/2} - 2p^6 5p {}^2P_{3/2}$	3.5	2.5	16	3
740.79	Fe VII	$3d 4p {}^3D_3 - 3d 4d {}^3F_4$			4.6	5
741.14	Fe VII	$3d 4p {}^3P_1 - 3d 4d {}^3P_0$			4.6	5
743.71	Ne I	$2p^6 {}^1S_0 - 2p^5 3s {}^3P_1$	5.9	4.0	11	1
744.91	S IV	$3s^2 3p {}^2P_{1/2} - 3s 3p^2 {}^2P_{3/2}$	8.6	5.6	13	1

Table 1—Continued

λ_{obs} Å	Line	Transition	L_{QS}^{peak} mW	L_{CH}^{peak} (sr m ² Å) ⁻¹	L_{SS}^{peak}	Ref.
745.38	Fe VII	$3d4p\ ^3F_2 - 3d4d\ ^3F_2$			5.8	5
745.55					5.3	3
745.84	N II	$2s^2 2p^2\ ^1S_0 - 2s2p^3\ ^1P_1$	4.2	2.7	3.2	1
746.65					3.5	3
746.99	N II	$2s^2 2p^2\ ^1D_2 - 2s^2 2p\ 3s\ ^1P_1$	6.8	4.2	2.5	1
747.37					5.3	3
748.40	S IV	$3s^2 3p\ ^2P_{1/2} - 3s3p^2\ ^2P_{1/2}$	13	8.4	32	1
749.01	Fe VII	$3d4p\ ^3F_3 - 3d4d\ ^3F_3$			8.1	5
749.54	Mg IX	$1s^2 2s\ 2p\ ^1P_1 - 1s^2 2p^2\ ^1D_2$	7.6	3.5	38	0
750.22	S IV	$3s^2 3p\ ^2P_{3/2} - 3s3p^2\ ^2P_{3/2}$	27	18	73	1
750.58	(a)				6.7	0
751.46	(a)				5.7	0
752.51	Fe VIII	$3p^5 3d^2\ ^2P_{1/2} - 3p^6 4d\ ^2D_{3/2}$			5	
753.22					9.0	3
753.74	S IV	$3s^2 3p\ ^2P_{3/2} - 3s3p^2\ ^2P_{1/2}$	8.3	5.3	14	1
754.93	Ar VI	$3s^2 3p\ ^2P_{1/2} - 3s3p^2\ ^2D_{3/2}$	4.7	2.8	27	0
756.70	Al VIII ?	$2s^2 2p^2\ ^3P_1 - 2s2p^3\ ^5S_2$	4.1	2.8	5.3	0
757.15	Fe VII	$3d4p\ ^3F_4 - 3d4d\ ^3F_4$			15	5
758.68	O V	$2s2p\ ^3P_1 - 2p^2\ ^3P_2$	21	16	603	1
759.34	S IV					1
759.43	O V	$2s2p\ ^3P_0 - 2p^2\ ^3P_1$	18	12	474	1
760.21	O V	$2s2p\ ^3P_1 - 2p^2\ ^3P_1$	19	11	362	1
760.43	O V	$2s2p\ ^3P_2 - 2p^2\ ^3P_2$	59	41	1865	1
761.13	O V	$2s2p\ ^3P_1 - 2p^2\ ^3P_0$	6.2	3.9	89	1
761.99	O V	$2s2p\ ^3P_2 - 2p^2\ ^3P_1$	21	15	547	1
762.65	Mg VIII	$2s^2 2p\ ^2P_{1/2} - 2s2p^2\ ^4P_{3/2}$	5.2	3.3	12	0
763.33	N III	$2s^2 2p\ ^2P_{1/2} - 2s2p^2\ ^2S_{1/2}$	14	9.6	14	1
764.36	N III	$2s^2 2p\ ^2P_{3/2} - 2s2p^2\ ^2S_{1/2}$	25	16	22	1
765.15	N IV	$2s^2\ ^1S_0 - 2s2p\ ^1P_1$	247	157	970	1
767.07	Ar VI	$3s^2 3p\ ^2P_{3/2} - 3s3p^2\ ^2D_{5/2}$	6.5	4.4	45	0
769.38	Mg VIII	$2s^2 2p\ ^2P_{1/2} - 2s2p^2\ ^4P_{1/2}$	6.6	4.3	25	0
770.42	Ne VIII	$1s^2 2s\ ^2S_{1/2} - 1s^2 2p\ ^2P_{3/2}$	241	174	1950	1
771.90	N III	$2s2p^2\ ^4P_{3/2} - 2p^3\ ^4S_{3/2}$	6.8	4.4	14	1
772.31	Mg VIII	$2s^2 2p\ ^2P_{3/2} - 2s2p^2\ ^4P_{5/2}$	13	9.3	190	0
772.34	N III	$2s2p^2\ ^4P_{5/2} - 2p^3\ ^4S_{3/2}$	13	9.3	190	1
772.54	Al VIII	$2s^2 2p^2\ ^3P_2 - 2s2p^3\ ^5S_2$	6.6	4.1	32	0
772.89	N III	$2s2p^2\ ^2D_{5/2} - 2p^3\ ^2P_{3/2}$	6.2	3.8	7.3	1

Table 1—Continued

λ_{obs}	Line	Transition	L_{QS}^{peak}	L_{CH}^{peak}	L_{SS}^{peak}	Ref.
Å			mW	(sr m ² Å) ⁻¹		
774.51	O V	$2s\ 2p\ ^1P_1 - 2p^2\ ^1S_0$	10	6.8	120	1
775.35			7.7	5.0	7.9	1
775.95	N II	$2s^2\ 2p^2\ ^1D_2 - 2s\ 2p^3\ ^1D_2$	11	7.5	7.9	1
776.23	S X	$2s^2\ 2p^3\ ^4S_{3/2} - 2s^2\ 2p^3\ ^2P_{3/2}$	7.6	3.7	14	0
776.62	(b)				16	0
777.94			7.1	5.1	7.6	3
[779.73]	O IV	$2s\ 2p^2\ ^2D_{5/2} - 2p^3\ ^2D_{3/2}$				1
[779.82]	O IV	$2s\ 2p^2\ ^2D_{3/2} - 2p^3\ ^2D_{3/2}$	11	7.6	75	1
779.91	O IV	$2s\ 2p^2\ ^2D_{5/2} - 2p^3\ ^2D_{5/2}$	11	7.4	75	1
780.00	O IV	$2s\ 2p^2\ ^2D_{3/2} - 2p^3\ ^2D_{5/2}$				1
780.30	Ne VIII	$1s^2\ 2s\ ^2S_{1/2} - 1s^2\ 2p\ ^2P_{1/2}$	127	90	982	1
782.34	Mg VIII	$2s^2\ 2p\ ^2P_{3/2} - 2s\ 2p^2\ ^4P_{3/2}$	10	6.8	81	0
783.01	S XI	$2s^2\ 2p^2\ ^3P_1 - 2s^2\ 2p^2\ ^1S_0$	7.1	4.4	8.8	0
784.52	Fe VII	$3d\ 4p\ ^3F_1 - 3d\ 4d\ ^3S_1$			10	3
784.81	Mn VII	$3p^6\ 4p\ ^2P_{1/2} - 3p^6\ 4d\ ^2D_{3/2}$			11	5
786.47	S V	$3s^2\ ^1S_0 - 3s\ 3p\ ^1P_1$	92	64	895	1
787.72	O IV	$2s^2\ 2p\ ^2P_{1/2} - 2s\ 2p^2\ ^2D_{3/2}$	164	105	1676	1
789.43	Mg VIII	$2s^2\ 2p\ ^2P_{3/2} - 2s\ 2p^2\ ^4P_{1/2}$	8.3	5.9	28	0
789.78	Na VIII	$2s^2\ ^1S_0 - 2s\ 2p\ ^3P_1$	9.0	6.5	35	0
[790.11]	O IV	$2s^2\ 2p\ ^2P_{3/2} - 2s\ 2p^2\ ^2D_{3/2}$				1
[790.19]	O IV	$2s^2\ 2p\ ^2P_{3/2} - 2s\ 2p^2\ ^2D_{5/2}$	305	215	3623	1
792.77	Fe VII	$3d\ 4p\ ^3F_2 - 3d\ 4d\ ^3G_3$			20	5
795.23	(a)				10	0
796.66	O II	$2s^2\ 2p^3\ ^2P_{3/2} - 2s\ 2p^4\ ^2D_{5/2}$	15	9.0	12	1
799.11	Fe VII	$3d\ 4p\ ^3D_3 - 3d\ 4d\ ^3D_3$			12	5
799.66	C II	$2s\ 2p^2\ ^2D_{5/2} - 2s\ 2p\ 3d\ ^2F_{7/2}$	10	6.4	10	3
799.94	C II	$2s\ 2p^2\ ^2D_{3/2} - 2s\ 2p\ 3d\ ^2F_{5/2}$	9.9	6.2	11	3
800.69	Cl VII	$2p^6\ 3s\ ^2S_{1/2} - 2p^6\ 3p\ ^2P_{3/2}$			20	0
801.69	Fe VII	$3d\ 4p\ ^3F_3 - 3d\ 4d\ ^3G_3$			25	5
803.46	(e)				18	0
[804.14]	S X	$2s^2\ 3s\ ^4D_{7/2} - 2p^2\ 3p\ ^4F_{9/2}$				5
[804.16]	Fe VII	$3d\ 4p\ ^3F_4 - 3d\ 4d\ ^3G_5$			47	5
806.31	C II	$2s\ 2p^2\ ^4P_{3/2} - 2s\ 2p\ 3s\ ^4P_{5/2}$	10	6.5	8.1	1
[806.53]	C II	$2s\ 2p^2\ ^4P_{1/2} - 2s\ 2p\ 3s\ ^4P_{3/2}$				1
[806.57]	C II	$2s\ 2p^2\ ^4P_{5/2} - 2s\ 2p\ 3s\ ^4P_{5/2}$	12	8.6	11	1
[806.68]	C II	$2s\ 2p^2\ ^4P_{3/2} - 2s\ 2p\ 3s\ ^4P_{3/2}$				1
[806.83]	C II	$2s\ 2p^2\ ^4P_{3/2} - 2s\ 2p\ 3s\ ^4P_{1/2}$	11	7.3	11	1

Table 1—Continued

λ_{obs} Å	Line	Transition	L_{QS}^{peak} mW	L_{CH}^{peak} (sr m ² Å) ⁻¹	L_{SS}^{peak}	Ref.
806.86	C II	$2s\ 2p^2\ ^4P_{5/2} - 2s\ 2p\ 3s\ ^4P_{3/2}$				1
809.66	S IV	$3s^2\ 3p\ ^2P_{1/2} - 3s\ 3p^2\ ^2S_{1/2}$	13	8.7	22	1
809.68	C II	$2s\ 2p^2\ ^2D_{5/2} - 2s\ 2p\ 3d\ ^2D_{5/2}$				1
811.55	Mn VII	$3p^6\ 4p\ ^2P_{3/2} - 3p^6\ 4d\ ^2D_{5/2}$			14	5
813.00	Cl VII	$2p^6\ 3s\ ^2S_{1/2} - 2p^6\ 3p\ ^2P_{1/2}$			16	0
813.38	Fe III	$3d^6\ ^5D_4 - 3d^5\ 4p\ ^5D_4$	12	7.5	11	4
814.24	Fe III	$3d^6\ ^5D_2 - 3d^5\ 4p\ ^5P_1$	12	7.0	12	4
815.05	Si IV	$2p^6\ 3p\ ^2P_{1/2} - 2p^6\ 4s\ ^2S_{1/2}$	14	8.5	17	1
815.95	S IV	$3s^2\ 3p\ ^2P_{3/2} - 3s\ 3p^2\ ^2S_{1/2}$	18	10	33	1
816.45			13	8.6	13	3
818.15	Si IV	$2p^6\ 3p\ ^2P_{3/2} - 2p^6\ 4s\ ^2S_{1/2}$	18	11	29	1
820.89			15	9.5	16	1
821.23	Ca IX	$3s\ 3p\ ^1P_1 - 3p^2\ ^1D_2$			29	0
822.19	Ar V	$3s^2\ 3p^2\ ^3P_0 - 3s\ 3p^3\ ^3D_1$	14	9.1	17	0
822.56			18	11	18	1
823.45	Si III	$3s\ 3p\ ^1P_1 - 3s\ 4d\ ^1D_2$	16	9.8	19	4
827.06	Ar V	$3s^2\ 3p^2\ ^3P_1 - 3s\ 3p^3\ ^3D_2$	15	10	19	0
832.75	O II	$2s^2\ 2p^3\ ^4S_{3/2} - 2s\ 2p^4\ ^4P_{1/2}$	72	49	59	1
832.94	O III	$2s^2\ 2p^2\ ^3P_0 - 2s\ 2p^3\ ^3D_1$	87	55	153	1
833.32	O II	$2s^2\ 2p^3\ ^4S_{3/2} - 2s\ 2p^4\ ^4P_{3/2}$	110	69	84	1
833.74	O III	$2s^2\ 2p^2\ ^3P_1 - 2s\ 2p^3\ ^3D_2$	204	126	383	1
834.45	O II	$2s^2\ 2p^3\ ^4S_{3/2} - 2s\ 2p^4\ ^4P_{5/2}$	151	96	100	1
835.09	O III	$2s^2\ 2p^2\ ^3P_2 - 2s\ 2p^3\ ^3D_2$	89	65	127	1
835.28	O III	$2s^2\ 2p^2\ ^3P_2 - 2s\ 2p^3\ ^3D_3$	290	179	589	1
849.29	S V	$3s\ 3p\ ^3P_1 - 3p^2\ ^3P_2$	24	15	38	0
852.17	S V	$3s\ 3p\ ^3P_0 - 3p^2\ ^3P_1$	23	15	44	0
854.71	Mg VII	$2s^2\ 2p^2\ ^3P_1 - 2s\ 2p^3\ ^5S_2$	31	18	140	0
854.80	S V	$3s\ 3p\ ^3P_2 - 3p^2\ ^3P_2$			0	
856.73	(f)				45	0
857.82	S V	$3s\ 3p\ ^3P_1 - 3p^2\ ^3P_0$	28	16	40	0
858.04	C II	$2s^2\ 2p\ ^2P_{1/2} - 2s^2\ 3s\ ^2S_{1/2}$	35	20	36	1
858.53	C II	$2s^2\ 2p\ ^2P_{3/2} - 2s^2\ 3s\ ^2S_{1/2}$	43	26	40	1
859.63	Fe III	$3d^6\ ^5D_2 - 3d^5\ 4p\ ^5D_3$			1	
859.72	Fe III	$3d^6\ ^5D_4 - 3d^5\ 4p\ ^5F_5$	35	21	34	1
860.48	S V	$3s\ 3p\ ^3P_2 - 3p^2\ ^3P_2$	29	17	50	0
861.76	Fe III	$3d^6\ ^5D_1 - 3d^5\ 4p\ ^5F_2$	34	20	38	1
861.83	Fe III	$3d^6\ ^5D_3 - 3d^5\ 4p\ ^5F_4$			1	

Table 1—Continued

λ_{obs} Å	Line	Transition	L_{QS}^{peak} mW	L_{CH}^{peak} (sr m ² Å) ⁻¹	L_{SS}^{peak}	Ref.
864.03	Fe III	$3d^6 \ ^5D_2 - 3d^5 4p \ ^5F_3$	31	19	45	1
868.13	Mg VII	$2s^2 2p^2 \ ^3P_2 - 2s 2p^3 \ ^5S_2$	33	21	226	0
872.12	Na VII	$2s^2 2p \ ^2P_{3/2} - 2s 2p^2 \ ^4P_{5/2}$			59	0
873.78	(b)				52	0
877.92	Ar VII	$3s^2 \ ^1S_0 - 3s 3p \ ^3P_1$			76	0
880.33	Na VII	$2s^2 2p \ ^2P_{3/2} - 2s 2p^2 \ ^4P_{3/2}$			57	0
885.33	(b)				63	0
895.17	Ne VII	$2s^2 \ ^1S_0 - 2s 2p \ ^3P_1$	49	35	396	0
903.59	C II	$2s^2 2p \ ^2P_{1/2} - 2s 2p^2 \ ^2P_{3/2}$	74	44	80	1
[903.99	C II	$2s^2 2p \ ^2P_{1/2} - 2s 2p^2 \ ^2P_{1/2}$	82	60	83	1
904.14	C II	$2s^2 2p \ ^2P_{3/2} - 2s 2p^2 \ ^2P_{3/2}$	120	74	101	1
904.46	C II	$2s^2 2p \ ^2P_{3/2} - 2s 2p^2 \ ^2P_{1/2}$	63	39	78	1
905.02	Si VII	$2p^3 3p \ ^5P_2 - 2p^3 3d \ ^5D_{2,3}$			103	0
914.29	H I Ly 18	$1s \ ^2S_{1/2} - 19p \ ^2P_{3/2}$	43	25	73	1
914.58	H I Ly 17	$1s \ ^2S_{1/2} - 18p \ ^2P_{3/2}$	41	25	72	1
914.92	H I Ly 16	$1s \ ^2S_{1/2} - 17p \ ^2P_{3/2}$	43	24	73	1
915.33	H I Ly 15	$1s \ ^2S_{1/2} - 16p \ ^2P_{3/2}$	43	24	77	1
915.60	N II	$2s^2 2p^2 \ ^3P_0 - 2s 2p^3 \ ^3P_1$	25	16	36	1
915.82	H I Ly 14	$1s \ ^2S_{1/2} - 15p \ ^2P_{3/2}$	43	26	84	1
916.00	N II	$2s^2 2p^2 \ ^3P_1 - 2s 2p^3 \ ^3P_{0,1,2}$	48	25	69	1
916.43	H I Ly 13	$1s \ ^2S_{1/2} - 14p \ ^2P_{3/2}$	45	25	80	1
916.70	N II	$2s^2 2p^2 \ ^3P_2 - 2s 2p^3 \ ^3P_{1,2}$	49	28	66	1
917.18	H I Ly 12	$1s \ ^2S_{1/2} - 13p \ ^2P_{3/2}$	44	26	89	1
918.13	H I Ly 11	$1s \ ^2S_{1/2} - 12p \ ^2P_{3/2}$	45	24	92	1
[918.73	O I	$2s^2 2p^4 \ ^3P_0 - 2s^2 2p^3 12d \ ^3D_1$	3.9	2.4	4.2	1
918.84	Si VII	$2p^3 3p \ ^3F_4 - 2p^3 3d \ ^3G_5$			1	
919.35	H I Ly 10	$1s \ ^2S_{1/2} - 11p \ ^2P_{3/2}$	49	26	91	1
919.65	O I	$2s^2 2p^4 \ ^3P_2 - 2s^2 2p^3 10d \ ^3D_3$	10	6.4	11	1
919.91	O I	$2s^2 2p^4 \ ^3P_2 - 2s^2 2p^3 11s \ ^3S_1$	4.8	2.6	4.2	1
919.97	O I	$2s^2 2p^4 \ ^3P_0 - 2s^2 2p^3 11d \ ^3D_1$			1	
920.97	H I Ly 9	$1s \ ^2S_{1/2} - 10p \ ^2P_{3/2}$	49	31	99	1
921.58	O I	$2s^2 2p^4 \ ^3P_0 - 2s^2 2p^3 10d \ ^3D_1$	5.2	2.9	11	1
[922.01	O I	$2s^2 2p^4 \ ^1D_2 - 2s^2 2p^3 3d \ ^1F_3$	17	10	78	1
921.99	N IV	$2s 2p \ ^3P_1 - 2p^2 \ ^3P_2$			1	
922.07	O I	$2s^2 2p^4 \ ^1D_2 - 2s^2 2p^3 3d \ ^1D_2$			1	
[922.53	N IV	$2s 2p \ ^3P_0 - 2p^2 \ ^3P_1$	7.3	4.1	57	1
922.46	O I	$2s^2 2p^4 \ ^1D_2 - 2s^2 2p^3 3d \ ^1P_1$			1	

Table 1—Continued

λ_{obs} Å	Line	Transition	L_{QS}^{peak} mW	L_{CH}^{peak} (sr m ² Å) ⁻¹	L_{SS}^{peak}	Ref.
923.15	H I Ly 8	$1s^2 S_{1/2}$ – $9p^2 P_{3/2}$	64	41	230	1
923.20	O I	$2s^2 2p^4 ^3P_1$ – $2s^2 2p^3 9d ^3D_2$				1
923.22	N IV	$2s 2p ^3P_2$ – $2p^2 ^3P_2$				1
923.68	N IV	$2s 2p ^3P_1$ – $2p^2 ^3P_0$				1
923.79	O I	$2s^2 2p^4 ^3P_0$ – $2s^2 2p^3 9d ^3D_1$	5.9	3.3	39	1
924.08	S VII	$2p^5 3s ^3P_1$ – $2p^5 3p ^3D_2$	4.2	2.3	9.8	5
924.28	N IV	$2s 2p ^3P_2$ – $2p^2 ^3P_1$	7.8	4.2	76	1
924.96	O I	$2s^2 2p^4 ^3P_2$ – $2s^2 2p^3 8d ^3D_3$	10	5.9	9.1	1
925.44	O I	$2s^2 2p^4 ^3P_2$ – $2s^2 2p^3 9s ^3S_1$	4.7	2.8	3.6	1
925.82	He II	$2p^2 P_{3/2}$ – $16d ^2D_{5/2}$	5.7	3.1	14	4
926.23	H I Ly 7	$1s^2 S_{1/2}$ – $8p^2 P_{3/2}$	64	39	130	1
926.29	O I	$2s^2 2p^4 ^3P_1$ – $2s^2 2p^3 8d ^3D_2$				1
926.81	O I	$2s^2 2p^4 ^3P_1$ – $2s^2 2p^3 9s ^3S_1$	5.7	3.7	3.9	1
926.90	O I	$2s^2 2p^4 ^3P_0$ – $2s^2 2p^3 8d ^3D_1$				1
927.19			2.2	1.3	4.7	1
927.39	O I	$2s^2 2p^4 ^3P_0$ – $2s^2 2p^3 9s ^3S_1$	2.0	1.3	2.1	1
927.85	He II	$2p^2 P_{3/2}$ – $15d ^2D_{5/2}$	3.5	1.7	15	1
928.01	Fe III	$3d^6 ^1F_3$ – $3d^5 4p ^1F_3$	1.8	1.0	4.8	1
928.47	Fe III	$3d^6 ^3G_5$ – $3d^5 4p ^3H_6$	2.2	1.1	4.3	1
929.17	Fe III	$3d^6 ^3G_4$ – $3d^5 4p ^3H_5$	1.9	1.1	2.9	1
929.52	O I	$2s^2 2p^4 ^3P_2$ – $2s^2 2p^3 7d ^3D_3$	12	7.6	11	1
930.09	Fe III	$3d^6 ^3G_3$ – $3d^5 4p ^3H_4$	2.6	1.5	2.7	1
930.32	He II	$2p^2 P_{3/2}$ – $14d ^2D_{5/2}$	8.6	5.4	24	1
930.26	O I	$2s^2 2p^4 ^3P_2$ – $2s^2 2p^3 8s ^3S_1$				1
930.75	H I Ly 6	$1s^2 S_{1/2}$ – $7p^2 P_{3/2}$	77	48	164	1
930.89	O I	$2s^2 2p^4 ^3P_1$ – $2s^2 2p^3 7d ^3D_2$				1
931.48	O I	$2s^2 2p^4 ^3P_0$ – $2s^2 2p^3 7d ^3D_1$	6.8	4.1	5.0	1
931.63	O I	$2s^2 2p^4 ^3P_1$ – $2s^2 2p^3 8s ^3S_1$				1
932.22	O I	$2s^2 2p^4 ^3P_0$ – $2s^2 2p^3 8s ^3S_1$	2.7	1.5	1.6	1
933.40	S VI	$2p^6 3s ^2S_{1/2}$ – $2p^6 3p ^2P_{3/2}$	57	31	1586	1
933.44	He II	$2p^2 P_{3/2}$ – $13d ^2D_{5/2}$				1
934.70	Fe III	$3d^6 ^3P_2$ – $3d^5 4p ^3S_1$	1.7	1.1	6.5	1
935.19	O I	$2s^2 2p^4 ^1D_2$ – $2s^2 2p^3 4s ^1D_2$	4.3	2.4	5.4	1
936.63	O I	$2s^2 2p^4 ^3P_2$ – $2s^2 2p^3 6d ^3D_3$	14	8.6	14	1
937.39	He II	$2p^2 P_{3/2}$ – $12d ^2D_{5/2}$	10	5.6	34	0
937.40	S II	$3s^2 3p^3 ^2D_{3/2}$ – $3s^2 3p^2 4s ^2D_{3/2}$				0
937.80	H I Ly 5	$1s^2 S_{1/2}$ – $6p^2 P_{3/2}$	107	68	210	1

Table 1—Continued

λ_{obs}	Line	Transition	L_{QS}^{peak}	L_{CH}^{peak}	L_{SS}^{peak}	Ref.
Å			mW (sr m ² Å) ⁻¹			
937.84	O I	$2s^2 2p^4 \ ^3P_2 - 2s^2 2p^3 7s \ ^3S_1$				1
938.02	O I	$2s^2 2p^4 \ ^3P_1 - 2s^2 2p^3 6d \ ^3D_2$				1
938.62	O I	$2s^2 2p^4 \ ^3P_0 - 2s^2 2p^3 6d \ ^3D_1$	8.3	4.9	8.3	1
939.24	O I	$2s^2 2p^4 \ ^3P_1 - 2s^2 2p^3 7s \ ^3S_1$	6.2	3.9	9.1	1
939.84	O I	$2s^2 2p^4 \ ^3P_0 - 2s^2 2p^3 7s \ ^3S_1$	3.6	2.3	3.5	1
941.47			2.4	1.4		1
942.39	Fe III	$3d^6 \ ^1F_3 - 3d^5 4p \ ^1G_4$	2.5	1.5	8.0	1
942.51	He II	$2p \ ^2P_{3/2} - 11d \ ^2D_{5/2}$	5.5	2.8	32	1
943.03			1.8	1.1	5.8	1
943.89			2.2	1.3	2.7	1
944.34	Si VIII	$2s^2 2p^3 \ ^4S_{3/2} - 2s^2 2p^3 \ ^2P_{3/2}$	14	8.7	17	0
944.55	S VI	$2p^6 3s \ ^2S_{1/2} - 2p^6 3p \ ^2P_{1/2}$	29	18	784	1
945.19	C I	$2s^2 2p^2 \ ^3P_0 - 2s 2p^3 \ ^3S_1$				1
945.33	C I	$2s^2 2p^2 \ ^3P_1 - 2s 2p^3 \ ^3S_1$	3.6	2.0	5.4	1
945.59	C I	$2s^2 2p^2 \ ^3P_2 - 2s 2p^3 \ ^3S_1$	3.7	2.2	5.8	1
945.99	C II	$2s 2p^2 \ ^2S_{1/2} - 2s 2p 3d \ ^2P_{1/2}$	2.2	1.3	6.5	1
946.19	C II	$2s 2p^2 \ ^2S_{1/2} - 2s 2p 3d \ ^2P_{3/2}$	2.7	1.4	8.6	1
946.65	Mg II	$2p^6 3s \ ^2S_{1/2} - 2p^6 6p \ ^2P_{3/2,1/2}$	1.8	1.0	6.9	1
948.31	Fe III	$3d^6 \ ^3P_2 - 3d^5 4p \ ^3D_3$	2.1	1.1	2.1	1
948.70	O I	$2s^2 2p^4 \ ^3P_2 - 2s^2 2p^3 5d \ ^3D_3$	9	11	18	1
949.22	Si VIII	$2s^2 2p^3 \ ^4S_{3/2} - 2s^2 2p^3 \ ^2P_{1/2}$				0
949.36	He II	$2p \ ^2P_{3/2} - 10d \ ^2D_{5/2}$	16	9.7	111	0
949.74	H I Ly 4	$1s \ ^2S_{1/2} - 5p \ ^2P_{3/2}$	177	109	348	1
950.11	O I	$2s^2 2p^4 \ ^3P_1 - 2s^2 2p^3 5d \ ^3D_2$	31	16	67	1
950.14	Si IX	$2s^2 2p^2 \ ^3P_1 - 2s^2 2p^2 \ ^1S_0$				1
950.34	Fe III	$3d^6 \ ^1I_6 - 3d^5 4p \ ^5G_6$	7.7	3.8	24	1
950.72	Fe III	$3d^6 \ ^3P_0 - 3d^5 4p \ ^3S_1$	15	9.2	30	1
950.73	O I	$2s^2 2p^4 \ ^3P_0 - 2s^2 2p^3 5d \ ^3D_1$				1
950.89	O I	$2s^2 2p^4 \ ^3P_2 - 2s^2 2p^3 6s \ ^3S_1$	9.4	6.1	9.9	1
952.34	O I	$2s^2 2p^4 \ ^3P_1 - 2s^2 2p^3 6s \ ^3S_1$	5.8	3.6	4.1	1
952.95	O I	$2s^2 2p^4 \ ^3P_0 - 2s^2 2p^3 6s \ ^3S_1$	3.9	2.5	1.8	1
953.42	N I	$2s^2 2p^3 \ ^4S_{3/2} - 2s^2 2p^2 3d \ ^4P_{1/2}$	3.0	1.8	1.6	1
953.66	N I	$2s^2 2p^3 \ ^4S_{3/2} - 2s^2 2p^2 3d \ ^4P_{3/2}$	3.6	2.0	3.1	1
953.98	N I	$2s^2 2p^3 \ ^4S_{3/2} - 2s^2 2p^2 3d \ ^4P_{5/2}$	3.3	1.8	3.7	1
954.52	/2					3
955.34	N IV	$2s 2p \ ^1P_1 - 2p^2 \ ^1S_0$	2.4	1.4	7.6	1
955.45			2.4	1.4	7.6	3

Table 1—Continued

λ_{obs} Å	Line	Transition	L_{QS}^{peak} mW	L_{CH}^{peak} (sr m ² Å) ⁻¹	L_{SS}^{peak}	Ref.
955.88					1.9	3
957.11			1.4	0.8	7.0	3
957.75	(a)		1.6	0.9	2.6	0
958.70	He II	$2p\ ^2P_{3/2} - 9d\ ^2D_{5/2}$	8.5	4.2	45	1
959.57	Fe III	$3d^6\ ^3P_1 - 3d^54p\ ^3D_2$	2.2	1.2	2.4	1
961.90	Fe III	$3d^6\ ^1D_2 - 3d^54p\ ^1D_2$	2.0	1.1	2.9	1
962.44			2.3	1.3	5.7	1
962.67	Fe III	$3d^6\ ^1S_0 - 3d^54p\ ^1P_1$	1.9	1.0	1.6	1
963.88	Fe III	$3d^6\ ^3P_0 - 3d^54p\ ^3D_1$				1
963.99	N I	$2s^22p^3\ ^4S_{3/2} - 2s^22p^24s\ ^4P_{5/2}$	4.3	2.4	3.9	1
964.63	N I	$2s^22p^3\ ^4S_{3/2} - 2s^22p^24s\ ^4P_{3/2}$	3.6	2.0	2.2	1
965.04	N I	$2s^22p^3\ ^4S_{3/2} - 2s^22p^24s\ ^4P_{1/2}$	2.8	1.7	2.0	1
965.28	(d)		1.8	1.1	5.6	0
966.68					4.7	3
967.20	Fe III	$3d^6\ ^3F_4 - 3d^54p\ ^3D_3$	2.9	1.7	6.7	1
968.95	Fe III	$3d^6\ ^3F_3 - 3d^54p\ ^3D_2$	2.5	1.6	2.9	1
970.00	Fe III	$3d^6\ ^3F_2 - 3d^54p\ ^3D_1$	2.2	1.5	2.9	1
971.45			10	6.4	8.0	1
971.72	O I	$2s^22p^4\ ^3P_2 - 2s^22p^34d\ ^3D_3$	28	17	25	1
972.12	He II	$2p\ ^2P_{3/2} - 8d\ ^2D_{5/2}$	27	16	75	0
972.54	H I Ly 3	$1s\ ^2S_{1/2} - 4p\ ^2P_{3/2}$	266	196	815	1
973.24	O I	$2s^22p^4\ ^3P_1 - 2s^22p^34d\ ^3D_2$	24	15	57	1
973.35	Ne VII	$2s2p\ ^1P_1 - 2p^2\ ^1D_2$	11	15	57	0
973.89	O I	$2s^22p^4\ ^3P_0 - 2s^22p^34d\ ^3D_1$	15	9.1	20	1
974.58	Si VIII	$2p^23p\ ^2F_{7/2} - 2p^23d\ ^2G_{9/2}$	3.4	2.3		5
975.85	(d)				6.0	0
976.44	O I	$2s^22p^4\ ^3P_2 - 2s^22p^35s\ ^3S_1$	12	8.3	11	1
977.03	C III	$2s^2\ ^1S_0 - 2s2p\ ^1P_1$	2412	1878	6713	1
977.96	O I	$2s^22p^4\ ^3P_1 - 2s^22p^35s\ ^3S_1$	9.8	6.6	10	1
978.62	O I	$2s^22p^4\ ^3P_0 - 2s^22p^35s\ ^3S_1$	7.2	4.7	12	1
979.03	Fe III	$3d^6\ ^1F_3 - 3d^54p\ ^1F_3$	5.7	3.1	0	1
979.84	N III	$2s2p^2\ ^2D_{3/2} - 2p^3\ ^2D_{3/2}$				1
979.91	N III	$2s2p^2\ ^2D_{5/2} - 2p^3\ ^2D_{5/2}$	4.0	2.5	6.3	1
980.40					3.5	3
981.40	Fe III	$3d^54s\ ^5P_2 - 3d^55p\ ^5P_2$	6.6	3.9	11	1
982.14			2.1	1.4	2.1	3
983.51	Fe III	$3d^6\ ^1G_4 - 3d^54p\ ^3H_5$	2.2	1.4	1.9	4

Table 1—Continued

λ_{obs} Å	Line	Transition	L_{QS}^{peak} mW	L_{CH}^{peak} (sr m ² Å) ⁻¹	L_{SS}^{peak}	Ref.
983.87	Fe III	$3d^6 \ ^3H_5$	– $3d^5 4p \ ^3G_4$	7.1	3.5	11 1
983.91	Fe III	$3d^6 \ ^1I_6$	– $3d^5 4p \ ^1K_7$			1
984.97				2.2	1.4	2.2 3
985.40				2.2	1.4	1.8 3
985.84	Fe III	$3d^6 \ ^3H_4$	– $3d^5 4p \ ^3G_3$	5.5	2.9	8.8 1
986.51	Fe III	$3d^6 \ ^3F_4$	– $3d^5 4p \ ^5D_3$			1
986.62	Fe III	$3d^6 \ ^1I_6$	– $3d^5 4p \ ^1H_5$	2.7	1.7	4.0 1
987.91	(a)					3.1 0
988.17	Fe III	$3d^6 \ ^3F_3$	– $3d^5 4p \ ^3D_2$	2.4	1.6	2.5 1
988.75	O I	$2s^2 2p^4 \ ^3P_2$	– $2s^2 2p^3 3s \ ^3D_3$	61	35	81 1
988.65	Na VI	$2s^2 2p^2 \ ^3P_2$	– $2s 2p^3 \ ^5S_2$			1
989.82	N III	$2s^2 2p \ ^2P_{1/2}$	– $2s 2p^2 \ ^2D_{3/2}$	81	37	219 1
990.19	O I	$2s^2 2p^4 \ ^3P_1$	– $2s^2 2p^3 3s \ ^3D_{2,1}$	42	24	41 1
990.79	O I	$2s^2 2p^4 \ ^3P_0$	– $2s^2 2p^3 3s \ ^3D_1$	21	12	21 1
991.23	Fe III	$3d^6 \ ^3F_4$	– $3d^5 4p \ ^3D_3$	9.5	4.4	13 1
991.59	N III	$2s^2 2p \ ^2P_{3/2}$	– $2s 2p^2 \ ^2D_{5/2,3/2}$	152	66	410 1
991.83	Fe III	$3d^6 \ ^1G_4$	– $3d^5 4p \ ^1H_5$	18	9.2	23 3
992.36	He II	$2p \ ^2P_{3/2}$	– $7d \ ^2D_{5/2}$	15	7.7	76 1
992.68	Si II	$3s^2 3p \ ^2P_{3/2}$	– $3s^2 4d \ ^2D_{5/2}$	11	6.7	24 1
992.73	Ne VI	$2s^2 2p \ ^2P_{1/2}$	– $2s 2p^2 \ ^4P_{3/2}$			1
993.08	Fe III	$3d^6 \ ^3G_4$	– $3d^5 4p \ ^3F_3$	5.0	2.9	8.8 1
993.52	Si III	$3s 3p \ ^3P_0$	– $3s 4s \ ^3S_1$	4.3	2.3	8.0 1
994.16				8.1	5.2	6.3 3
994.26	Fe III	$3d^6 \ ^3P_2$	– $3d^5 4p \ ^3P_1$			3
994.59	K XIII	$2s^2 2p^3 \ ^4S_{3/2}$	– $2s^2 2p^3 \ ^2D_{3/2}$	3.2	2.1	5.9 3
994.59	Si VIII	$2p^2 3p \ ^4D_{7/2}$	– $2p^2 3d \ ^4F_{9/2}$			4
994.77	Fe III	$3d^6 \ ^3G_3$	– $3d^5 4p \ ^3F_2$	6.6	3.4	14 1
995.22	Fe III	$3d^6 \ ^3F_4$	– $3d^5 4p \ ^3G_{4,5}$	4.2	2.4	4.5 1
995.63						4.6 3
996.00	S II	$3s^2 3p^3 \ ^2D_{5/2}$	– $3s^2 3p^2 3d \ ^2F_{7/2}$	6.6	3.5	15 1
997.09	Fe III	$3d^6 \ ^3P_2$	– $3d^5 4p \ ^3P_2$	6.4	3.9	46 1
997.18	Ne VI	$2s^2 2p \ ^2P_{1/2}$	– $2s 2p^2 \ ^4P_{1/2}$	6.4	3.9	46 0
997.40	Si III	$3s 3p \ ^3P_2$	– $3s 4s \ ^3S_1$	8.0	4.1	20 1
997.64	Fe III	$3d^6 \ ^3F_3$	– $3d^5 4p \ ^3G_4$	4.0	2.6	10 1
998.05						10 3
999.27	Ne VI	$2s^2 2p \ ^2P_{3/2}$	– $2s 2p^2 \ ^4P_{5/2}$	9.8	6.1	261 0
999.38	Fe III	$3d^6 \ ^3F_2$	– $3d^5 4p \ ^3G_3$			1

Table 1—Continued

λ_{obs} Å	Line	Transition	L_{QS}^{peak} mW	L_{CH}^{peak} (sr m ² Å) ⁻¹	L_{SS}^{peak} (sr m ² Å) ⁻¹	Ref.
999.50	O I	$2s^2 2p^4 \ 1D_2 - 2s^2 2p^3 3s \ 1P_1$	31	19	40	1
999.85					19	3
1000.18	Ar VI	$3s^2 3p \ 2P_{3/2} - 3s 3p^2 \ 4P_{5/2}$	7.6	4.9	19	0
1000.49	S II	$3s^2 3p^3 \ 2D_{3/2} - 3s^2 3p^2 3d \ 2F_{5/2}$	5.7	3.4	14	1
1000.85	S II	$3s^2 3p^3 \ 2D_{5/2} - 3s^2 3p^2 3d \ 2F_{5/2}$	3.3	2.2	6.5	1
1005.12	Fe III	$3d^5 4p \ 7P_3 - 3d^5 5s \ 5G_4$	3.8	2.4	4.1	1
1005.33	Si III	$3s 3d \ 3D_4 - 3s 6f \ 3F_{4,3}$	3.2	2.2	3.5	4
1005.79	Ne VI	$2s^2 2p \ 2P_{3/2} - 2s 2p^2 \ 4P_{3/2}$	6.6	4.6	147	0
1006.01	N III	$2s 2p^2 \ 2S_{1/2} - 2p^3 \ 2P_{3/2}$			1	
1006.11	S II	$3s^2 3p^3 \ 2D_{5/2} - 3s^2 3p^2 3d \ 4D_{7/2}$	6.9	3.9	10	1
1006.33	Fe III	$3d^6 \ 1G_4 - 3d^5 4p \ 3I_5$	4.6	2.8	2.9	1
1006.92	S II	$3s^2 3p^3 \ 2D_{3/2} - 3s^2 3p^2 3d \ 4D_{1/2}$	4.0	2.5	4.5	1
1007.11	Fe III	$3d^6 \ 3P_1 - 3d^5 4p \ 3P_1$	3.8	2.5	4.2	1
1008.93			10	6.6	5.7	1
1009.85	C II	$2s 2p^2 \ 4P_{1/2} - 2p^3 \ 4S_{3/2}$	10	3.9	8.2	1
1010.01	Fe III	$3d^6 \ 3P_1 - 3d^5 4p \ 3P_2$			1	
1010.03	C II	$2s 2p^2 \ 4P_{3/2} - 2p^3 \ 4S_{3/2}$	16	7.8	14	1
1010.29	Ne VI	$2s^2 2p \ 2P_{3/2} - 2s 2p^2 \ 4P_{1/2}$	21	5.8	63	0
1010.37	C II	$2s 2p^2 \ 4P_{5/2} - 2p^3 \ 4S_{3/2}$	21	10	63	1
1011.61					7.6	3
1012.41	Fe III	$3d^6 \ 3P_0 - 3d^5 4p \ 3P_1$			1	
1012.45	S III	$3s^2 3p^2 \ 3P_0 - 3s 3p^3 \ 3P_1$	6.4	3.7	12	1
1012.65			4.1	2.4	10	3
1013.88			3.5	2.3	6.8	3
1014.39	S II	$3s^2 3p^3 \ 2D_{5/2} - 3s^2 3p^2 4s \ 2P_{3/2}$	5.6	3.0	5.5	1
1015.50	S III	$3s^2 3p^2 \ 3P_1 - 3s 3p^3 \ 3P_1$	8.8	4.5	15	1
1015.77	S III	$3s^2 3p^2 \ 3P_1 - 3s 3p^3 \ 3P_2$	6.7	4.0	13	1
1016.40			4.1	2.5	3.3	3
1017.24	Fe III	$3d^6 \ 3H_6 - 3d^5 4p \ 3H_6$	10	5.7	15	1
1017.75	Fe III	$3d^6 \ 3H_5 - 3d^5 4p \ 3H_5$	8.0	4.5	10	1
1018.29	Fe III	$3d^6 \ 3H_4 - 3d^5 4p \ 3H_4$	7.5	4.1	9.0	1
1019.48	S II	$3s^2 3p^3 \ 2D_{3/2} - 3s^2 3p^2 4s \ 2P_{1/2}$	4.8	3.0	9.2	1
1019.78	Fe III	$3d^6 \ 3D_3 - 3d^5 4p \ 3P_2$	5.0	2.9	5.6	1
1020.67	Si II	$3s^2 3p \ 2P_{1/2} - 3s^2 5s \ 2S_{1/2}$	4.8	3.2	6.5	1
1021.08	S III	$3s^2 3p^2 \ 3P_2 - 3s 3p^3 \ 3P_1$	7.8	4.8	14	1
1021.30	S III	$3s^2 3p^2 \ 3P_2 - 3s 3p^3 \ 3P_2$	14	8.0	29	1
1021.56	Fe III	$3d^6 \ 3D_2 - 3d^5 4p \ 3P_1$	5.3	3.6	4.8	1

Table 1—Continued

λ_{obs} Å	Line	Transition	L_{QS}^{peak} mW	L_{CH}^{peak} (sr m ² Å) ⁻¹	L_{SS}^{peak} (sr m ² Å) ⁻¹	Ref.
1023.73	Si II	$3s^2 3p\ ^2P_{3/2} - 3s^2 5s\ ^2S_{1/2}$	7.9	5.2	8.8	1
1024.20	Fe III	$3d^6\ ^3D_1 - 3d^5 4p\ ^3P_0$	9.7	6.6	12	1
1024.62					19	3
1025.27	He II	$2p\ ^2P_{3/2} - 4d\ ^2D_{5/2}$	120	86	283	1
1025.72	H I Ly 2	$1s\ ^2S_{1/2} - 3p\ ^2P_{3/2}$	1092	692	3392	1
1025.76	O I	$2s^2 2p^4\ ^3P_2 - 2s^2 2p^3 3d\ ^3D_3$			1	
1026.76	Fe III	$3d^6\ ^3G_5 - 3d^5 4p\ ^3G_5$	19	13	21	1
1027.44	O I	$2s^2 2p^4\ ^3P_1 - 2s^2 2p^3 3d\ ^3D_2$	124	73	187	1
1028.15	O I	$2s^2 2p^4\ ^3P_0 - 2s^2 2p^3 3d\ ^3D_1$	55	36	146	1
1028.95	(e)		6.4	3.6	15	0
1030.05			6.5	4.1		3
1030.87	S II	$3s^2 3p^3\ ^2P_{1/2} - 3s^2 3p^2 4s\ ^2D_{3/2}$			1	
1030.92	Fe III	$3d^6\ ^3G_4 - 3d^5 4p\ ^3G_4$	7.2	4.4	13	1
1031.39	S II	$3s^2 3p^3\ ^2P_{3/2} - 3s^2 3p^2 4s\ ^2D_{5/2}$	9.3	6.3	38	1
1031.93	O VI	$2s\ ^2S_{1/2} - 2p\ ^2P_{3/2}$	1140	602	70382	1
1033.30	Fe III	$3d^6\ ^3G_3 - 3d^5 4p\ ^3G_3$	6.4	4.5	18	1
1033.42	N I	$2s^2 2p^3\ ^2D_{5/2} - 2s^2 2p^2 9d\ ^2D_{5/2}$			1	
1035.78	Fe III	$3d^6\ ^3F_3 - 3d^5 4p\ ^3F_3$	9.1	5.8	17	1
1036.34	C II	$2s^2 2p\ ^2P_{1/2} - 2s 2p^2\ ^2S_{1/2}$	206	110	223	1
1037.00	C II	$2s^2 2p\ ^2P_{3/2} - 2s 2p^2\ ^2S_{1/2}$	239	130	242	1
1037.64	O VI	$2s\ ^2S_{1/2} - 2p\ ^2P_{1/2}$	545	303	25689	1
1038.36	Fe III	$3d^6\ ^3F_2 - 3d^5 4p\ ^3F_2$	9.4	6.0	27	1
1039.22	O I	$2s^2 2p^4\ ^3P_2 - 2s^2 2p^3 4s\ ^3S_1$	29	19	36	1
1040.94	O I	$2s^2 2p^4\ ^3P_1 - 2s^2 2p^3 4s\ ^3S_1$	29	19	21	1
1041.69	O I	$2s^2 2p^4\ ^3P_0 - 2s^2 2p^3 4s\ ^3S_1$	27	16	22	1
1043.08	N I	$2s^2 2p^3\ ^2D_{5/2} - 2s^2 2p^2 7d\ ^4D_{7/2}$	7.1	4.5	6.7	1
1043.17	N I	$2s^2 2p^3\ ^2D_{5/2} - 2s^2 2p^2 7d\ ^2F_{7/2}$			1	
1043.52					8.1	3
1044.08	N I	$2s^2 2p^3\ ^2D_{3/2} - 2s^2 2p^2 7d\ ^2P_{1/2}$	6.9	4.4	6.3	1
1044.19	N I	$2s^2 2p^3\ ^2D_{5/2} - 2s^2 2p^2 7d\ ^2P_{3/2}$			1	
1044.43	He I/2	$1s^2\ ^1S_0 - 1s 4p\ ^1P_1$			0	
1045.75	Al IV?	$2s^2 2p^5 3s\ ^3P_1 - 2s^2 2p^5 3p\ ^1S_0$	8.6	5.5	5.2	1
1048.22	Ar I	$3p^6\ ^1S_0 - 3p^5 4s\ ^1P_1$	8.1	5.5	5	
1049.07	S II	$3s^2 3p^3\ ^2D_{3/2} - 3s^2 3p^2 3d\ ^4F_{3/2}$	7.3	4.9	7.7	1
1049.25	Si VII	$2s^2 2p^4\ ^3P_1 - 2s^2 2p^4\ ^1S_0$	7.8	5.6	58	0
1049.86	S I	$3s^2 3p^4\ ^3P_2 - 3s^2 3p^3 5s\ ^3P_2$	7.2	5.1	4.8	1
1050.30	S I	$3s^2 3p^4\ ^3P_2 - 3s^2 3p^3 5s\ ^3P_1$	11	8.2	4.1	1

Table 1—Continued

λ_{obs} Å	Line	Transition	L_{QS}^{peak} mW	L_{CH}^{peak} (sr m ² Å) ⁻¹	L_{SS}^{peak}	Ref.
1050.51			8.4	5.5	3.7	1
1051.60	O III/2	$2s^2 2p^2 {}^1D_2 - 2s 2p^3 {}^1P_1$				4
1052.08	N I	$2s^2 2p^3 {}^2D_{5/2} - 2s^2 2p^2 6d {}^4D_{7/2}$				1
1052.22	N I	$2s^2 2p^3 {}^2D_{5/2} - 2s^2 2p^2 6d {}^2F_{7/2}$	9.0	6.2	5.0	1
1052.83	N I	$2s^2 2p^3 {}^2D_{5/2} - 2s^2 2p^2 7s {}^2P_{3/2}$	7.8	5.1	4.9	4
1053.09	N I	$2s^2 2p^3 {}^2D_{3/2} - 2s^2 2p^2 6d {}^4P_{5/2}$				4
1053.18	N I	$2s^2 2p^3 {}^2D_{3/2} - 2s^2 2p^2 6d {}^2P_{1/2}$	9.2	6.0	4.5	4
1053.87	Al VII	$2s^2 2p^3 {}^4S_{3/2} - 2s^2 2p^3 {}^2P_{3/2}$	7.6	5.1	19	0
1054.65			9.4	6.0	5.3	3
1054.90			9.6	6.8	4.8	3
1056.67	S I	$3s^2 3p^4 {}^3P_0 - 3s^2 3p^3 5s {}^3P_1$				0
1056.81	Al VII	$2s^2 2p^3 {}^4S_{3/2} - 2s^2 2p^3 {}^2P_{1/2}$	9.9	6.6	12	0
1057.79	Al VIII	$2s^2 2p^2 {}^3P_1 - 2s^2 2p^2 {}^1S_0$	7.5	5.2	13	0
1059.02			9.9	6.7	6.5	3
1059.44			14	9.0	7.2	3
1061.27	Fe III	$3d^6 {}^3D_1 - 3d^5 4p {}^3D_1$	9.7	5.9	7.2	1
1061.71	Fe III	$3d^6 {}^3D_2 - 3d^5 4p {}^3D_2$	10	6.6	7.7	1
1061.83	Fe III	$3d^6 {}^3D_1 - 3d^5 4p {}^3D_2$				1
1062.25	Fe III	$3d^6 {}^3D_2 - 3d^5 4p {}^3D_3$	9.3	6.4	7.5	1
1062.66	S IV	$3s^2 3p {}^2P_{1/2} - 3s 3p {}^2D_{3/2}$	33	17	135	1
1063.29	Fe III	$3d^6 {}^3D_3 - 3d^5 4p {}^3D_2$	10	7.4	9.3	1
1063.58			10	6.9	12	3
1063.87	Fe III	$3d^6 {}^3D_3 - 3d^5 4p {}^3D_3$	12	8.4	10	1
1064.65	Fe III	$3d^6 {}^3F_2 - 3d^5 4p {}^3G_3$	12	8.1	10	1
1065.52			11	8.3	8.3	3
1065.86	C II	$2s 2p^2 {}^2D_{5/2} - 2p^3 {}^2P_{3/2}$	12	8.0	9.6	1
1066.13	C II	$2s 2p^2 {}^2D_{3/2} - 2p^3 {}^2P_{1/2}$				4
1066.14	Fe III	$3d^6 {}^3G_5 - 3d^5 4p {}^3H_6$				1
1066.18	Fe III	$3d^6 {}^1S_0 - 3d^5 4p {}^3P_1$	15	9.3	12	1
1066.65	Si IV	$2p^6 3d {}^2D_{5/2} - 2p^6 4f {}^2F_{7/2}$	22	14	33	1
1066.66	Ar I	$3p^6 {}^1S_0 - 3p^5 4s {}^1P_1$				5
1067.31	N I	$2s^2 2p^3 {}^2D_{3/2} - 2s^2 2p^2 5d {}^2D_{3/2}$				4
1067.38	N I	$2s^2 2p^3 {}^2D_{5/2} - 2s^2 2p^2 5d {}^4D_{7/2}$	11	7.5	8.1	4
1067.62	N I	$2s^2 2p^3 {}^2D_{5/2} - 2s^2 2p^2 5d {}^2F_{7/2}$	12	8.0	8.1	4
1067.83	O IV	$2s^2 3d {}^2D_{5/2} - 2s^2 4f {}^2F_{7/2}$	10	6.9	18	0
1068.19	Fe III	$3d^6 {}^3G_4 - 3d^5 4p {}^3H_5$	11	6.9	10	1
1068.48	N I	$2s^2 2p^3 {}^2D_{3/2} - 2s^2 2p^2 5d {}^4P_{5/2}$	13	9.1	8.4	4

Table 1—Continued

λ_{obs}	Line	Transition	L_{QS}^{peak}	L_{CH}^{peak}	L_{SS}^{peak}	Ref.
Å			mW	(sr m ² Å) ⁻¹		
1069.08	Fe III	$3d^6 \ ^3G_3$ – $3d^5 4p \ ^3H_4$	11	7.9	9.0	1
1071.44	N I ?	$2s^2 2p^3 \ ^2D_{3/2}$ – $2s^2 2p^2 6s \ ^4P_{1/2}$	12	7.3		5
1071.76	Fe III	$3d^6 \ ^3G_4$ – $3d^5 4p \ ^3F_3$	12	8.1	9.4	1
1072.99	S IV	$3s^2 3p \ ^2P_{3/2}$ – $3s 3p^2 \ ^2D_{5/2}$	46	27	237	1
1073.53	S IV	$3s^2 3p \ ^2P_{3/2}$ – $3s 3p^2 \ ^2D_{3/2}$	13	9.0	28	1
[1074.01	Fe VII	$3d 4s \ ^1D_2$ – $3d 4p \ ^1P_1$				5
1074.06	He I/2	$1s^2 \ ^1S_0$ – $1s 3p \ ^1P_1$				0
1074.97	Fe III	$3d^6 \ ^3G_3$ – $3d^5 4p \ ^3F_2$	12	8.2	13	1
1077.14	S III	$3s^2 3p^2 \ ^1D_2$ – $3s 3p^3 \ ^1D_2$	26	16	42	1
1083.99	N II	$2s^2 2p^2 \ ^3P_0$ – $2s 2p^3 \ ^3D_1$	59	34	95	1
[1084.56	N II	$2s^2 2p^2 \ ^3P_1$ – $2s 2p^3 \ ^3D_1$				1
1084.58	N II	$2s^2 2p^2 \ ^3P_1$ – $2s 2p^3 \ ^3D_2$	116	69	181	1
1084.94	He II	$2p \ ^2P_{3/2}$ – $5d \ ^2D_{5/2}$	64	31	202	1
1085.54	N II	$2s^2 2p^2 \ ^3P_2$ – $2s 2p^3 \ ^3D_2$	83	53	105	1
1085.71	N II	$2s^2 2p^2 \ ^3P_2$ – $2s 2p^3 \ ^3D_3$	211	121	353	1
[1087.80	ne IV/2	$2s^2 2p^3 \ ^3S_{3/2}$ – $2s 2p^4 \ ^4P_{5/2}$			22	5
1087.86	Fe VII	$3d 4s \ ^3D_2$ – $3d 4p \ ^3P_1$				5
1092.73	C II	$2s 2p^2 \ ^2P_{3/2}$ – $2s 2p 3d \ ^2P_{3/2}$	20	15	20	4
1093.10			18	12	19	3
1095.37	Fe VII	$3d 4s \ ^3D_3$ – $3d 4p \ ^3P_2$			26	5
[1096.57	S II	$3s^2 3p^3 \ ^2D_{3/2}$ – $3s 3p^4 \ ^2P_{1/2}$				1
1096.61	Fe III	$3d^6 \ ^3F_4$ – $3d^5 4p \ ^3D_3$	20	12	18	1
[1097.20	N I	$2s^2 2p^3 \ ^2D_{5/2}$ – $2s^2 2p^2 4d \ ^2F_{7/2}$	22	14	21	1
1097.38	S I	$3s^2 3p^4 \ ^3P_1$ – $3s^2 3p^3 4d \ ^3P_2$				1
[1098.05	N I	$2s^2 2p^3 \ ^2D_{3/2}$ – $2s^2 2p^2 4d \ ^4P_{5/2}$	29	9	21	1
1098.24	Fe III	$3d^6 \ ^3P_2$ – $3d^5 4p \ ^3D_3$				1
[1098.26	N I	$2s^2 2p^3 \ ^2D_{3/2}$ – $2s^2 2p^2 4d \ ^2F_{5/2}$				1
1098.92			20	12	32	3
1099.45	S IV ?		18	11	26	5
1102.38	S II	$3s^2 3p^3 \ ^2D_{5/2}$ – $3s 3p^4 \ ^2P_{3/2}$	23	14	20	1
1103.60	C I	$2s^2 2p^2 \ ^3P_2$ – $2s^2 2p 22d \ ^1F_3$	18	12	24	4
1103.86	C I	$2s^2 2p^2 \ ^3P_2$ – $2s^2 2p 21d \ ^1F_3$	19	13	23	4
1104.16	C I	$2s^2 2p^2 \ ^3P_2$ – $2s^2 2p 20d \ ^1P_1$	19	13	26	4
1104.55	C I	$2s^2 2p^2 \ ^3P_2$ – $2s^2 2p 19d \ ^1F_3$	20	12	22	4
1104.96	C I	$2s^2 2p^2 \ ^3P_2$ – $2s^2 2p 18d \ ^1P_1$	19	12	26	4
1105.14	C I	$2s^2 2p^2 \ ^3P_1$ – $2s^2 2p 17d \ ^1P_1$	15	10	15	4
1105.47	C I	$2s^2 2p^2 \ ^3P_2$ – $2s^2 2p 17d \ ^1F_3$	20	13	25	4

Table 1—Continued

λ_{obs} Å	Line	Transition	L_{QS}^{peak} mW	L_{CH}^{peak} (sr m ² Å) ⁻¹	L_{SS}^{peak}	Ref.
1105.75	C I	$2s^2 2p^2 {}^3P_1 - 2s^2 2p 16d {}^1P_1$	16	11	21	4
1106.07	C I	$2s^2 2p^2 {}^3P_2 - 2s^2 2p 16d {}^1P_1$	20	12	25	4
1106.29	C I	$2s^2 2p^2 {}^3P_0 - 2s^2 2p 15d {}^1P_1$	16	11	17	4
1106.50	C I	$2s^2 2p^2 {}^3P_1 - 2s^2 2p 15d {}^1P_1$	20	13	27	4
[1106.70	O IV/2	$2s^2 2p {}^2P_{1/2} - 2s 2p^2 {}^2P_{3/2}$				4
[1106.80	C I	$2s^2 2p^2 {}^3P_2 - 2s^2 2p 15d {}^1P_1$	24	15	63	4
1107.34	C I	$2s^2 2p^2 {}^3P_1 - 2s^2 2p 14d {}^1P_1$	18	13	21	4
1107.70	C I	$2s^2 2p^2 {}^3P_2 - 2s^2 2p 14d {}^1F_3$	24	15	32	4
1108.10	C I	$2s^2 2p^2 {}^3P_1 - 2s^2 2p 14d {}^3D_1$	22	15	81	4
1108.16	O IV/2	$2s^2 2p {}^2P_{1/2} - 2s 2p^2 {}^2P_{1/2}$				1
[1108.37	Si III	$3s 3p {}^3P_0 - 3s 3d {}^3D_1$	32	18	78	1
[1108.48	S IV	$3s 3p^2 {}^2S_{1/2} - 3s^2 4p {}^2P_{3/2}$				1
1108.44	C I	$2s^2 2p^2 {}^3P_1 - 2s^2 2p 13d {}^1P_1$	32	18	78	4
1108.80	C I	$2s^2 2p^2 {}^3P_2 - 2s^2 2p 13d {}^1F_3$	26	17	41	4
1109.03	C I	$2s^2 2p^2 {}^3P_0 - 2s^2 2p 13d {}^3D_1$	27	15	210	4
1109.12	O IV/2	$2s^2 2p {}^2P_{3/2} - 2s 2p^2 {}^2P_{3/2}$				1
1109.24	C I	$2s^2 2p^2 {}^3P_1 - 2s^2 2p 13d {}^3D_1$	19	12	90	1
1109.60	C I	$2s^2 2p^2 {}^3P_0 - 2s^2 2p 12d {}^1P_1$	18	12	20	4
[1109.84	C I	$2s^2 2p^2 {}^3P_1 - 2s^2 2p 12d {}^1P_1$				1
[1110.00	Si III	$3s 3p {}^3P_1 - 3s 3d {}^3D_2$	41	23	134	1
[1110.17	C I	$2s^2 2p^2 {}^3P_2 - 2s^2 2p 12d {}^1P_1$				1
[1110.19	C I	$2s^2 2p^2 {}^3P_2 - 2s^2 2p 12d {}^1F_3$	32	19	40	1
[1110.44						3
[1110.52	O IV/2	$2s^2 2p {}^2P_{3/2} - 2s 2p^2 {}^2P_{1/2}$				0
[1110.67						3
1111.01	C I	$2s^2 2p^2 {}^3P_2 - 2s^2 2p 12d {}^3F_3$	15	10	17	1
1111.42	C I	$2s^2 2p^2 {}^3P_0 - 2s^2 2p 11d {}^1P_1$	12	9.0	15	1
1111.60	C I	$2s^2 2p^2 {}^3P_1 - 2s^2 2p 11d {}^1P_1$	19	13	24	1
[1111.96	C I	$2s^2 2p^2 {}^3P_2 - 2s^2 2p 11d {}^1P_1$	30	18	39	1
[1111.99	C I	$2s^2 2p^2 {}^3P_2 - 2s^2 2p 11d {}^1F_3$				1
1112.22	C I	$2s^2 2p^2 {}^3P_0 - 2s^2 2p 11d {}^1D_1$	18	11	18	1
1112.47	C I	$2s^2 2p^2 {}^3P_1 - 2s^2 2p 11d {}^3D_1$	19	12	30	1
[1112.80	C I	$2s^2 2p^2 {}^3P_2 - 2s^2 2p 11d {}^3D_1$	16	10	16	1
[1112.82	C I	$2s^2 2p^2 {}^3P_2 - 2s^2 2p 11d {}^3F_3$				1
[1113.15	S III					1
[1113.23	Si III	$3s 3p {}^3P_2 - 3s 3d {}^3D_3$	71	36	207	1
1114.00	C I	$2s^2 2p^2 {}^3P_1 - 2s^2 2p 10d {}^1P_1$	21	14	26	1

Table 1—Continued

λ_{obs} Å	Line	Transition	L_{QS}^{peak} mW (sr m ² Å) ⁻¹	L_{CH}^{peak}	L_{SS}^{peak}	Ref.	
1114.39	C I	$2s^2 2p^2 {}^3P_2 - 2s^2 2p 10d {}^1F_3$	32	21	45	1	
1114.64	C I	$2s^2 2p^2 {}^3P_0 - 2s^2 2p 10d {}^3D_1$	19	13	21	1	
1114.86	C I	$2s^2 2p^2 {}^3P_1 - 2s^2 2p 10d {}^3D_1$	21	14	28	1	
1115.17	C I	$2s^2 2p^2 {}^3P_2 - 2s^2 2p 10d {}^3D_1$				1	
1115.21	C I	$2s^2 2p^2 {}^3P_2 - 2s^2 2p 10d {}^3F_3$	17	11	26	1	
1115.52	Ca x/2	$2p^6 3s {}^2S_{1/2} - 2p^6 3p {}^2P_{3/2}$				0	
1117.20	C I	$2s^2 2p^2 {}^3P_1 - 2s^2 2p 9d {}^1P_1$	22	15	59	1	
1117.24	Ne VI/2	$2s^2 2p {}^2P_{1/2} - 2s 2p^2 {}^2D_{3/2}$				0	
1117.24	Ca v/2	$3s^2 3p^4 {}^1D_2 - 3s 3p^5 {}^3P_1$				5	
1117.58	C I	$2s^2 2p^2 {}^3P_2 - 2s^2 2p 9d {}^3P_2$	33	20	64	1	
1117.58	Fe VII	$3d 4s {}^1D_2 - 3d 4p {}^3P_0$				5	
1117.72	C I	$2s^2 2p^2 {}^3P_2 - 2s^2 2p 9d {}^3D_3$				1	
1117.88	C I	$2s^2 2p^2 {}^3P_0 - 2s^2 2p 9d {}^3D_1$	23	15	37	1	
1117.98	P V	$2p^6 3s {}^2S_{1/2} - 2p^6 3p {}^2P_{3/2}$				1	
1118.07	C I	$2s^2 2p^2 {}^3P_1 - 2s^2 2p 9d {}^3D_1$				1	
1118.18	C I	$2s^2 2p^2 {}^3P_1 - 2s^2 2p 9d {}^3F_2$	23	15	43	1	
1118.41	C I	$2s^2 2p^2 {}^3P_2 - 2s^2 2p 9d {}^3D_1$				1	
1118.49	C I	$2s^2 2p^2 {}^3P_2 - 2s^2 2p 9d {}^3F_3$	18	12	25	1	
1118.90				16	9.4	3	
1119.10	H ₂	1 - 3 Q3 (C-X)	11	8.0	764	4	
1121.47	C I	$2s^2 2p^2 {}^3P_0 - 2s^2 2p 8d {}^3P_1$				1	
1121.65	C I	$2s^2 2p^2 {}^3P_1 - 2s^2 2p 8d {}^3P_1$	21	14	29	1	
1121.91	C I	$2s^2 2p^2 {}^3P_2 - 2s^2 2p 8d {}^3P_1$	18	11	22	1	
1122.13	C I	$2s^2 2p^2 {}^3P_2 - 2s^2 2p 8d {}^3P_2$	30	18	48	1	
1122.33	C I	$2s^2 2p^2 {}^3P_2 - 2s^2 2p 8d {}^3D_3$				1	
1122.44	C I	$2s^2 2p^2 {}^3P_0 - 2s^2 2p 8d {}^3D_1$				1	
1122.52	Si IV	$2p^6 3p {}^2P_{1/2} - 2p^6 3d {}^2D_{3/2}$	105	61	189	1	
1122.53	Fe III	$3d^6 {}^5D_4 - 3d^5 4p {}^5P_3$				1	
1122.65	C I	$2s^2 2p^2 {}^3P_1 - 2s^2 2p 8d {}^3D_1$				0	
1122.76	Ne VII/2	$2s 2p {}^3P_1 - 2p^2 {}^3P_1$				0	
1122.79	C I	$2s^2 2p^2 {}^3P_1 - 2s^2 2p 8d {}^3F_2$				0	
1122.99	C I	$2s^2 2p^2 {}^3P_2 - 2s^2 2p 8d {}^3D_1$				1	
1123.11	C I	$2s^2 2p^2 {}^3P_2 - 2s^2 2p 8d {}^3F_3$	21	13	32	1	
1123.46	Ne VII/2	$2s 2p {}^3P_2 - 2p^2 {}^3P_2$				1	
1124.13				8.7	5.5	10	3
1124.88	Fe III	$3d^6 {}^5D_3 - 3d^5 4p {}^5P_2$	38	23	41	1	
1125.66	Ne VI/2	$2s^2 2p {}^2P_{3/2} - 2s 2p^2 {}^2D_{5/2}$			*2511	1	

Table 1—Continued

λ_{obs} Å	Line	Transition	L_{QS}^{peak} mW	L_{CH}^{peak} (sr m ² Å) ⁻¹	L_{SS}^{peak} (sr m ² Å) ⁻¹	Ref.
1126.72	Fe III	$3d^6 \ 5D_2$ – $3d^5 4p \ 5P_1$	17	10	17	1
1126.85	S III	$3s \ 3p^3 \ 3D_2$ – $3s^2 3p \ 4p \ 3P_1$				1
1128.04	Si XI	$2s^2 \ 1S_0$ – $2s \ 2p \ 3P_2$				1
1128.06	Fe III	$3d^6 \ 5D_3$ – $3d^5 4p \ 5P_3$	39	24	55	1
1128.35	Si IV	$2p^6 3p \ 2P_{3/2}$ – $2p^6 3d \ 2D_{5/2}$	48	26	240	1
1128.72	Fe III	$3d^6 \ 5D_2$ – $3d^5 4p \ 5P_2$	49	30	72	1
1129.04	Ne VII/2	$2s \ 2p \ 3P_2$ – $2p^2 \ 3P_1$				0
1129.14	C I	$2s^2 2p^2 \ 3P_2$ – $2s^2 2p \ 7d \ 3D_{3,2}$	55	34	95	1
1129.19	Fe III	$3d^6 \ 5D_1$ – $3d^5 4p \ 5P_1$				1
1129.60	C I	$2s^2 2p^2 \ 3P_1$ – $2s^2 2p \ 7d \ 3F_2$	21	14	36	1
1129.92	C I	$2s^2 2p^2 \ 3P_2$ – $2s^2 2p \ 7d \ 3F_3$	22	14	38	1
1130.40	Fe III	$3d^6 \ 5D_0$ – $3d^5 4p \ 5P_1$	15	9.1	18	1
1131.01	Si VI	$2p^4 3s \ 4P_{5/2}$ – $2p^4 3p \ 4D_{7/2}$				3
1131.20	Fe III	$3d^6 \ 5D_1$ – $3d^5 4p \ 5P_2$	10	6.9	18	1
1131.62	S II	$3s^2 3p^3 \ 2P_{3/2}$ – $3s^2 3p^2 4s \ 2P_{1/2}$	12	8.1	14	1
1131.92	Fe III	$3d^6 \ 5D_2$ – $3d^5 4p \ 5P_3$	9.4	6.3	9.2	1
1132.35			6.7	4.5	7.8	3
1132.88			7.1	4.7	8.8	3
1133.68	Al VI ?	$2s^2 2p^4 \ 3P_2$ – $2s^2 2p^4 \ 1S_0$	35	21	70	1
1134.16	N I	$2s^2 2p^3 \ 4S_{3/2}$ – $2s \ 2p^4 \ 4P_{1/2}$	24	16	15	1
1134.40	N I	$2s^2 2p^3 \ 4S_{3/2}$ – $2s \ 2p^4 \ 4P_{3/2}$	38	25	27	1
1134.98	N I	$2s^2 2p^3 \ 4S_{3/2}$ – $2s \ 2p^4 \ 4P_{5/2}$	46	31	37	1
1135.40	Si VII	$2p^3 3s \ 5S_2$ – $2p^3 3p \ 5P_3$	10	6.8	16	3
1135.55			1	6.4	16	3
1136.56	Ne V	$2s^2 2p^2 \ 3P_1$ – $2s \ 2p^3 \ 5S_2$	8.3	5.4	89	1
1136.82	Ne V/2	$2s^2 2p^2 \ 3P_0$ – $2s \ 2p^3 \ 3D_1$				0
1137.23	Si VII	$2p^3 3s \ 3D_2$ – $2p^3 3p \ 3F_3$	8.6	5.7	12	0
1138.00			8.4	5.6	5.9	3
1138.38	C I	$2s^2 2p^2 \ 3P_0$ – $2s^2 2p \ 6d \ 3P_1$	15	9.8	16	1
1138.56	C I	$2s^2 2p^2 \ 3P_1$ – $2s^2 2p \ 6d \ 3P_0$	26	16	43	4
1138.94	C II	$2s \ 2p^2 \ 2P_{1/2}$ – $2s \ 2p \ 3d \ 2D_{3/2}$				1
1138.95	C I	$2s^2 2p^2 \ 3P_2$ – $2s^2 2p \ 6d \ 3P_1$	30	18	49	1
1139.09	C I	$2s^2 2p^2 \ 3P_2$ – $2s^2 2p \ 6d \ 3P_2$				1
1139.38	C II	$2s \ 2p^2 \ 2P_{3/2}$ – $2s \ 2p \ 3d \ 2D_{5/2}$	23	14	28	4
1139.72	Ne V/2	$2s^2 2p^2 \ 3P_1$ – $2s \ 2p^3 \ 3D_2$				0
1139.77	C I	$2s^2 2p^2 \ 3P_1$ – $2s^2 2p \ 7s \ 3P_2$				1
1139.81	C I	$2s^2 2p^2 \ 3P_2$ – $2s^2 2p \ 6d \ 3D_3$	42	25	111	1

Table 1—Continued

λ_{obs} Å	Line	Transition	L_{QS}^{peak} mW	L_{CH}^{peak} (sr m ² Å) ⁻¹	L_{SS}^{peak}	Ref.
1140.35	C I	$2s^2 2p^2 {}^3P_1 - 2s^2 2p 6d {}^3F_2$	25	15	33	1
1140.62	C I	$2s^2 2p^2 {}^3P_2 - 2s^2 2p 6d {}^3F_3$	24	16	34	1
1141.29	Fe III	$3d^6 {}^1G_4 - 3d^5 4p {}^1H_5$	10	7.1	10	1
1141.45	Fe VII	$3d4s {}^3D_3 - 3d4p {}^3F_4$			25	5
1141.68	C II	$2s 2p^2 {}^2D_{5/2} - 2s^2 4p {}^2P_{3/2}$	10	6.6	1	1
[1142.29	Si III	$3p^2 {}^3P_1 - 3p 3d {}^3D_1$			0	
1142.36	Si VII	$2p^3 3s {}^5S_2 - 2p^3 3p {}^5P_2$	16	10	16	0
[1142.45					3	
1142.60	Fe III	$3d^6 {}^3D_2 - 3d^5 4p {}^3F_3$	9.1	6.6	10	3
1143.00	Fe III	$3d^6 {}^3D_3 - 3d^5 4p {}^3F_4$	10	7.2	5.6	1
1143.22	Fe II	$3d^6 4s {}^6D_{9/2} - 3d^5 4s 4p {}^6F_{9/2}$	9.2	6.2	5.9	4
1143.67	Fe III	$3d^6 {}^3D_1 - 3d^5 4p {}^3F_2$	13	8.9	5.2	1
1144.28	Ne V/2	$2s^2 2p^2 {}^3P_2 - 2s 2p^3 {}^3D_2$			0	
1144.74	Ne V/2	$2s^2 2p^2 {}^3P_2 - 2s 2p^3 {}^3D_3$			0	
1144.94	Fe II	$3d^6 4s {}^6D_{9/2} - 3d^5 4s 4p {}^6F_{11/2}$	11	7.2	18	4
1145.66	Ne V	$2s^2 2p^2 {}^3P_2 - 2s 2p^3 {}^5S_2$	13	8.6	143	0
[1146.83	Fe II	$3d^6 4s {}^6D_{3/2} - 3d^5 4s 4p {}^6D_{5/2}$	9.9	6.6	8.4	4
[1146.95	Fe II	$3d^6 4s {}^6D_{7/2} - 3d^5 4s 4p {}^6F_{5/2}$			4	
1147.41	Fe II	$3d^6 4s {}^6D_{7/2} - 3d^5 4s 4p {}^6F_{7/2}$	9.2	6.3	5.6	4
[1148.06	Ca X/2	$2p^6 3s {}^2S_{1/2} - 2p^6 3p {}^2P_{1/2}$			0	
1148.08	Fe II	$3d^6 4s {}^6D_{3/2} - 3d^5 4s 4p {}^6D_{3/2}$	8.9	5.9	19	4
1148.28	Fe II	$3d^6 4s {}^6D_{7/2} - 3d^5 4s 4p {}^6F_{9/2}$	9.4	6.5	7.6	4
1148.69	Si VI	$2p^4 3s {}^4P_{3/2} - 2p^4 3p {}^4D_{5/2}$	9.9	7.0	8.1	4
1148.96	Fe II	$3d^6 4s {}^6D_{3/2} - 3d^5 4s 4p {}^6F_{1/2}$	8.5	5.9	9.6	4
1149.59	Fe II	$3d^6 4s {}^6D_{1/2} - 3d^5 4s 4p {}^6D_{3/2}$	8.3	6.0	10	4
1149.96	S I ?	$3s^2 3p^4 {}^1D_2 - 3s^2 3p^3 9s {}^1D_2$	9.9	6.9	4.1	4
1150.47	Fe II	$3d^6 4s {}^6D_{1/2} - 3d^5 4s 4p {}^6F_{1/2}$	8.7	6.5	5.7	4
1150.80	O III	$2s 2p^3 {}^3S_1 - 2p^4 {}^3P_1$	14	10	5.0	1
1151.15	Fe II	$3d^6 4s {}^6D_{5/2} - 3d^5 4s 4p {}^6F_{7/2}$	9.6	6.8	5.5	4
1152.15	O I	$2s^2 2p^4 {}^1D_2 - 2s^2 2p^3 3s {}^1D_2$	104	69	57	1
1152.88	Fe II	$3d^6 4s {}^6D_{3/2} - 3d^5 4s 4p {}^6F_{3/2}$	10	6.9	6.6	4
1153.27	Fe II	$3d^6 4s {}^6D_{3/2} - 3d^5 4s 4p {}^6F_{5/2}$	9.8	6.8	4.2	4
1154.00			10	7.4	3	
1154.40	Fe II	$3d^6 4s {}^6D_{1/2} - 3d^5 4s 4p {}^6F_{3/2}$	9.7	6.9	3.7	4
1155.00	Fe VII	$3d4s {}^3D_2 - 3d4p {}^3F_3$	9.2	6.6	5.2	5
1155.82	C I	$2s^2 2p^2 {}^3P_0 - 2s^2 2p 5d {}^3P_1$	20	13	14	4
[1156.00	S I	$3s^2 3p^4 {}^3P_2 - 3s^2 3p^3 3d {}^3P_2$	38	24	31	1

Table 1—Continued

λ_{obs} Å	Line	Transition	L_{QS}^{peak} mW	L_{CH}^{peak} (sr m ² Å) ⁻¹	L_{SS}^{peak} (sr m ² Å) ⁻¹	Ref.
1156.03	C I	$2s^2 2p^2 \ ^3P_1$ – $2s^2 2p \ ^5d \ ^3P_1$				1
1156.27	S I	$3s^2 3p^4 \ ^3P_2$ – $3s^2 3p^3 3d \ ^3P_1$	39	26	17	1
1156.56	C I	$2s^2 2p^2 \ ^3P_2$ – $2s^2 2p \ ^5d \ ^3P_2$	23	13	25	4
1157.40	C I	$2s^2 2p^2 \ ^3P_1$ – $2s^2 2p \ ^6s \ ^1P_1$	21	14	18	1
1157.50	(d)					1
1157.79	C I	$2s^2 2p^2 \ ^3P_1$ – $2s^2 2p \ ^5d \ ^3D_2$	23	16	24	4
1157.91	C I	$2s^2 2p^2 \ ^3P_0$ – $2s^2 2p \ ^5d \ ^3D_1$				4
1158.02	C I	$2s^2 2p^2 \ ^3P_2$ – $2s^2 2p \ ^5d \ ^3D_3$	35	22	45	4
1158.13	C I	$2s^2 2p^2 \ ^3P_2$ – $2s^2 2p \ ^5d \ ^3D_2$				4
1158.32	C I	$2s^2 2p^2 \ ^3P_0$ – $2s^2 2p \ ^6s \ ^3P_1$				4
1158.40	C I	$2s^2 2p^2 \ ^3P_2$ – $2s^2 2p \ ^6s \ ^3P_2$	25	16	40	4
1158.67	C I	$2s^2 2p^2 \ ^3P_1$ – $2s^2 2p \ ^6s \ ^3P_0$				4
1158.73	C I	$2s^2 2p^2 \ ^3P_1$ – $2s^2 2p \ ^5d \ ^3F_2$	24	17	23	4
1158.97	C I	$2s^2 2p^2 \ ^3P_2$ – $2s^2 2p \ ^5d \ ^3F_3$	26	17	23	4
1159.51	Ni II	$3d^8 4s \ ^4F_{9/2}$ – $3d^7 4s \ ^4p \ ^4G_{9/2}$	11	8.6	6.0	4
1160.51			13	9.0	5.9	3
1160.79	S I	$3s^2 3p^4 \ ^1D_2$ – $3s^2 3p^3 8s \ ^1D_2$	14	9.5	5.2	4
1161.35	S I	$3s^2 3p^4 \ ^3P_1$ – $3s^2 3p^3 3d \ ^3P_2$	32	23	11	1
1161.58	S I	$3s^2 3p^4 \ ^3P_1$ – $3s^2 3p^3 3d \ ^3P_1$	28	19	10	1
1161.72	S I	$3s^2 3p^4 \ ^3P_1$ – $3s^2 3p^3 3d \ ^3P_0$	31	21	16	1
1161.76	Si XI/2	$2s^2 \ ^1S_0$ – $2s \ ^2p \ ^3P_1$				0
1161.97	S I	$3s^2 3p^4 \ ^1D_2$ – $3s^2 3p^3 6d \ ^1D_2$	20	13	9.0	1
1163.85	H ₂	1 - 4 Q3 (C-X)	18	14	1267	4
1163.90	Fe VII	$3d4s \ ^3D_2$ – $3d4p \ ^3D_3$				5
1163.88	N I	$2s^2 2p^3 \ ^2D_{5/2}$ – $2s^2 2p^2 3d \ ^2D_{5/2}$				1
1163.98	S I	$3s^2 3p^4 \ ^3P_0$ – $3s^2 3p^3 3d \ ^3P_1$	30	21	1267	1
1164.00	N I	$2s^2 2p^3 \ ^2D_{3/2}$ – $2s^2 2p^2 3d \ ^2D_{5/2}$				1
1165.74	Ca VIII/2	$3s^2 3p \ ^2P_{1/2}$ – $3s \ ^3p^2 \ ^2D_{3/2}$				3
1166.18	Fe VII	$3d4s \ ^3D_1$ – $3d4p \ ^3F_2$				22
1167.45	N I	$2s^2 2p^3 \ ^2D_{5/2}$ – $2s^2 2p^2 3d \ ^2F_{7/2}$	30	21	17	4
1168.06	S I	$3s^2 3p^4 \ ^3P_2$ – $3s^2 3p^3 3d \ ^1D_2$	17	12	10	4
1168.33	N I	$2s^2 2p^3 \ ^2D_{3/2}$ – $2s^2 2p^2 3d \ ^4P_{5/2}$				1
1168.54	N I	$2s^2 2p^3 \ ^2D_{3/2}$ – $2s^2 2p^2 3d \ ^2F_{5/2}$	82	39	204	1
1168.55	Fe II	$3d^6 4s \ ^4H_{11/2}$ – $3d^5 4s \ ^4p \ ^2H_{9/2}$				1
1168.68	He I/2	$1s^2 \ ^1S_0$ – $1s \ ^2p \ ^1P_1$	*2606	*1443	*10617	1
1169.69	N I ?	$2s^2 2p^3 \ ^2D_{5/2}$ – $2s^2 2p^2 3d \ ^4F_{7/2}$	18	13	7.1	4
1170.18			24	18		3

Table 1—Continued

λ_{obs} Å	Line	Transition	L_{QS}^{peak} mW	L_{CH}^{peak} (sr m ² Å) ⁻¹	L_{SS}^{peak} (sr m ² Å) ⁻¹	Ref.
1171.60	Ar VII/2	$3s^2 \ ^1S_0$ – $3s \ 3p \ ^1P_1$				0
1171.95	(d)		37	25	21	0
1174.88	C III	$2s \ 2p \ ^3P_1$ – $2p^2 \ ^3P_2$	184	112	389	1
1175.24	C III	$2s \ 2p \ ^3P_0$ – $2p^2 \ ^3P_1$	150	96	319	1
1175.59	C III	$2s \ 2p \ ^3P_1$ – $2p^2 \ ^3P_1$	334	319	1218	1
1175.74	C III	$2s \ 2p \ ^3P_2$ – $2p^2 \ ^3P_2$	559	319	1218	1
1175.98	C III	$2s \ 2p \ ^3P_1$ – $2p^2 \ ^3P_0$	166	98	289	1
1176.37	C III	$2s \ 2p \ ^3P_2$ – $2p^2 \ ^3P_1$	178	105	346	1
1177.67	N I	$2s^2 \ 2p^3 \ ^2D_{3/2}$ – $2s^2 \ 2p^2 \ ^2P_{1/2}$	21	13	17	4
1178.04	Si III	$3p^2 \ ^3P_2$ – $3s \ 5p \ ^3P_2$	24	16	15	4
1181.59	S I	$3s^2 \ 3p^4 \ ^1D_2$ – $3s^2 \ 3p^3 \ ^5D_1$	21	14	11	4
1183.45	N I ?	$2s^2 \ 2p^3 \ ^2D_{3/2}$ – $2s^2 \ 2p^2 \ ^4P_{5/2}$	19	12	11	4
1183.83	Fe II	$3d^6 \ 4s \ ^4D_{7/2}$ – $3d^5 \ 4s \ 4p \ ^4F_{9/2}$	20	13	10	4
1185.31					12	3
1185.71	Fe II ?	$3d^7 \ ^4F_{7/2}$ – $3d^6 \ 4p \ ^4D_{5/2}$	19	13	7.9	4
1187.42	Fe II	$3d^6 \ 4s \ ^4D_{7/2}$ – $3d^5 \ 4s \ 4p \ ^2G_{9/2}$	18	11	11	4
1188.83	C I	$2s^2 \ 2p^2 \ ^3P_0$ – $2s^2 \ 2p \ 4d \ ^3P_1$	24	16	30	4
1189.00	C I	$2s^2 \ 2p^2 \ ^3P_0$ – $2s^2 \ 2p \ 4d \ ^3P_1$	26	17	42	4
1189.24	C I	$2s^2 \ 2p^2 \ ^3P_1$ – $2s^2 \ 2p \ 4d \ ^3P_2$	26	16	36	4
1189.45	C I	$2s^2 \ 2p^2 \ ^3P_2$ – $2s^2 \ 2p \ 4d \ ^3P_1$	25	16	34	4
1189.63	C I	$2s^2 \ 2p^2 \ ^3P_2$ – $2s^2 \ 2p \ 4d \ ^3P_2$	27	17	55	4
1189.84	Mg VII	$2s^2 \ 2p^2 \ ^3P_1$ – $2s^2 \ 2p^2 \ ^1S_0$	21	14	129	0
1190.10	Mg VI	$2s^2 \ 2p^3 \ ^4S_{3/2}$ – $2s^2 \ 2p^3 \ ^2P_{3/2}$	25	18	526	0
1190.17	S III	$3s^2 \ 3p^2 \ ^3P_0$ – $3s \ 3p^3 \ ^3D_1$	28	19	526	4
1190.42	Si II	$3s^2 \ 3p \ ^2P_{1/2}$ – $3s \ 3p^2 \ ^2P_{3/2}$	98	55	183	4
1190.92			23	14	18	3
1191.68	Mg VI	$2s^2 \ 2p^3 \ ^4S_{3/2}$ – $2s^2 \ 2p^3 \ ^2P_{1/2}$	22	14	135	0
1191.84	C I	$2s^2 \ 2p^2 \ ^3P_2$ – $2s^2 \ 2p \ 4d \ ^1F_3$	25	16	65	4
1193.00	C I	$2s^2 \ 2p^2 \ ^3P_1$ – $2s^2 \ 2p \ 4d \ ^3D_2$	39	25	77	4
1193.24	C I	$2s^2 \ 2p^2 \ ^3P_2$ – $2s^2 \ 2p \ 4d \ ^3D_3$			4	
1193.26	C I	$2s^2 \ 2p^2 \ ^3P_1$ – $2s^2 \ 2p \ 4d \ ^3D_1$			4	
1193.29	Si II	$3s^2 \ 3p \ ^2P_{1/2}$ – $3s \ 3p^2 \ ^2P_{1/2}$	67	42	136	4
1193.68	C I	$2s^2 \ 2p^2 \ ^3P_1$ – $2s^2 \ 2p \ 5s \ ^3P_2$	32	20	59	0
1193.98	Ca VIII/2	$3s^2 \ 3p \ ^2P_{3/2}$ – $3s \ 3p^2 \ ^2D_{5/2}$			0	
1194.04	S III	$3s^2 \ 3p^2 \ ^3P_1$ – $3s \ 3p^3 \ ^3D_2$	44	30	117	0
1194.49	C I	$2s^2 \ 2p^2 \ ^3P_2$ – $2s^2 \ 2p \ 4d \ ^3F_3$	115	68	231	4
1194.40	S III	$3s^2 \ 3p^2 \ ^3P_1$ – $3s \ 3p^3 \ ^3D_1$			4	

Table 1—Continued

λ_{obs} Å	Line	Transition	L_{QS}^{peak} mW	L_{CH}^{peak} (sr m ² Å) ⁻¹	L_{SS}^{peak} (sr m ² Å) ⁻¹	Ref.
1194.50	Si II	$3s^2 3p \ ^2P_{3/2} - 3s 3p^2 \ ^2P_{3/2}$				4
1196.22	S X	$2s^2 2p^3 \ ^4S_{3/2} - 2s^2 2p^3 \ ^2D_{5/2}$	27	15	25	0
1197.40	Si II	$3s^2 3p \ ^2P_{3/2} - 3s 3p^2 \ ^2P_{3/2}$	65	41	118	4
1199.19	O III/2	$2s^2 2p^2 \ ^1D_2 - 2s 2p^3 \ ^1D_2$				0
1199.20	S V	$3s^2 \ ^1S_0 - 3s 3p \ ^3P_1$	65	43	551	0
1199.55	N I	$2s^2 2p^3 \ ^4S_{3/2} - 2s^2 2p^2 3s \ ^4P_{5/2}$	117	75	124	4
1200.22	N I	$2s^2 2p^3 \ ^4S_{3/2} - 2s^2 2p^2 3s \ ^4P_{3/2}$	103	64	110	4
1200.71	N I	$2s^2 2p^3 \ ^4S_{3/2} - 2s^2 2p^2 3s \ ^4P_{1/2}$	84	56	81	4
1200.99	S III	$3s^2 3p^2 \ ^3P_2 - 3s 3p^3 \ ^3D_3$	67	45	140	4
1201.47			40	26	44	3
1201.73	S III	$3s^2 3p^2 \ ^3P_2 - 3s 3p^3 \ ^3D_2$	32	21	56	4
1202.00			42	27	53	3
1202.69			43	30	45	3
1203.41			50	31	69	3
1204.30	S V	$3s^2 \ ^1S_0 - 3s 3p \ ^3P_1$	70	45	63	0
1204.33	S I	$3s^2 3p^4 \ ^3P_2 - 3s^2 3p^3 15d \ ^3D_3$				0
1205.57	S I	$3s^2 3p^4 \ ^3P_2 - 3s^2 3p^3 14d \ ^3D_3$	60	33	65	4
1206.51	Si III	$3s^2 \ ^1S_0 - 3s 3p \ ^1P_1$	2391	1318	8487	0
1207.00			77	52	72	3
1207.76	S I	$3s^2 3p^4 \ ^3P_2 - 3s^2 3p^3 13d \ ^3S_1$	55	41	62	4
1208.32	Si XI	$2s 2p \ ^1P_1 - 2p^2 \ ^1D_2$				5
1208.39	Fe VII	$3d 4s \ ^3D_2 - 3d 4p \ ^3D_2$	62	40	87	5
1208.88	S I	$3s^2 3p^4 \ ^3P_2 - 3s^2 3p^3 12d \ ^3D_3$	78	58	813	4
1208.94	H ₂	1 - 5 Q3 (C-X)	78	58	813	4
1209.20			70	49	80	3
1210.18	S I	$3s^2 3p^4 \ ^3P_1 - 3s^2 3p^3 15d \ ^3D_2$	78	55	81	3
1211.22	S I	$3s^2 3p^4 \ ^3P_2 - 3s^2 3p^3 11d \ ^3D_3$	117	87	109	3
1213.00	S X	$2s^2 2p^3 \ ^4S_{3/2} - 2s^2 2p^3 \ ^2D_{3/2}$	269	171	264	0
1215.66	H I Ly 1	$1s \ ^2S_{1/2} - 2p \ ^2P_{3/2,1/2}$	73912	36942	147390	0
1218.34	O V	$2s^2 \ ^1S_0 - 2s 2p \ ^3P_1$	464	395	5667	0
1219.59	Mg X/2	$2s \ ^2S_{1/2} - 2p \ ^2P_{3/2}$				0
1224.50	S I	$3s^2 3p^4 \ ^3P_2 - 3s^2 3p^3 8d \ ^3D_3$	60	43	57	4
1228.06			44	31	38	3
1229.61	S I	$3s^2 3p^4 \ ^3P_2 - 3s^2 3p^3 9s \ ^3S_1$	33	22	30	4
1230.47	S I	$3s^2 3p^4 \ ^3P_1 - 3s^2 3p^3 8d \ ^3D_2$	28	20	24	4
1234.14	S II	$3s^2 3p^3 \ ^2P_{3/2} - 3s 3p^4 \ ^2P_{3/2}$	23	15	20	4
1235.62	S I	$3s^2 3p^4 \ ^3P_1 - 3s^2 3p^3 9s \ ^3S_1$	21	15	15	4

Table 1—Continued

λ_{obs} Å	Line	Transition	L_{QS}^{peak} mW	L_{CH}^{peak} (sr m ² Å) ⁻¹	L_{SS}^{peak} (sr m ² Å) ⁻¹	Ref.
1237.02			23	16	16	3
1238.82	N V	$2s\ ^2S_{1/2}$ – $2p\ ^2P_{3/2}$	218	134	2356	0
1239.89	Fe II	$3d^64s\ ^2H_{9/2}$ – $3d^54s4p\ ^2H_{9/2}$				4
1239.93	Mg II	$2p^63s\ ^2S_{1/2}$ – $2p^64p\ ^2P_{3/2}$	18	13	14	4
1240.39	Mg II	$2p^63s\ ^2S_{1/2}$ – $2p^64p\ ^2P_{1/2}$	19	13		4
1241.95	Fe XII	$3s^23p^3\ ^4S_{3/2}$ – $3s^23p^3\ ^2P_{3/2}$	31	17	46	0
1242.24	C I	$2s^22p^2\ ^1D_2$ – $2s^22p\ 24d\ ^1F_3$	20	12	17	4
1242.80	N V	$2s\ ^2S_{1/2}$ – $2p\ ^2P_{1/2}$	137	68	1211	0
1243.18	N I	$2s^22p^3\ ^2D_{5/2}$ – $2s^22p^23s\ ^2D_{5/2}$	39	24	23	4
1243.31	N I	$2s^22p^3\ ^2D_{3/2}$ – $2s^22p^23s\ ^2D_{3/2}$				4
1243.52	C I	$2s^22p^2\ ^1D_2$ – $2s^22p\ 20d\ ^1F_3$	24	15	15	4
1243.78	C I	$2s^22p^2\ ^1D_2$ – $2s^22p\ 22d\ ^3F_3$	14	9.2	13	4
1244.00	C I	$2s^22p^2\ ^1D_2$ – $2s^22p\ 19d\ ^1F_3$	23	15	25	4
1244.51	C I	$2s^22p^2\ ^1D_2$ – $2s^22p\ 18d\ ^1F_3$	28	17		4
1244.99	C I	$2s^22p^2\ ^1D_2$ – $2s^22p\ 19d\ ^3F_3$	18	11		4
1245.18	C I	$2s^22p^2\ ^1D_2$ – $2s^22p\ 17d\ ^1F_3$	25	16		4
1245.53	C I	$2s^22p^2\ ^1D_2$ – $2s^22p\ 18d\ ^3F_3$	17	11		4
1245.94	C I	$2s^22p^2\ ^1D_2$ – $2s^22p\ 16d\ ^1F_3$	30	19	16	4
1246.17	C I	$2s^22p^2\ ^1D_2$ – $2s^22p\ 17d\ ^3F_3$	17	11	11	4
1246.87	C I	$2s^22p^2\ ^1D_2$ – $2s^22p\ 15d\ ^1F_3$	37	23	39	4
1247.16	S I	$3s^23p^4\ ^3P_2$ – $3s^23p^36d\ ^3D_3$	28	19	11	4
1247.41	C III	$2s\ 2p\ ^1P_1$ – $2p^2\ ^1S_0$	15	9.4	23	0
1247.86	C I	$2s^22p^2\ ^1D_2$ – $2s^22p\ 15d\ ^3F_3$	31	21	34	4
1248.00	C I	$2s^22p^2\ ^1D_2$ – $2s^22p\ 14d\ ^1F_3$	35	24	38	4
1248.88						4
1249.00	C I	$2s^22p^2\ ^1D_2$ – $2s^22p\ 14d\ ^3F_3$	26	16	31	4
1249.40	Si X/2	$2s^22p\ ^2P_{3/2}$ – $2s\ 2p^2\ ^4P_{5/2}$				0
1249.41	C I	$2s^22p^2\ ^1D_2$ – $2s^22p\ 13d\ ^1F_3$				4
1249.90	Mg X/2	$2s\ ^2S_{1/2}$ – $2p\ ^2P_{1/2}$				*1880
1250.09	Si II	$3s\ 3p^2\ ^2D_{3/2}$ – $3p^3\ ^2D_{3/2}$	17	6.7	86	4
1250.41	Si II	$3s\ 3p^2\ ^2D_{5/2}$ – $3p^3\ ^2D_{5/2}$				4
1250.42	C I	$2s^22p^2\ ^1D_2$ – $2s^22p\ 13d\ ^3F_3$				4
1250.58	S II	$3s^23p^3\ ^4S_{3/2}$ – $3s\ 3p^4\ ^4P_{1/2}$	49	28	24	4
1251.16	Si II	$3s\ 3p^2\ ^4P_{5/2}$ – $3p^3\ ^4S_{3/2}$	48	30	69	4
1251.17	C I	$2s^22p^2\ ^1D_2$ – $2s^22p\ 12d\ ^1F_3$				4
1251.48	Si V ?	$2s^22p^53p\ ^3P_2$ – $2s^22p^53p\ ^3D_3$	9.6	6.1	41	5
1251.76	Si V ?	$2s^22p^53p\ ^1P_1$ – $2s^22p^53p\ ^3P_1$	8.6	5.1	28	5

Table 1—Continued

λ_{obs} Å	Line	Transition	L_{QS}^{peak} mW	L_{CH}^{peak} (sr m ² Å) ⁻¹	L_{SS}^{peak} (sr m ² Å) ⁻¹	Ref.
1252.21	C I	$2s^2 2p^2 {}^1D_2 - 2s^2 2p 12d {}^3F_3$	32	20	38	4
1253.32	S I	$3s^2 3p^4 {}^3P_1 - 3s^2 3p^3 6d {}^3D_2$				4
1253.47	C I	$2s^2 2p^2 {}^1D_2 - 2s^2 2p 11d {}^1F_3$	48	32	85	4
1253.80	S II	$3s^2 3p^3 {}^4S_{3/2} - 3s 3p^4 {}^4P_{3/2}$	81	47	48	4
1254.11	H ₂	1 - 6 Q3 (C-X)	9.3	6.5	137	3
1254.51	C I	$2s^2 2p^2 {}^1D_2 - 2s^2 2p 11d {}^3F_3$	33	21	45	4
1255.28	Si I	$3s^2 3p^2 {}^3P_0 - 3s 3p^3 {}^3S_1$	35	24	18	4
1255.34						4
1256.09	S I	$3s^2 3p^4 {}^3P_0 - 3s^2 3p^5 6d {}^3D_1$	15	10	6.8	4
1256.49	Si I	$3s^2 3p^2 {}^3P_1 - 3s 3p^3 {}^3S_1$	97	63	109	4
1256.50	C I	$2s^2 2p^2 {}^1D_2 - 2s^2 2p 10d {}^1F_3$				4
1257.24					21	3
1257.58	C I	$2s^2 2p^2 {}^1D_2 - 2s^2 2p 10d {}^3F_3$	41	26	53	4
1257.87	H ₂ ?	1 - 3 R3 (X-B)	13	9.6	24	3
1258.78	Si I	$3s^2 3p^2 {}^3P_2 - 3s 3p^3 {}^3S_1$	104	68	61	4
1259.53	S II	$3s^2 3p^3 {}^4S_{3/2} - 3s 3p^4 {}^4P_{5/2}$				4
1259.54	O V/2	$2s^2 {}^1S_0 - 2s 2p {}^1P_1$	*3657	*2086	*122284	0
1260.44	Si II	$3s^2 3p {}^2P_{1/2} - 3s^2 3d {}^2D_{3/2}$	193	110	303	4
1260.53	Fe II	$3d^6 4s {}^6D_{9/2} - 3d^5 4s 4p {}^6P_{7/2}$				4
1260.61	C I	$2s^2 2p^2 {}^1D_2 - 2s^2 2p 9d {}^1F_3$	84	56	155	4
1260.94	C I	$2s^2 2p^2 {}^3P_1 - 2s^2 2p 9d {}^3P_0$	26	18	78	4
1261.11	Ca VII/2	$3s^2 3p^2 {}^3P_1 - 3s 3p^3 {}^3D_2$				0
1261.12	C I	$2s^2 2p^2 {}^3P_1 - 2s^2 2p 3d {}^3P_2$				4
1261.43	C I	$2s^2 2p^2 {}^3P_2 - 2s^2 2p 3d {}^3P_1$				4
1261.55	C I	$2s^2 2p^2 {}^3P_2 - 2s^2 2p 3d {}^3P_2$	31	20	93	4
1261.64	Mg VI	$2p^2 3p {}^4D_{5/2} - 2p^2 3d {}^4F_{7/2}$	46	30	123	3
1261.72	C I	$2s^2 2p^2 {}^1D_2 - 2s^2 2p 9d {}^3F_3$				4
1262.21	Fe II	$3d^7 {}^4P_{3/2} - 3d^6 4p {}^4D_{5/2}$	10	6.5	7.9	4
1262.86	S I	$3s^2 3p^4 {}^3P_2 - 3s^2 3p^3 7s {}^3S_1$	20	14	9.6	4
1264.74	Si II	$3s^2 3p {}^2P_{3/2} - 3s^2 3d {}^2D_{5/2}$	479	262	665	4
1265.00	Si II	$3s^2 3p {}^2P_{3/2} - 3s^2 3d {}^2D_{3/2}$	206	133	256	4
1265.65	Fe II	$3d^6 4s {}^4G_{9/2} - 3d^5 4s 4p {}^4H_{11/2}$	14	9.8	15	4
1265.78	Fe II	$3d^7 {}^2H_{9/2} - 3d^6 4p {}^2G_{7/2}$				4
1266.27	C I	$2s^2 2p^2 {}^1D_2 - 2s^2 2p 8d {}^1P_1$	46	31	60	4
1266.37	Mg VI	$2p^2 3p {}^4D_{7/2} - 2p^2 3d {}^4F_{7/2}$	78	49	157	3
1266.42	C I	$2s^2 2p^2 {}^1D_2 - 2s^2 2p 8d {}^1F_3$	78	49	157	4
1266.67	Fe II	$3d^6 4s {}^6D_{7/2} - 3d^5 4s 4p {}^6P_{7/2}$	21	13	17	4

Table 1—Continued

λ_{obs} Å	Line	Transition	L_{QS}^{peak} mW	L_{CH}^{peak} (sr m ² Å) ⁻¹	L_{SS}^{peak} (sr m ² Å) ⁻¹	Ref.
1267.55	Mg VI	$2p^2 3p \ ^4D_{3/2} - 2p^2 3d \ ^4F_{3/2}$			63	3
1267.60	C I	$2s^2 2p^2 \ ^1D_2 - 2s^2 2p 8d \ ^3F_3$	50	32		4
1267.76	Ca VI/2	$3s^2 3p^3 \ ^4S_{3/2} - 3s 3p^4 \ ^4P_{3/2}$				3
1268.12	Fe II	$3d^7 \ ^4P_{5/2} - 3d^5 4s 4p \ ^4F_{5/2}$	11	8.2	4.9	4
1269.06	(a)/2					3
1269.21	S I	$3s^2 3p^4 \ ^3P_1 - 3s^2 3p^3 7s \ ^3S_1$	10	7.3	7.6	4
1270.14	C I	$2s^2 2p^2 \ ^3P_0 - 2s^2 2p 3d \ ^1P_1$	13	8.8	5.8	4
1270.41	C I	$2s^2 2p^2 \ ^3P_1 - 2s^2 2p 3d \ ^1P_1$	12	9.0	6.7	4
1270.78	S I	$3s^2 3p^4 \ ^3P_2 - 3s^2 3p^3 5d \ ^3D_3$	57	38	23	4
1271.23	Mg II	$2p^6 3p \ ^2P_{1/2} - 2p^6 8d \ ^2D_{3/2}$	10	7.2	7.0	4
1271.93	H ₂	1 - 3 P5 (X-B)				4
1271.94	Mg II	$2p^6 3p \ ^2P_{1/2} - 2p^6 9s \ ^2S_{1/2}$	13	10	23	4
1271.98	Fe II	$3d^6 4s \ ^6D_{5/2} - 3d^5 4s 4p \ ^6P_{5/2}$				4
1271.98	C II/2	$2s^2 2p \ ^2P_{1/2} - 2s^2 4s \ ^2S_{1/2}$				1
1272.08	S I	$3s^2 3p^4 \ ^3P_0 - 3s^2 3p^3 7s \ ^3S_1$	14	10	25	4
1272.18	N IV ?	$2s 3p \ ^3P_1 - 2p 3p \ ^3D_2$	14	10	25	3
1272.66	Fe II	$3d^6 4s \ ^6D_{5/2} - 3d^5 4s 4p \ ^6P_{3/2}$	16	11	8.7	4
1274.11	C I	$2s^2 2p^2 \ ^3P_2 - 2s^2 2p 3d \ ^1F_3$	23	16	20	4
1274.76	C I	$2s^2 2p^2 \ ^1D_2 - 2s^2 2p 7d \ ^1P_1$	43	27	47	4
1274.95	Ar VII/2	$3s 3p \ ^3P_1 - 3p^2 \ ^3P_1$				3
1274.98	C I	$2s^2 2p^2 \ ^1D_2 - 2s^2 2p 7d \ ^1F_3$	85	53	175	4
1275.29	C I	$2s^2 2p^2 \ ^1D_2 - 2s^2 2p 7d \ ^3D_3$	23	16	17	4
1275.35	Fe II	$3d^7 \ ^4P_{1/2} - 3d^6 5p \ ^4P_{1/2}$				4
1275.81	Fe II	$3d^7 \ ^2D_{5/2} - 3d^6 4p \ ^2F_{7/2}$	19	12	10	4
1276.22	C I	$2s^2 2p^2 \ ^1D_2 - 2s^2 2p 8s \ ^3P_1$				4
1276.29	C I	$2s^2 2p^2 \ ^1D_2 - 2s^2 2p 7d \ ^3F_3$	56	36	67	4
1276.48	C I	$2s^2 2p^2 \ ^3P_0 - 2s^2 2p 4s \ ^1P_1$	21	14	15	4
1276.75	C I	$2s^2 2p^2 \ ^3P_1 - 2s^2 2p 4s \ ^1P_1$	24	16	22	4
1276.80	Fe II	$3d^7 \ ^4P_{1/2} - 3d^6 5p \ ^4P_{3/2}$				4
1277.24	C I	$2s^2 2p^2 \ ^3P_1 - 2s^2 2p 3d \ ^3D_1$				4
1277.28	C I	$2s^2 2p^2 \ ^3P_1 - 2s^2 2p 3d \ ^3D_2$	43	27	79	4
1277.55	C I	$2s^2 2p^2 \ ^3P_2 - 2s^2 2p 3d \ ^3D_3$	46	29	82	4
1277.64	Fe II	$3d^6 4s \ ^6D_{1/2} - 3d^5 4s 4p \ ^6P_{3/2}$				4
1277.72	C I	$2s^2 2p^2 \ ^3P_2 - 2s^2 2p 3d \ ^3D_2$	41	26	57	4
1277.88	Si X/2	$2s^2 2p \ ^2P_{3/2} - 2s 2p^2 \ ^4P_{3/2}$				0
1277.95	C I	$2s^2 2p^2 \ ^3P_2 - 2s^2 2p 3d \ ^3D_1$	35	23	37	4
1278.36	Ca VII/2	$3s^2 3p^2 \ ^3P_2 - 3s 3p^3 \ ^3D_3$			*535	0

Table 1—Continued

λ_{obs} Å	Line	Transition	L_{QS}^{peak} mW	L_{CH}^{peak} (sr m ² Å) ⁻¹	L_{SS}^{peak} (sr m ² Å) ⁻¹	Ref.
1279.06	C I	$2s^2 2p^2 {}^3P_1$ – $2s^2 2p 3d {}^3F_2$	35	23	37	4
1279.23	C I	$2s^2 2p^2 {}^3P_2$ – $2s^2 2p 3d {}^3F_3$	38	24	50	4
1279.50	C I	$2s^2 2p^2 {}^3P_2$ – $2s^2 2p 3d {}^3F_2$	35	24	33	4
1279.89	C I	$2s^2 2p^2 {}^3P_1$ – $2s^2 2p 4s {}^3P_2$	37	24	37	4
[1280.10	S I	$3s^2 3p^4 {}^3P_0$ – $3s^2 3p^3 5d {}^3D_1$	38	26	31	4
1280.13	C I	$2s^2 2p^2 {}^3P_0$ – $2s^2 2p 4s {}^3P_1$			4	
[1280.33	C I	$2s^2 2p^2 {}^3P_2$ – $2s^2 2p 4s {}^3P_2$	39	26	56	4
1280.40	C I	$2s^2 2p^2 {}^3P_1$ – $2s^2 2p 4s {}^3P_1$			4	
1280.60	C I	$2s^2 2p^2 {}^3P_1$ – $2s^2 2p 4s {}^3P_0$	34	23	31	4
1280.85	C I	$2s^2 2p^2 {}^3P_2$ – $2s^2 2p 4s {}^3P_1$	31	21	34	4
1283.06	Fe II	$3d^7 {}^2H_{11/2}$ – $3d^6 4p {}^2H_{11/2}$	15	10	7.7	4
1283.92	Ca VI/2	$3s^2 3p^3 {}^4S_{3/2}$ – $3s 3p^4 {}^4P_{5/2}$			*343	3
1285.49					12	3
1285.69	H ₂	1 - 3 P7 (X-B)	11	8.1	10	4
[643.10	Ca V/2	$3s^2 3p^4 {}^3P_1$ – $3s 3p^5 {}^3P_0$			3	
[1286.43	H ₂	3 - 4 P5 (X-B)	12	9.3	9.1	4
1287.21	Ca II	$3d {}^2D_{3/2}$ – $10f {}^2F_{5/2}$	11	8.0	8.6	4
1287.61	C I	$2s^2 2p^2 {}^3P_1$ – $2s^2 2p 3d {}^1D_2$	17	11	5.6	4
1288.04	C I	$2s^2 2p^2 {}^1D_2$ – $2s^2 2p 6d {}^1P_1$	44	31	37	4
1288.27	O II/2	$2s^2 2p^3 {}^2P_{3/2}$ – $2p 2p^4 {}^2S_{1/2}$			0	
1288.42	C I	$2s^2 2p^2 {}^1D_2$ – $2s^2 2p 6d {}^1F_3$	96	63	182	4
1288.71	C I	$2s^2 2p^2 {}^1D_2$ – $2s^2 2p 7s {}^1P_1$	35	22	21	4
1288.92	C I	$2s^2 2p^2 {}^1D_2$ – $2s^2 2p 6d {}^3D_3$	31	20	21	4
1289.31	Fe II	$3d^6 4s {}^4P_{5/2}$ – $3d^5 4s 4p {}^4D_{7/2}$	12	8.4	5.2	4
[1289.89	C I	$2s^2 2p^2 {}^1D_2$ – $2s^2 2p 7s {}^3P_1$			4	
[1289.98	C I	$2s^2 2p^2 {}^1D_2$ – $2s^2 2p 6d {}^3F_3$	56	39	62	4
1291.30	C I	$2s^2 2p^2 {}^1D_2$ – $2s^2 2p 6d {}^1D_2$	29	20	18	4
1291.58	Fe II	$3d^7 {}^4P_{5/2}$ – $3d^6 4p {}^4P_{3/2}$	14	9.8	7.9	4
1292.42	Fe II	$3d^7 {}^4P_{3/2}$ – $3d^6 5p {}^4D_{3/2}$	12	9.3	4.6	4
1293.14	Ca V/2	$3s^2 3p^4 {}^3P_2$ – $3s 3p^5 {}^3P_2$			*149	0
1293.88	Mg V ?	$2s^2 2p^4 {}^3P_2$ – $2s^2 2p^4 {}^1S_0$			7.2	5
1294.58	Si III	$3s 3p {}^3P_1$ – $3p^2 {}^3P_2$	22	11	88	0
1294.91	Fe II	$3d^7 {}^4P_{3/2}$ – $3d^6 4p {}^4P_{3/2}$	12	7.8	4.7	4
1295.65	S I	$3s^2 3p^4 {}^3P_2$ – $3s^2 3p^3 4s {}^3P_2$	57	40	26	4
1296.16	S I	$3s^2 3p^4 {}^3P_2$ – $3s^2 3p^3 4s {}^3P_1$	42	28	21	4
1296.77	Si III	$3s 3p {}^3P_0$ – $3p^2 {}^3P_1$	20	11	78	0
1298.96	Si III	$3s 3p {}^3P_2$ – $3p^2 {}^3P_2$	50	25	263	0

Table 1—Continued

λ_{obs} Å	Line	Transition	L_{QS}^{peak} mW	L_{CH}^{peak} (sr m ² Å) ⁻¹	L_{SS}^{peak}	Ref.
1299.43	Fe II	$3d^7 \ 4P_{3/2} - 3d^6 4p \ 4S_{3/2}$	16	11	12	4
1299.83			13	8.7	7.3	3
1300.91	S I	$3s^2 3p^4 \ 1D_2 - 3s^2 3p^3 5s \ 1D_2$	167	125	104	4
1301.16	Si III	$3s 3p \ 3P_1 - 3p^2 \ 3P_0$	17	10	44	4
1302.17	O I	$2s^2 2p^4 \ 3P_2 - 2s^2 2p^3 3s \ 3S_1$	2234	1318	3650	4
1302.34	S I	$3s^2 3p^4 \ 3P_1 - 3s^2 3p^3 4s \ 3P_2$			4	
1302.87	S I	$3s^2 3p^4 \ 3P_1 - 3s^2 3p^3 4s \ 3P_1$	45	29	18	4
1303.11	S I	$3s^2 3p^4 \ 3P_1 - 3s^2 3p^3 4s \ 3P_0$	38	27	23	4
1303.32	Si III	$3s 3p \ 3P_2 - 3p^2 \ 3P_1$	38	16	99	0
1303.43	S I	$3s^2 3p^4 \ 3P_2 - 3s^2 3p^3 6s \ 3S_1$	38	25	99	4
1304.37	Si II	$3s^2 3p \ 2P_{1/2} - 3s 3p^2 \ 2S_{1/2}$	204	139	222	4
1304.86	O I	$2s^2 2p^4 \ 3P_1 - 2s^2 2p^3 3s \ 3S_1$	2331	1432	3862	4
1305.59	Si II	$3s 3p^2 \ 2D_{5/2} - 3s 3p 3d \ 2F_{7/2}$	23	16	27	4
1306.03	O I	$2s^2 2p^4 \ 3P_0 - 2s^2 2p^3 3s \ 3S_1$	2524	1698	4284	4
1308.13			16	10	3	
1309.28	Si II	$3s^2 3p \ 2P_{3/2} - 3s 3p^2 \ 2S_{1/2}$	325	213	273	4
1310.19	C I	$2s^2 2p^2 \ 1D_2 - 2s^2 2p 5d \ 3P_1$	26	18	10	4
1310.19	S I	$3s^2 3p^4 \ 3P_1 - 3s^2 3p^3 6s \ 3S_1$			4	
1310.54	N I	$2s^2 2p^3 \ 2P_{3/2} - 2s^2 2p^2 3d \ 2D_{5/2}$			4	
1310.64	C I	$2s^2 2p^2 \ 1D_2 - 2s^2 2p 5d \ 1P_1$	48	31	50	4
1310.94	N I	$2s^2 2p^3 \ 2P_{1/2} - 2s^2 2p^2 3d \ 2D_{3/2}$	17	11	7.0	4
1311.36	C I	$2s^2 2p^2 \ 1D_2 - 2s^2 2p 5d \ 1F_3$	92	57	190	4
1311.93	C I	$2s^2 2p^2 \ 1D_2 - 2s^2 2p 6s \ 1P_1$	39	27	36	4
1312.25	C I	$2s^2 2p^2 \ 1D_2 - 2s^2 2p 5d \ 3D_3$	32	21	30	4
1312.59	Si III	$3s 3p \ 1P_1 - 3s 4s \ 1S_0$	17	10	29	4
1312.85	C I	$2s^2 2p^2 \ 1D_2 - 2s^2 2p 5d \ 3D_1$	13	9.2	4.6	4
1313.25	S I	$3s^2 3p^4 \ 3P_0 - 3s^2 3p^3 6s \ 3S_1$	22	15	9.7	4
1313.39	C I	$2s^2 2p^2 \ 1D_2 - 2s^2 2p 6s \ 3P_1$			4	
1313.46	C I	$2s^2 2p^2 \ 1D_2 - 2s^2 2p 5d \ 3F_3$	54	37	77	4
1314.67	S IV/2	$3s^2 3p \ 2P_{1/2} - 3s^2 3d \ 2D_{3/2}$			*275	1
1315.92	C I	$2s^2 2p^2 \ 1D_2 - 2s^2 2p 5d \ 1D_2$	47	29	57	4
1316.54	S I	$3s^2 3p^4 \ 3P_2 - 3s^2 3p^3 4d \ 3D_3$	109	73	61	4
1316.62	S I	$3s^2 3p^4 \ 3P_2 - 3s^2 3p^3 4d \ 3D_2$			4	
1317.22	Ni II	$3d^9 \ 2D_{5/2} - 3d^8 4p \ 2F_{7/2}$	56	37	17	4
1317.84					10	3
1318.98	N I	$2s^2 2p^3 \ 2P_{1/2} - 2s^2 2p^2 3d \ 2P_{1/2}$	154	120	105	4
1319.68	N I	$2s^2 2p^3 \ 2P_{3/2} - 2s^2 2p^2 3d \ 2P_{3/2}$			4	

Table 1—Continued

λ_{obs} Å	Line	Transition	L_{QS}^{peak} mW	L_{CH}^{peak} (sr m ² Å) ⁻¹	L_{SS}^{peak} (sr m ² Å) ⁻¹	Ref.
1319.76	S V/2	$3s\ 3p\ ^3P_1 - 3s\ 3d\ ^3D_2$				0
1322.24	Mn XII	$3s^2\ 3p^2\ ^3P_1 - 3s^2\ 3p^2\ ^1S_0$	14	9.7	7.9	5
1322.84	S IV/2	$3s^2\ 3p\ ^2P_{3/2} - 3s^2\ 3d\ ^2D_{5/2}$			*419	1
1323.52	S I	$3s^2\ 3p^4\ ^3P_1 - 3s^2\ 3p^3\ (^4S)4d\ ^3D_2$	71	48	30	4
1323.91	C II	$2s\ 2p^2\ ^2D_{3/2} - 2p^3\ ^2D_{3/2}$				4
1323.95	C II	$2s\ 2p^2\ ^2D_{5/2} - 2p^3\ ^2D_{5/2}$	22	12	14	4
1324.59	Mg V	$2s^2\ 2p^4\ ^3P_1 - 2s^2\ 2p^4\ ^1S_0$	13	9.7	121	0
1326.40	S V/2	$3s\ 3p\ ^3P_2 - 3s\ 3d\ ^3D_3$			*235	1
1326.63	S I	$3s^2\ 3p^4\ ^3P_0 - 3s^2\ 3p^3\ 4d\ ^3D_1$	53	35	19	4
1327.92	N I	$2s^2\ 2p^3\ ^2P_{1/2} - 2s^2\ 2p^2\ ^2F_{1/2}$	15	10	2.9	4
1328.83	C I	$2s^2\ 2p^2\ ^3P_0 - 2s\ 2p^3\ ^3P_1$	79	49	109	4
1329.10	C I	$2s^2\ 2p^2\ ^3P_1 - 2s\ 2p^3\ ^3P_{2,1,0}$	81	50	127	4
1329.58	C I	$2s^2\ 2p^2\ ^3P_2 - 2s\ 2p^3\ ^3P_{2,1}$	74	49	110	4
1330.95	Fe II	$3d^6\ 4s\ ^2F_{7/2} - 3d^5\ 4s\ 4p\ ^2D_{5/2}$	17	11	9.9	4
1333.47			16	11	13	3
1333.79	S I	$3s^2\ 3p^4\ ^3P_2 - 3s^2\ 3p^3\ 4d\ ^5D_3$	22	15	15	4
1334.53	C II	$2s^2\ 2p\ ^2P_{1/2} - 2s\ 2p^2\ ^2D_{3/2}$	2957	1430	3150	4
1335.20	Ni II	$3d^9\ ^2D_{3/2} - 3d^8\ 4p\ ^2F_{5/2}$	46	32	18	4
1335.71	C II	$2s^2\ 2p\ ^2P_{3/2} - 2s\ 2p^2\ ^2D_{5/2}$	3530	1759	4600	4
1337.84			20	13	12	4
1338.57	H ₂	0 - 4 P2 (X-B)	18	13	25	4
1338.61	O IV	$2s\ 2p^2\ ^2P_{1/2} - 2p^3\ ^2D_{3/2}$				4
1339.57			17	11	9.3	3
1340.39	Ni II	$3d^8\ 4p\ ^2F_{7/2} - 3d^8\ 6d\ ^2H_{9/2}$	17	11	4.6	4
1341.20			21	15	8.7	3
1342.28			23	16	16	3
1342.90			16	12	21	3
1343.64			16	10	21	3
1345.16			17	12	9.9	3
1345.51					9.8	3
1345.95	Ni II ?	$3d^9\ ^2D_{5/2} - 3d^8\ 4p\ ^4S_{3/2}$	17	12	4.6	4
1347.06			21	13	23	3
1348.79			19	12	11	3
1349.43	Fe XII	$3s^2\ 3p^3\ ^4S_{3/2} - 3s^2\ 3p^3\ ^2P_{1/2}$	20	12	39	0
1350.12					8.0	3
1351.66	Cl I	$3s^2\ 3p^5\ ^2P_{1/2} - 3s^2\ 3p^4\ 4s\ ^2P_{1/2}$	313	194	130	4
1353.02	Si IX/2	$2s^2\ 2p^2\ ^3P_1 - 2s\ 2p^3\ ^5S_2$				3

Table 1—Continued

λ_{obs} Å	Line	Transition	L_{QS}^{peak} mW	L_{CH}^{peak} (sr m ² Å) ⁻¹	L_{SS}^{peak}	Ref.
1354.29	C I	$2s^2 2p^2 \ ^1D_2 - 2s^2 2p \ 4d \ ^1P_1$	55	36	53	4
1354.80			23	14	9.9	3
1355.60	O I	$2s^2 2p^4 \ ^3P_2 - 2s^2 2p^3 3s \ ^5S_2$	345	199	297	4
1355.84	C I	$2s^2 2p^2 \ ^1D_2 - 2s^2 2p \ 4d \ ^1F_3$	114	69	262	4
1356.47	H ₂	$0 - 4 R7 \ (X-B)$			12	3
1357.13	C I	$2s^2 2p^2 \ ^1D_2 - 2s^2 2p \ 5s \ ^1P_1$	58	37	58	4
1357.66	C I	$2s^2 2p^2 \ ^1D_2 - 2s^2 2p \ 4d \ ^3D_3$	55	34	37	4
1358.19	C I	$2s^2 2p^2 \ ^1D_2 - 2s^2 2p \ 4d \ ^3D_1$	34	20	12	4
1358.51	O I	$2s^2 2p^4 \ ^3P_1 - 2s^2 2p^3 3s \ ^5S_2$	126	75	82	4
1358.77			40	25		3
1359.28	C I	$2s^2 2p^2 \ ^1D_2 - 2s^2 2p \ 4d \ ^3F_3$	83	52	86	4
1359.44	C I	$2s^2 2p^2 \ ^1D_2 - 2s^2 2p \ 5s \ ^3P_1$				4
1360.17	Fe II	$3d^6 4s \ ^6D_{1/2} - 3d^6 4p \ ^2D_{3/2}$	31	19	33	4
1360.78	Al IX/2	$2s^2 2p \ ^2P_{1/2} - 2s \ 2p^2 \ ^4P_{3/2}$				0
1361.37	Fe II	$3d^7 \ ^4P_{5/2} - 3d^6 4p \ ^4D_{7/2}$	78	45	71	4
1361.40	S III/2	$3s^2 3p^2 \ ^3P_2 - 3s^2 3p \ 3d \ ^3D_3$				1
1362.75	Fe II	$3d^6 4s \ ^4P_{5/2} - 3d^5 4s \ 4p \ ^4P_{5/2}$	24	15	12	4
1363.48	Na IX/2	$2s \ ^2S_{1/2} - 2p \ ^2P_{3/2}$			*284	0
1364.16	C I	$2s^2 2p^2 \ ^1D_2 - 2s^2 2p \ 4d \ ^1D_2$	101	62	142	4
1364.38	Fe II	$3d^7 \ ^4P_{5/2} - 3d^6 4p \ ^4D_{5/2}$	34	22	9.3	4
1364.87	Na V	$2s^2 2p^3 \ ^4S_{3/2} - 2s^2 2p^3 \ ^2P_{3/2}$	22	13	11	3
1365.51	Na V	$2s^2 2p^3 \ ^4S_{3/2} - 2s^2 2p^3 \ ^2P_{1/2}$	22	13	11	3
1366.39	Fe II	$3d^6 4s \ ^4F_{7/2} - 3d^5 4s \ 4p \ ^4P_{5/2}$	28	17		4
1366.43					16	3
1367.23					10	3
1368.09	Fe II	$3d^7 \ ^4P_{3/2} - 3d^6 4p \ ^4D_{5/2}$	53	32	10	4
1368.45						3
1368.57	Fe II	$3d^6 4s \ ^4P_{3/2} - 3d^5 4s \ 4p \ ^4P_{1/2}$	24	17	15	4
1369.55					17	3
1369.71	Fe II	$3d^7 \ ^4P_{5/2} - 3d^6 4p \ ^2F_{7/2}$	29	18	6.3	4
1370.00	N III/2	$2s^2 2p \ ^2P_{1/2} - 2s \ 2p^2 \ ^2P_{3/2}$				1
1370.12	Ni II	$3d^9 \ ^2D_{5/2} - 3d^8 4p \ ^2P_{3/2}$	70	42	21	4
1371.00	N III/2	$2s^2 2p \ ^2P_{1/2} - 2s \ 2p^2 \ ^2P_{1/2}$				1
1371.02	Fe II	$3d^6 4s \ ^4H_{13/2} - 3d^5 4s \ 4p \ ^4G_{11/2}$	37	22	37	4
1371.32	O V	$2s \ 2p \ ^1P_1 - 2p^2 \ ^1D_2$	46	25	889	0
1371.58	N III/2	$2s^2 2p \ ^2P_{3/2} - 2s \ 2p^2 \ ^2P_{3/2}$				1
1372.29	Fe II	$3d^7 \ ^4P_{3/2} - 3d^6 4p \ ^4D_{3/2}$	49	29	8.9	4

Table 1—Continued

λ_{obs} Å	Line	Transition	L_{QS}^{peak} mW (sr m ² Å) ⁻¹	L_{CH}^{peak} mW (sr m ² Å) ⁻¹	L_{SS}^{peak} mW (sr m ² Å) ⁻¹	Ref.
1372.70	N III/2	$2s^2 2p \ ^2P_{3/2} - 2s 2p^2 \ ^2P_{1/2}$				1
1372.92	Fe VIII/2	$3p^5 3d^2 \ ^2P_{3/2} - 3p^6 4d \ ^2D_{5/2}$				17 5
1374.06	C II/2					3
1374.08	Ni II	$3d^9 \ ^2D_{3/2} - 3d^8 4p \ ^2S_{1/2}$	45	28	13	4
1374.69	C II/2	$2s^2 2p \ ^2P_{3/2} - 2s^2 3d \ ^2D_{5/2}$				1
1375.20	Fe II	$3d^6 4s \ ^4H_{11/2} - 3d^5 4s 4p \ ^4G_{9/2}$	33	20	9.3	4
1376.67	Fe II	$3d^7 \ ^4P_{1/2} - 3d^6 4p \ ^4D_{3/2}$	42	25	8.4	4
1378.56	Ni II	$3d^8 4p \ ^2F_{5/2} - 3d^8 6d \ ^2D_{5/2}$	30	19	9.2	4
1379.18	Mg VIII/2	$2s 2p^2 \ ^2P_{3/2} - 2p^3 \ ^2D_{5/2}$				0
1379.47	Fe II	$3d^6 4s \ ^4H_{9/2} - 3d^5 4s 4p \ ^4G_{7/2}$	32	19	12	4
1379.59	Ni II	$3d^8 4s \ ^4P_{3/2} - 3d^7 4s 4p \ ^4D_{5/2}$	55	34	12	4
1380.23			31	18	8.3	3
1381.05	C III/2	$2s 2p \ ^1P_1 - 2s 3s \ ^1S_0$				1
1381.30	Ni II	$3d^9 \ ^2D_{3/2} - 3d^8 4p \ ^2P_{1/2}$	59	39	10	4
1381.55	S I	$3s^2 3p^4 \ ^3P_2 - 3s 3p^5 \ ^3P_1$	38	24	14	4
1382.88	Ca IX/2	$3s^2 \ ^1S_0 - 3s 3p \ ^3P_1$			*137	0
1384.71			28	16	9.7	3
1385.51	S I	$3s^2 3p^4 \ ^3P_1 - 3s 3p^5 \ ^3P_0$	34	20	5.8	4
1385.74					14	3
1386.79					10	3
1387.22	Fe II	$3d^7 \ ^2H_{11/2} - 3d^5 4s 4p \ ^4F_{9/2}$	45	28	10	4
1387.32					3	
1387.98	Mg IX/2	$2s^2 \ ^1S_0 - 2s 2p \ ^3P_2$				0
1388.32	Na IX/2	$2s \ ^2S_{1/2} - 2p \ ^2P_{1/2}$				0
1388.44	S I	$3s^2 3p^4 \ ^3P_2 - 3s 3p^5 \ ^3P_2$				4
1389.44	Si IX/2	$2s^2 2p^2 \ ^3P_2 - 2s 2p^3 \ ^5S_2$				0
1389.56	K XII ?					5
1392.15	Fe II	$3d^7 \ ^2H_{11/2} - 3d^6 4p \ ^2G_{9/2}$	39	24	10	4
1392.59	S I	$3s^2 3p^4 \ ^3P_0 - 3s 3p^5 \ ^3P_1$	38	24	6.8	4
1392.82	Fe II	$3d^7 \ ^2H_{9/2} - 3d^6 4p \ ^2G_{7/2}$	58	34	12	4
1393.33	Ni II	$3d^9 \ ^2D_{5/2} - 3d^8 4p \ ^2D_{5/2}$	67	39	51	4
1393.78	Si IV	$3s \ ^2S_{1/2} - 3p \ ^2P_{3/2}$	809	405	9943	0
1394.28	Fe VIII/2	$3p^6 4p \ ^2P_{1/2} - 3p^6 4d \ ^2D_{3/2}$				5
1396.11	S I	$3s^2 3p^4 \ ^3P_1 - 3s 3p^5 \ ^3P_2$	48	31	20	4
1397.22	O IV	$2s^2 2p \ ^2P_{1/2} - 2s 2p^2 \ ^4P_{3/2}$	34	23	83	0
1398.06	Si IV	$3s^2 3p \ ^2P_{1/2} - 3s 3p^2 \ ^4P_{3/2}$			12	4
1398.78			42	26	8.1	4

Table 1—Continued

λ_{obs} Å	Line	Transition	L_{QS}^{peak} mW	L_{CH}^{peak} (sr m ² Å) ⁻¹	L_{SS}^{peak} (sr m ² Å) ⁻¹	Ref.	
1398.95	H ₂	0 - 5 P2 (X-B)				4	
1399.03	Ni II	$3d^9 2D_{3/2} - 3d^8 4p 2P_{3/2}$	50	32	21	4	
1399.77	O IV	$2s^2 2p 2P_{1/2} - 2s 2p^2 4P_{1/2}$	47	29	428	0	
1399.97	Fe II	$3d^6 4s 4P_{1/2} - 3d^5 4s 4p 6D_{3/2}$	38	22	92	4	
1400.52	Ar VIII/2	$2p^6 3s 2S_{1/2} - 2p^6 3p 2P_{3/2}$				0	
1401.16	O IV	$2s^2 2p 2P_{3/2} - 2s 2p^2 4P_{5/2}$	117	69	2162	0	
1401.51	S I	$3s^2 3p^4 3P_2 - 3s^2 3p^3 5s 3S_1$	66	42	56	4	
1402.77	Si IV	$3s 2S_{1/2} - 3p 2P_{1/2}$	375	229	4016	0	
1404.64	O III/2	$2s^2 2p^2 3P_0 - 2s 2p^3 3P_1$				1	
1404.79	S IV	$3s^2 3p 2P_{1/2} - 3s 3p^2 4P_{1/2}$	85	56	622	0	
1404.82	O IV	$2s^2 2p 2P_{3/2} - 2s 2p^2 4P_{3/2}$				0	
1405.61	Fe II	$3d^7 4F_{9/2} - 3d^6 4p 2F_{7/2}$	79	51	89	4	
1405.64	O III/2	$2s^2 2p^2 3P_1 - 2s 2p^3 3P_0$				1	
1405.80	O III/2	$2s^2 2p^2 3P_1 - 2s 2p^3 3P_2$				1	
1406.04	S IV	$3s^2 3p 2P_{3/2} - 3s 3p^2 4P_{5/2}$	54	32	186	0	
1407.39	O IV	$2s^2 2p 2P_{3/2} - 2s 2p^2 4P_{1/2}$	51	35	394	0	
1407.70	O III/2	$2s^2 2p^2 3P_2 - 2s 2p^3 3P_2$				1	
1409.07	Si II	$3s 3p^2 2D_{3/2} - 3s 3p 3d 2P_{1/2}$	40	24	11	4	
1409.34	S I	$3s^2 3p^4 3P_1 - 3s^2 3p^3 5s 3S_1$	65	42	17	4	
1411.07	Ni II	$3d^9 2D_{3/2} - 3d^8 4p 2D_{3/2}$	83	53	16	4	
1411.30			45	26	12	3	
1411.95	N I	$2s^2 2p^3 2P_{3/2} - 2s^2 2p^2 3s 2D_{5/2}$	63	39	62	4	
1412.10	Mg IX/2	$2s^2 1S_0 - 2s 2p 3P_1$			*317	0	
1412.85	Fe II	$3d^7 4F_{9/2} - 3d^6 4p 4D_{7/2}$	93	58	13	4	
1412.87	Ni II	$3d^9 2D_{5/2} - 3d^8 4p 4D_{7/2}$				4	
1412.87	S I	$3s^2 3p^4 3P_0 - 3s^2 3p^3 5s 3S_1$				4	
1413.02	S VI/2	$2p^6 3p 2P_{1/2} - 2p^6 3d 2D_{3/2}$				4	
1413.65						16	3
1414.30	Ni II	$3d^9 2D_{5/2} - 3d^8 4p 4D_{3/2}$	42	27	6.3	4	
1414.36	S I	$3s^2 3p^4 3P_2 - 3s^2 3p^3 5s 5S_2$				4	
1415.73	Ni II	$3d^9 2D_{5/2} - 3d^8 4p 4D_{5/2}$	53	33	6.6	4	
1415.77	Fe II	$3d^6 4s 4G_{11/2} - 3d^5 4s 4p 2H_{11/2}$				4	
1416.73	Fe II	$3d^7 4F_{7/2} - 3d^6 4p 2F_{7/2}$	46	29	9.1	4	
1416.93	S IV	$3s^2 3p 2P_{3/2} - 3s 3p^2 4P_{3/2}$	48	29	110	4	
1417.70	Ni II	$3d^8 4s 4P_{5/2} - 3d^7 4s 4p 4G_{7/2}$				4	
1417.73	Fe II	$3d^6 4s 4H_{9/2} - 3d^5 4s 4p 4H_{9/2}$	43	29	10	4	
1418.38	Ar V/2	$3s^2 3p^2 3P_1 - 3s 3p^3 3P_2$				1	

Table 1—Continued

λ_{obs} Å	Line	Transition	L_{QS}^{peak} mW	L_{CH}^{peak} (sr m ² Å) ⁻¹	L_{SS}^{peak} (sr m ² Å) ⁻¹	Ref.
1418.85	Fe II	$3d^7 \ ^4F_{9/2} - 3d^6 \ ^4p \ ^4F_{7/2}$	57	38	12	4
1420.89	Fe II	$3d^6 \ ^4s \ ^4H_{7/2} - 3d^5 \ ^4s \ ^4p \ ^4H_{7/2}$	42	24	8.6	4
1421.44	Fe II	$3d^7 \ ^4F_{5/2} - 3d^6 \ ^4p \ ^2P_{3/2}$	41	25	7.6	4
1421.62	(a)/2				0	
1422.54	Fe II	$3d^6 \ ^4s \ ^4F_{3/2} - 3d^6 \ ^4p \ ^4F_{3/2}$	44	27	10	4
1423.21	Ni II	$3d^9 \ ^2D_{3/2} - 3d^8 \ ^4p \ ^2D_{5/2}$	49	32	8.2	4
1423.86	S IV	$3s^2 \ ^3p \ ^2P_{3/2} - 3s \ ^3p^2 \ ^4P_{1/2}$			34	4
1424.07	Fe II	$3d^7 \ ^4F_{7/2} - 3d^6 \ ^4p \ ^4F_{9/2}$	47	29	9.0	4
[1424.72	Fe II	$3d^7 \ ^4F_{7/2} - 3d^6 \ ^4p \ ^4D_{5/2}$	90	55	13	4
1424.79	Fe II	$3d^6 \ ^4s \ ^4D_{5/2} - 3d^5 \ ^4s \ ^4p \ ^4P_{3/2}$			4	
1425.03	S I	$3s^2 \ ^3p^4 \ ^3P_2 - 3s^2 \ ^3p^3 \ ^3d \ ^3D_3$	222	147	110	4
1425.19	S I	$3s^2 \ ^3p^4 \ ^3P_2 - 3s^2 \ ^3p^3 \ ^3d \ ^3D_{2,1}$	160	108	55	4
1425.42	S VI/2	$2p^6 \ ^3p \ ^2P_{3/2} - 2p^6 \ ^3d \ ^2D_{5/2,3/2}$			1	
1426.49	H ₂	0 - 5 P7 (X-B)			26	5
1427.18	Fe II	$3d^7 \ ^4F_{3/2} - 3d^6 \ ^4p \ ^2P_{1/2}$	48	30	9.6	4
1427.68	Ar VIII/2	$2p^6 \ ^3s \ ^2S_{1/2} - 2p^6 \ ^3p \ ^2P_{1/2}$			*134	0
1430.18	Fe II	$3d^7 \ ^4F_{7/2} - 3d^6 \ ^4p \ ^4F_{7/2}$	55	34	12	4
1431.03					24	3
1431.32	Ar V/2	$3s^2 \ ^3p^2 \ ^3P_2 - 3s \ ^3p^3 \ ^3P_{2,1}$			3	
1431.60	C I	$2s \ ^2p^3 \ ^5S_2 - 2s \ ^2p^2 \ ^3s \ ^5P_3$	90	54	31	4
1432.11	C I	$2s \ ^2p^3 \ ^5S_2 - 2s \ ^2p^2 \ ^3s \ ^5P_2$	102	64	52	4
1432.53	C I	$2s \ ^2p^3 \ ^5S_2 - 2s \ ^2p^2 \ ^3s \ ^5P_1$	89	54	44	4
1432.87	Fe II	$3d^6 \ ^4s \ ^4F_{9/2} - 3d^5 \ ^4s \ ^4p \ ^4F_{9/2}$	50	35	11	4
1433.29	S I	$3s^2 \ ^3p^4 \ ^3P_1 - 3s^2 \ ^3p^3 \ ^3d \ ^3D_2$	175	136	79	4
1434.96	Fe II	$3d^7 \ ^4F_{5/2} - 3d^6 \ ^4p \ ^4D_{3/2}$	74	49	23	4
1436.52	(e)/2				*215	0
[1436.97	S I	$3s^2 \ ^3p^4 \ ^3P_0 - 3s^2 \ ^3p^3 \ ^3d \ ^3D_1$	150	95	41	4
1437.00	O II/2	$2s^2 \ ^2p^3 \ ^2D_{5/2} - 2s \ ^2p^4 \ ^2D_{5/2}$			1	
1438.13	Fe II	$3d^7 \ ^4F_{7/2} - 3d^6 \ ^4p \ ^4P_{5/2}$	54	37	16	4
1439.11			46	32	23	3
1439.86					21	3
[1440.79	Fe II	$3d^7 \ ^4F_{3/2} - 3d^6 \ ^4p \ ^4D_{3/2}$	56	39	13	4
1440.91	Fe II	$3d^7 \ ^4F_{5/2} - 3d^6 \ ^4p \ ^4F_{5/2}$	56	36	11	4
1441.12	Fe II	$3d^6 \ ^4s \ ^4F_{5/2} - 3d^5 \ ^4s \ ^4p \ ^4F_{5/2}$	52	32	11	4
1442.56	Fe VIII/2	$3p^6 \ ^4p \ ^2P_{3/2} - 3p^6 \ ^4d \ ^2D_{5/2}$			*208	5
1442.75	Fe II	$3d^7 \ ^4F_{3/2} - 3d^6 \ ^4p \ ^4D_{1/2}$	74	49	4	
1444.09					26	3

Table 1—Continued

λ_{obs} Å	Line	Transition	L_{QS}^{peak} mW	L_{CH}^{peak} (sr m ² Å) ⁻¹	L_{SS}^{peak} (sr m ² Å) ⁻¹	Ref.	
1444.30	S I	$3s^2 3p^4 {}^3P_2$ – $3s^2 3p^3 4s {}^1D_2$	83	57	25	4	
1445.10	Ni II	$3d^9 {}^2D_{3/2}$ – $3d^8 4p {}^4D_{3/2}$	58	39	13	4	
1445.77	Si VIII	$2s^2 2p^3 {}^4S_{3/2}$ – $2s^2 2p^3 {}^2D_{3/2}$	60	38	113	0	
1446.12	H ₂	1 - 6 P5 (X-B)	53	34	30	5	
1446.59	Ni II	$3d^9 {}^2D_{3/2}$ – $3d^8 4p {}^4D_{5/2}$	62	39	11	4	
1447.27	Fe II	$3d^7 {}^4F_{3/2}$ – $3d^6 4p {}^4P_{1/2}$	57	37	11	4	
1448.23	S I	$3s^2 3p^4 {}^1D_2$ – $3s^2 3p^3 4s {}^1P_1$	66	45	15	4	
1450.01	Ni II	$3d^9 {}^2D_{5/2}$ – $3d^8 4p {}^2P_{3/2}$	60	41	11	4	
1453.08			59	39		3	
1454.85	Ni II	$3d^9 {}^2D_{5/2}$ – $3d^8 4p {}^2D_{5/2}$	96	63	0	4	
1456.13	C I	$2s^2 2p^2 {}^1S_0$ – $2s^2 2p 14d {}^1P_1$	63	41	14	4	
1456.23						3	
1457.38	S III/2	$3s^2 3p^2 {}^3P_2$ – $3s 3p^3 {}^3S_1$				1	
1457.49	C I	$2s^2 2p^2 {}^1S_0$ – $2s^2 2p 14d {}^3D_1$	60	40	22	4	
1458.14			60	43	23	3	
1459.03	C I	$2s^2 2p^2 {}^1D_2$ – $2s^2 2p 3d {}^1P_1$	98	63	60	4	
1459.31	Fe II	$3d^5 4s^2 {}^6S_{5/2}$ – $3d^6 5p {}^6P_{3/2}$	60	39	25	4	
1460.45	C I	$2s^2 2p^2 {}^1S_0$ – $2s^2 2p 12d {}^1P_1$	59	41	18	4	
1461.85	C I	$2s^2 2p^2 {}^1S_0$ – $2s^2 2p 12d {}^3D_1$	60	43	13	4	
1463.34	C I	$2s^2 2p^2 {}^1D_2$ – $2s^2 2p 3d {}^1F_3$	168	107	337	4	
1463.38	Fe X	$3s^2 3p^4 3d {}^4F_{9/2}$ – $3s^2 3p^4 3d {}^2F_{7/2}$				0	
1463.55	C I	$2s^2 2p^2 {}^1S_0$ – $2s^2 2p 11d {}^1P_1$	69	47	38	4	
1464.59			62	45	13	3	
1465.00	C I	$2s^2 2p^2 {}^1S_0$ – $2s^2 2p 11d {}^3D_1$	63	42	21	4	
1465.05	Fe II	$3d^5 4s^2 {}^6S_{5/2}$ – $3d^6 5p {}^6P_{5/2}$				4	
1466.21			68	45	12	3	
1467.09	Fe XI	$3s^2 3p^4 {}^3P_1$ – $3s^2 3p^4 {}^1S_0$				35	5
1467.27	Ni II	$3d^9 {}^2D_{5/2}$ – $3d^8 4p {}^2D_{3/2}$				4	
1467.40	C I	$2s^2 2p^2 {}^1D_2$ – $2s^2 2p 4s {}^1P_1$	120	77	100	4	
1467.76	Ni II	$3d^9 {}^2D_{5/2}$ – $3d^8 4p {}^2F_{7/2}$				4	
1467.88	C I	$2s^2 2p^2 {}^1D_2$ – $2s^2 2p 3d {}^3D_3$	110	78	26	4	
1468.41	C I	$2s^2 2p^2 {}^1D_2$ – $2s^2 2p 3d {}^3D_1$	136	93	41	4	
1469.12	C I	$2s^2 2p^2 {}^1S_0$ – $2s^2 2p 10d {}^3D_1$	55	39	10	4	
1470.09	C I	$2s^2 2p^2 {}^1D_2$ – $2s^2 2p 3d {}^3F_3$	134	94	49	4	
1470.45	C I	$2s^2 2p^2 {}^1D_2$ – $2s^2 2p 3d {}^3F_2$	60	44	9.8	4	
1471.83	S I	$3s^2 3p^4 {}^1D_2$ – $3s^2 3p^3 4s {}^3P_2$	71	49	20	4	
1472.23	C I	$2s^2 2p^2 {}^1D_2$ – $2s^2 2p 4s {}^3P_1$	115	73	27	4	

Table 1—Continued

λ_{obs} Å	Line	Transition	L_{QS}^{peak} mW	L_{CH}^{peak} (sr m ² Å) ⁻¹	L_{SS}^{peak}	Ref.
1472.97	S I	$3s^2 3p^4 \ ^3P_2 - 3s^2 3p^3 3d \ ^5D_3$	563	361	212	4
1473.24	C I	$2s^2 2p^2 \ ^1S_0 - 2s^2 2p 9d \ ^1P_1$	85	61	33	4
1473.99	S I	$3s^2 3p^4 \ ^3P_2 - 3s^2 3p^3 4s \ ^3D_3$	430	305	187	4
1474.38	S I	$3s^2 3p^4 \ ^3P_2 - 3s^2 3p^3 4s \ ^3D_2$	239	173	63	4
1474.58	S I	$3s^2 3p^4 \ ^3P_2 - 3s^2 3p^3 4s \ ^3D_1$	130	91	20	4
1474.75	C I	$2s^2 2p^2 \ ^1S_0 - 2s^2 2p 9d \ ^3D_1$	77	56	16	4
1476.77			74	51		4
1477.24	Ni II	$3d^9 \ ^2D_{5/2} - 3d^8 4p \ ^2F_{5/2}$	81	60	48	4
1477.84	Fe VII/2	$3d4p \ ^3P_2 - 3d4d \ ^3P_2$			*825	5
1480.06	Fe VII	$3d4p \ ^1F_3 - 3d4d \ ^1G_4$				5
1480.22	Ar VIII/2	$2p^6 4d \ ^2D_{5/2} - 2p^6 5p \ ^2P_{3/2}$			*3630	3
1481.00	C I	$2s^2 2p^2 \ ^1S_0 - 2s^2 2p 8d \ ^3P_1$				4
1481.12	C I	$2s^2 2p^2 \ ^1S_0 - 2s^2 2p 8d \ ^1P_1$	101	69	39	4
1481.45	C I	$2s^2 2p^2 \ ^1S_0 - 2s^2 2p 9s \ ^1P_1$	78	56	74	4
1481.68	S I	$3s^2 3p^4 \ ^3P_1 - 3s^2 3p^3 3d \ ^5D_2$				4
1481.62	Fe VII/2	$3d4p \ ^3D_3 - 3d4d \ ^3F_4$				5
1481.76	C I	$2s^2 2p^2 \ ^1D_2 - 2s^2 2p 3d \ ^1D_2$	407	297		4
1482.36	Fe VII/2	$3d4p \ ^3P_1 - 3d4d \ ^3P_0$			*861	5
1482.39	Ni II	$3d^9 \ ^2D_{3/2} - 3d^8 4p \ ^2P_{3/2}$	82	56		4
1482.72	C I	$2s^2 2p^2 \ ^1S_0 - 2s^2 2p 8d \ ^3D_1$	79	58	33	4
1483.04	S I	$3s^2 3p^4 \ ^3P_1 - 3s^2 3p^3 4s \ ^3D_2$	272	193	131	4
1483.23	S I	$3s^2 3p^4 \ ^3P_1 - 3s^2 3p^3 4s \ ^3D_1$	153	107	50	4
1485.62	S I	$3s^2 3p^4 \ ^3P_0 - 3s^2 3p^3 3d \ ^5D_1$	249	133	36	4
1486.53	N IV	$2s^2 \ ^1S_0 - 2s 2p \ ^3P_1$	148	79		0
1487.15	S I	$3s^2 3p^4 \ ^3P_0 - 3s^2 3p^3 4s \ ^3D_1$	227	124		4
1489.82	S IV/2	$3s^2 3p \ ^2P_{1/2} - 3s 3p^2 \ ^2P_{3/2}$				1
1492.58	C I	$2s^2 2p^2 \ ^1S_0 - 2s^2 2p 7d \ ^3P_1$	118	129		4
1492.63	N I	$2s^2 2p^3 \ ^2D_{5/2} - 2s^2 2p^2 3s \ ^2P_{3/2}$				4
1492.74	C I	$2s^2 2p^2 \ ^1S_0 - 2s^2 2p 7d \ ^1P_1$	152	143		4
1492.82	N I	$2s^2 2p^3 \ ^2D_{3/2} - 2s^2 2p^2 3s \ ^2P_{3/2}$				4
1493.96	Fe II	$3d^7 \ ^2G_{7/2} - 3d^6 4p \ ^2G_{7/2}$				4
1493.98	N II/2	$2s^2 2p^2 \ ^1D_2 - 2s^2 2p 3s \ ^1P_1$				1
1494.53	C I	$2s^2 2p^2 \ ^1S_0 - 2s^2 2p 7d \ ^3D_1$	115	118		4
1496.80	S IV/2	$3s^2 3p \ ^2P_{1/2} - 3s 3p^2 \ ^2P_{1/2}$				1
1500.44	S IV/2	$3s^2 3p \ ^2P_{3/2} - 3s 3p^2 \ ^2P_{3/2}$				1
1500.44	Ni II	$3d^9 \ ^2D_{3/2} - 3d^8 4p \ ^2D_{3/2}$				4
1510.86	Ni II	$3d^9 \ ^2D_{3/2} - 3d^8 4p \ ^2F_{5/2}$	221			4

Table 1—Continued

λ_{obs} Å	Line	Transition	L_{QS}^{peak} mW (sr m ² Å) ⁻¹	L_{CH}^{peak} mW (sr m ² Å) ⁻¹	L_{SS}^{peak} mW (sr m ² Å) ⁻¹	Ref.
1510.98	C I	$2s^2 2p^2 {}^1S_0 - 2s^2 2p 6d {}^1P_1$				4
1517.36	O V/2	$2s 2p {}^3P_1 - 2p^2 {}^3P_2$				1
1518.86	O V/2	$2s 2p {}^3P_0 - 2p^2 {}^3P_1$				1
1520.42	O V/2	$2s 2p {}^3P_1 - 2p^2 {}^3P_1$				1
1520.86	O V/2	$2s 2p {}^3P_2 - 2p^2 {}^3P_2$				1
1523.26	Si I	$3s^2 3p^2 {}^3P_2 - 3s^2 3p 26d {}^3D_3$				4
1523.37	Fe II	$3d^7 {}^4F_{9/2} - 3d^6 4p {}^2H_{11/2}$	140			4
1523.98	O V/2	$2s 2p {}^3P_2 - 2p^2 {}^3P_1$				1
1524.72	Si I	$3s^2 3p^2 {}^3P_2 - 3s^2 3p 22d {}^3P_{1,2}$	135			4
1524.83	Si I	$3s^2 3p^2 {}^3P_1 - 3s^2 3p 17d {}^3P_{0,1}$	135			4
1526.71	Si II	$3s^2 3p {}^2P_{1/2} - 3s^2 4s {}^2S_{1/2}$	767			4
1527.35	Si I	$3s^2 3p^2 {}^3P_1 - 3s^2 3p 15d {}^3P_{0,2}$	165			4
1528.28	Si I	$3s^2 3p^2 {}^3P_2 - 3s^2 3p 17d {}^3P_1$	137			4
1528.36	Si I	$3s^2 3p^2 {}^3P_2 - 3s^2 3p 17d {}^3D_3$				4
1528.72	N III/2	$2s^2 2p {}^2P_{3/2} - 2s 2p^2 {}^2S_{1/2}$				1
1529.46	Si I	$3s^2 3p^2 {}^3P_2 - 3s^2 3p 16d {}^3P_{2,3}$	149			4
1530.30	N IV/2	$2s^2 {}^1S_0 - 2s 2p {}^1P_1$	*276			1
1530.88	Si I	$3s^2 3p^2 {}^3P_2 - 3s^2 3p 15d {}^3P_2$	161			4
1530.93	Si I	$3s^2 3p^2 {}^3P_2 - 3s^2 3p 15d {}^3D_3$				4
1531.60	Si I	$3s^2 3p^2 {}^3P_1 - 3s^2 3p 17d {}^3D_2$	142			4
1532.45	Si I	$3s^2 3p^2 {}^3P_2 - 3s^2 3p 14d {}^3P_1$	160			4
1532.63	Si I	$3s^2 3p^2 {}^3P_2 - 3s^2 3p 20d {}^1F_3$	166			4
1533.41	Si I	$3s^2 3p^2 {}^3P_1 - 3s^2 3p 14s {}^1P_1$				4
1533.43	Si II	$3s^2 3p {}^2P_{3/2} - 3s^2 4s {}^2S_{1/2}$	696			4
1534.11	Si I	$3s^2 3p^2 {}^3P_1 - 3s^2 3p 12d {}^3D_1$	184			4
1534.18	Si I	$3s^2 3p^2 {}^3P_1 - 3s^2 3p 15d {}^3D_2$				4
1534.71	Si I	$3s^2 3p^2 {}^3P_2 - 3s^2 3p 13d {}^3P_{2,3}$	185			4
1537.01	Si I	$3s^2 3p^2 {}^3P_1 - 3s^2 3p 11d {}^3P_{0,1}$	171			4
1537.29	Si I	$3s^2 3p^2 {}^3P_2 - 3s^2 3p 12d {}^3P_2$	178			4
1537.47	Si I	$3s^2 3p^2 {}^3P_2 - 3s^2 3p 12d {}^3D_3$				4
1537.52	Si I	$3s^2 3p^2 {}^3P_1 - 3s^2 3p 11d {}^3D_1$	191			4
1537.62	Si I	$3s^2 3p^2 {}^3P_2 - 3s^2 3p 15d {}^1F_3$				4
1537.94	Si I	$3s^2 3p^2 {}^3P_2 - 3s^2 3p 12d {}^3F_3$	188			4
1538.79			172			4
1539.54	Si I	$3s^2 3p^2 {}^3P_2 - 3s^2 3p 14d {}^3D_2$				4
1539.70	Si I	$3s^2 3p^2 {}^3P_2 - 3s^2 3p 14d {}^1F_3$	158			4
1540.71	Si I	$3s^2 3p^2 {}^3P_1 - 3s^2 3p 12d {}^3D_2$	1206			4

Table 1—Continued

λ_{obs} Å	Line	Transition	L_{QS}^{peak} mW	L_{CH}^{peak} (sr m ² Å) ⁻¹	L_{SS}^{peak} (sr m ² Å) ⁻¹	Ref.
1540.78	Si I	$3s^2 3p^2 {}^3P_2 - 3s^2 3p 11d {}^3P_2$				4
1540.85	Ne VIII/2	$1s^2 2s {}^2S_{1/2} - 1s^2 2p {}^2P_{3/2}$	*479			1
1541.20	Si I	$3s^2 3p^2 {}^3P_1 - 3s^2 3p 12s {}^3P_2$	205			4
1541.32	Si I	$3s^2 3p^2 {}^3P_2 - 3s^2 3p 13d {}^1F_3$				4
1541.52	C I	$2s^2 2p^2 {}^1S_0 - 2s^2 2p 5d {}^3P_1$	190			4
1541.57	Si I	$3s^2 3p^2 {}^3P_1 - 3s^2 3p 10d {}^3P_1$				4
1542.18	C I	$2s^2 2p^2 {}^1S_0 - 2s^2 2p 5d {}^1P_1$	262			4
1542.43	Si I	$3s^2 3p^2 {}^3P_2 - 3s^2 3p 13d {}^1D_2$	170			4
1543.72	Si I	$3s^2 3p^2 {}^3P_1 - 3s^2 3p 11d {}^3D_2$	190			4
1543.96	C I	$2s^2 2p^2 {}^1S_0 - 2s^2 2p 6s {}^1P_1$	185			4
1544.18	Si I	$3s^2 3p^2 {}^3P_2 - 3s^2 3p 12d {}^3D_2$	164			4
1544.59	Si I	$3s^2 3p^2 {}^3P_2 - 3s^2 3p 12d {}^1F_3$	241			4
1544.67	Si I	$3s^2 3p^2 {}^3P_2 - 3s^2 3p 12s {}^3P_2$				4
1544.76	N III/2	$2s 2p^2 {}^4P_{5/2} - 2p^3 {}^4S_{3/2}$				1
1545.06	Si I	$3s^2 3p^2 {}^3P_2 - 3s^2 3p 10d {}^3P_1$	215			4
1545.16	Si I	$3s^2 3p^2 {}^3P_1 - 3s^2 3p 11d {}^1D_2$				4
1545.25	C I	$2s^2 2p^2 {}^1S_0 - 2s^2 2p 5d {}^3D_1$				4
1545.58	Si I	$3s^2 3p^2 {}^3P_2 - 3s^2 3p 10d {}^3D_3$	244			4
1545.61	Si I	$3s^2 3p^2 {}^3P_0 - 3s^2 3p 9d {}^3P_1$				4
1545.75	Si I	$3s^2 3p^2 {}^3P_2 - 3s^2 3p 10d {}^3P_2$				4
1546.59	Si I	$3s^2 3p^2 {}^3P_2 - 3s^2 3p 10d {}^3F_3$				4
1546.67	Si I	$3s^2 3p^2 {}^3P_0 - 3s^2 3p 9d {}^3D_1$	198			4
1547.13	Si I	$3s^2 3p^2 {}^3P_1 - 3s^2 3p 11s {}^3P_2$	168			4
1547.36	Si I	$3s^2 3p^2 {}^3P_1 - 3s^2 3p 9d {}^3P_{0,1}$	222			4
1548.21	C IV	$2s {}^2S_{1/2} - 2p {}^2P_{3/2}$	1449			4
1548.72	Si I	$3s^2 3p^2 {}^3P_1 - 3s^2 3p 10d {}^3D_2$	328			4
1549.02	O V/2	$2s 2p {}^1P_1 - 2p^2 {}^1S_0$				1
1550.26	Fe II	$3d^7 {}^4F_{9/2} - 3d^6 4p {}^4F_{7/2}$	282			4
1550.77	C IV	$2s {}^2S_{1/2} - 2p {}^2P_{1/2}$	889			4
1551.24	Si I	$3s^2 3p^2 {}^3P_2 - 3s^2 3p 9d {}^3P_2$	285			4
1551.86	Si I	$3s^2 3p^2 {}^3P_2 - 3s^2 3p 9d {}^3D_3$	331			4
1552.21	Si I	$3s^2 3p^2 {}^3P_2 - 3s^2 3p 10d {}^1F_3$	280			4
1552.81	Fe II	$3d^6 4s {}^4D_{1/2} - 3d^5 4s 4p {}^4D_{1/2}$				4
1552.96	Si I	$3s^2 3p^2 {}^3P_0 - 3s^2 3p 9d {}^1P_1$	216			4
1553.37	Si I	$3s^2 3p^2 {}^3P_0 - 3s^2 3p 10s {}^1P_1$	210			4
1554.64	Ca II	$3d {}^2D_{5/2} - 5f {}^2F_{7/2}$	243			4
1554.70	Si I	$3s^2 3p^2 {}^3P_1 - 3s^2 3p 9d {}^3D_2$				4

Table 1—Continued

λ_{obs} Å	Line	Transition	L_{QS}^{peak} mW (sr m ² Å) ⁻¹	L_{CH}^{peak}	L_{SS}^{peak}	Ref.
1555.51	Si I	$3s^2 3p^2 \ ^3P_0 - 3s^2 3p \ 8d \ ^3D_1$				4
1555.66	Si I	$3s^2 3p^2 \ ^3P_1 - 3s^2 3p \ 8d \ ^3P_0$	231			4
1556.04	Si I	$3s^2 3p^2 \ ^3P_2 - 3s^2 3p \ 9d \ ^3F_2$				4
1556.16	Si I	$3s^2 3p^2 \ ^3P_1 - 3s^2 3p \ 8d \ ^3P_1$	265			4
1556.54	Si I	$3s^2 3p^2 \ ^3P_1 - 3s \ 3p^3 \ ^1D_2$	265			4
1558.24	Si I	$3s^2 3p^2 \ ^3P_2 - 3s^2 3p \ 9d \ ^3D_2$	264			4
1558.45	Si I	$3s^2 3p^2 \ ^3P_1 - 3s^2 3p \ 9d \ ^1D_2$	353			4
1558.55	Fe II	$3d^7 \ ^4F_{5/2} - 3d^6 4p \ ^2D_{5/2}$				4
1558.68	Fe II	$3d^7 \ ^4F_{3/2} - 3d^6 4p \ ^2D_{3/2}$	417			4
1559.08	Fe II	$3d^7 \ ^4F_{9/2} - 3d^6 4p \ ^4F_{9/2}$	655			4
1559.36	Si I	$3s^2 3p^2 \ ^3P_2 - 3s^2 3p \ 9d \ ^1F_3$	335			4
1559.49						4
1559.64	O IV/2	$2s \ 2p^2 \ ^2D_{3/2} - 2p^3 \ ^2D_{3/2}$				1
1559.81	O IV/2	$2s \ 2p^2 \ ^2D_{5/2} - 2p^3 \ ^2D_{5/2}$				1
1559.99	O IV/2	$2s \ 2p^2 \ ^2D_{3/2} - 2p^3 \ ^2D_{5/2}$				1
1560.07	Si I	$3s^2 3p^2 \ ^3P_2 - 3s^2 3p \ 8d \ ^3P_2$	368			4
1560.31	C I	$2s^2 2p^2 \ ^3P_0 - 2s \ 2p^3 \ ^3D_1$	1045			4
1560.68	Ne VIII/2	$1s^2 2s \ ^2S_{1/2} - 1s^2 2p \ ^2P_{1/2}$	*297			1
1560.68	C I	$2s^2 2p^2 \ ^3P_1 - 2s \ 2p^3 \ ^3D_2$				4
1560.93	Si I	$3s^2 3p^2 \ ^3P_2 - 3s^2 3p \ 8d \ ^3D_1$	396			4
1561.06	Fe II	$3d^7 \ ^4F_{9/2} - 3d^6 4p \ ^4G_{7/2}$				4
1561.34	C I	$2s^2 2p^2 \ ^3P_2 - 2s^2 2p^3 \ ^3D_{3,2,1}$	1258			4
1561.82	Si I	$3s^2 3p^2 \ ^3P_1 - 3s^2 3p \ 8d \ ^3D_2$	263			4
1562.00	Si I	$3s^2 3p^2 \ ^3P_2 - 3s^2 3p \ 9d \ ^1D_2$	305			4
1562.29	Si I	$3s^2 3p^2 \ ^3P_1 - 3s^2 3p \ 10s \ ^3P_1$	280			4
1563.33	Si I	$3s^2 3p^2 \ ^3P_2 - 3s^2 3p \ 8d \ ^1F_3$	324			4
1563.79	Fe II	$3d^7 \ ^4F_{7/2} - 3d^6 4p \ ^4F_{7/2}$	647			4
1564.61	Si I	$3s^2 3p^2 \ ^3P_1 - 3s^2 3p \ 8d \ ^3F_2$				4
1564.68	Mg VIII/2	$2s^2 2p \ ^2P_{3/2} - 2s \ 2p^2 \ ^4P_{3/2}$				0
1565.31	Si I	$3s^2 3p^2 \ ^3P_0 - 3s^2 3p \ 9s \ ^1P_1$	306			4
1565.38	Si I	$3s^2 3p^2 \ ^3P_2 - 3s^2 3p \ 8d \ ^3D_2$				4
1566.82	Fe II	$3d^7 \ ^4F_{9/2} - 3d^6 4p \ ^4G_{9/2}$	540			4
1567.73	Si I	$3s^2 3p^2 \ ^3P_1 - 3s^2 3p \ 9s \ ^3P_2$	305			4
1568.02	Fe II	$3d^7 \ ^4F_{5/2} - 3d^6 4p \ ^4F_{3/2}$	415			4
1568.20	Si I	$3s^2 3p^2 \ ^3P_1 - 3s^2 3p \ 7d \ ^3P_1$	361			4
1568.62	Si I	$3s^2 3p^2 \ ^3P_0 - 3s^2 3p \ 7d \ ^3D_1$	299			4
1569.32	Si I	$3s^2 3p^2 \ ^3P_2 - 3s^2 3p \ 8d \ ^3F_3$	335			4

Table 1—Continued

λ_{obs} Å	Line	Transition	L_{QS}^{peak} mW	L_{CH}^{peak} $(\text{sr m}^2 \text{ Å})^{-1}$	L_{SS}^{peak}	Ref.
1569.67	Fe II	$3d^7 \ 4F_{9/2}$ – $3d^6 4p \ 4G_{11/2}$	525			4
1570.24	Fe II	$3d^7 \ 4F_{5/2}$ – $3d^6 4p \ 4F_{5/2}$	581			4
1570.52	Si I	$3s^2 3p^2 \ 3P_1$ – $3s^2 3p \ 7d \ 3D_1$	274			4
1571.14	Fe II	$3d^7 \ 4F_{7/2}$ – $3d^6 4p \ 4G_{5/2}$	383			4
[1571.32	Si I	$3s^2 3p^2 \ 3P_2$ – $3s^2 3p \ 9s \ 3P_2$				4
[1571.41	Si I	$3s^2 3p^2 \ 3P_1$ – $3s^2 3p \ 7d \ 3D_2$	387			4
1571.80	Si I	$3s^2 3p^2 \ 3P_2$ – $3s^2 3p \ 7d \ 3P_1$	347			4
1572.72	Si I	$3s^2 3p^2 \ 3P_0$ – $3s^2 3p \ 9s \ 3P_1$	466			4
[1572.98	S V/2	$3s^2 \ 1S_0$ – $3s \ 3p \ 1P_1$	*174			1
1573.00	Fe II	$3d^6 4s \ 4D_{5/2}$ – $3d^6 4p \ 4P_{5/2}$				4
1573.63	Si I	$3s^2 3p^2 \ 3P_2$ – $3s^2 3p \ 7d \ 3P_2$	428			4
[1573.88	Si I	$3s^2 3p^2 \ 3P_2$ – $3s^2 3p \ 7d \ 3D_3$	603			4
[1574.04	Fe II	$3d^7 \ 2H_{11/2}$ – $3d^6 4p \ 2G_{9/2}$				4
[1574.81	Si I	$3s^2 3p^2 \ 3P_1$ – $3s^2 3p \ 9s \ 3P_0$	785			4
1574.92	Fe II	$3d^7 \ 4F_{3/2}$ – $3d^6 4p \ 4F_{3/2}$	785			4
[1574.99	S X/2	$2s^2 2p^3 \ 4S_{3/2}$ – $2s^2 2p^3 \ 2P_{3/2}$				5
[1575.11	Si I	$3s^2 3p^2 \ 3P_0$ – $3s^2 3p \ 7d \ 1P_1$	582			4
1575.46	O IV/2	$2s^2 2p \ 2P_{1/2}$ – $2s \ 2p^2 \ 2D_{3/2}$	*296			1
1576.83	Si I	$3s^2 3p^2 \ 3P_2$ – $3s^2 3p \ 7d \ 1F_3$	396			4
[1577.04	Si I	$3s^2 3p^2 \ 3P_1$ – $3s^2 3p \ 7d \ 1P_1$				4
[1577.17	Fe II	$3d^7 \ 4F_{3/2}$ – $3d^6 4p \ 4F_{5/2}$	477			4
1578.48	Si I	$3s^2 3p^2 \ 3P_2$ – $3s^2 3p \ 7d \ 3D_2$	402			4
[1580.30	Si I	$3s^2 3p^2 \ 3P_1$ – $3s^2 3p \ 7d \ 3F_2$				4
[1580.40	O IV/2	$2s^2 2p \ 2P_{3/2}$ – $2s \ 2p^2 \ 2D_{5/2}$	*526			1
1580.63	Fe II	$3d^7 \ 4F_{7/2}$ – $3d^6 4p \ 4G_{9/2}$	2782			4
1581.27	Fe II	$3d^7 \ 4F_{5/2}$ – $3d^6 4p \ 4G_{5/2}$	481			4
[1584.29						4
1584.35	Si I	$3s^2 3p^2 \ 3P_2$ – $3s^2 3p \ 7d \ 3F_3$	469			4
1584.95	Fe II	$3d^7 \ 4F_{5/2}$ – $3d^6 4p \ 4G_{7/2}$	625			4
[1585.99	Fe II	$3d^7 \ 2D_{3/2}$ – $3d^6 4p \ 2D_{3/2}$	492			4
[1586.14	Si I	$3s^2 3p^2 \ 3P_1$ – $3s^2 3p \ 6d \ 3P_0$				4
1588.29	Fe II	$3d^7 \ 4F_{3/2}$ – $3d^6 4p \ 4G_{5/2}$	891			4
1588.65			522			4
1590.10			529			4
1592.42	Si I	$3s^2 3p^2 \ 3P_2$ – $3s^2 3p \ 6d \ 3P_2$	619			4
1593.32	O II/2	$2s^2 2p^3 \ 2P_{3/2}$ – $2s \ 2p^4 \ 2D_{5/2}$				1
1594.57	Si I	$3s^2 3p^2 \ 3P_2$ – $3s^2 3p \ 6d \ 3D_3$	687			4

Table 1—Continued

λ_{obs} Å	Line	Transition	L_{QS}^{peak} mW	L_{CH}^{peak} (sr m ² Å) ⁻¹	L_{SS}^{peak}	Ref.
1594.95	Si I	$3s^2 3p^2 \ ^3P_2$ – $3s^2 3p \ 6d \ ^3P_2$	638			4
1595.76	Si I	$3s^2 3p^2 \ ^3P_0$ – $3s^2 3p \ 6d \ ^1P_1$	606			4
1597.96	Si I	$3s^2 3p^2 \ ^3P_2$ – $3s^2 3p \ 6d \ ^1F_3$	592			4
1602.21	Fe II	$3d^7 \ ^4F_{9/2}$ – $3d^6 4p \ ^2F_{7/2}$	716			4
1602.58	Fe II	$3d^6 4p \ ^6F_{11/2}$ – $3d^6 5d \ ^6G_{13/2}$	826			4
1602.97	C I	$2s^2 2p^2 \ ^1S_0$ – $2s^2 2p \ 4d \ ^1P_1$	848			4
1605.32	Fe II	$3d^7 \ ^2G_{9/2}$ – $3d^6 4p \ ^2F_{7/2}$	712			4
1605.84	Si I	$3s^2 3p^2 \ ^3P_1$ – $3s^2 3p \ 6d \ ^3F_2$	705			4
1606.96	C I	$2s^2 2p^2 \ ^1S_0$ – $2s^2 2p \ 5s \ ^1P_1$	745			4
1608.43	C I	$2s^2 2p^2 \ ^1S_0$ – $2s^2 2p \ 4d \ ^3D_1$				4
1608.46	Fe II	$3d^6 4s \ ^6D_{9/2}$ – $3d^6 4p \ ^6P_{7/2}$	1092			4
1610.93	Fe II	$3d^7 \ ^4F_{9/2}$ – $3d^6 4p \ ^4G_{9/2}$				4
1611.20	Fe II	$3d^6 4s \ ^6D_{9/2}$ – $3d^6 4p \ ^4F_{7/2}$				4